UNIVERSIDADE FEDERAL DE SÃO CARLOS
CENTRO DE CIÊNCIAS EXATAS E DE TECNOLOGIA
PROGRAMA DE PÓS-GRADUAÇãO EM MATEMÁTICA

Singular perturbation of a saddle-node boundary equilibrium

Jackson Cunha

São Carlos-SP

Agosto de 2024

UNIVERSIDADE FEDERAL DE SÃO CARLOS
CENTRO DE CIÊNCIAS EXATAS E DE TECNOLOGIA
PROGRAMA DE PÓS-GRADUAÇÃO EM MATEMÁTICA

Singular perturbation of a saddle-node boundary equilibrium

Jackson Cunha

Orientador(a): Prof. Dr. Tiago Carvalho

Tese apresentada ao Programa de Pós-Graduação em Matemática da Universidade Federal de São Carlos como parte dos requisitos para a obtenção do Título de Doutor em Matemática.

São Carlos-SP

Agosto de 2024

UNIVERSIDADE FEDERAL DE SÃO CARLOS

Centro de Ciências Exatas e de Tecnologia
Programa de Pós-Graduação em Matemática

Folha de Aprovação

Defesa de Tese de Doutorado do candidato Jackson Luiz Orione Rafael Cunha, realizada em 22/08/2024.

Comissão Julgadora:

Prof. Dr. Tiago de Carvalho (USP)

Prof. Dr. Francisco Braun (UFSCar)

Prof. Dr. Luiz Fernando Gonçalves (UFG)

Prof. Dr. Pedro Toniol Cardin (UNESP)

Prof. Dr. Durval José Tonon (UFG)

O Relatório de Defesa assinado pelos membros da Comissão Julgadora encontra-se arquivado junto ao Programa de Pós-Graduação em Matemática.

Dedico este trabalho

aos meus pais,

Jaider e Maria do Carmo.

Agradecimentos

A realização desta tese de doutorado só foi possível graças ao apoio e colaboração de muitas pessoas, às quais sou profundamente grato.

Primeiramente, gostaria de expressar minha sincera gratidão ao meu orientador, Tiago de Carvalho, por sua orientação, paciência e incentivo constante ao longo deste percurso. Seu conhecimento e suas sugestões foram fundamentais para a conclusão deste trabalho.

Agradeço também aos membros da banca examinadora, pelas valiosas contribuições e pelo tempo dedicado à avaliação desta tese. Suas observações e críticas foram essenciais para aprimorar a qualidade do trabalho.

Aos meus colegas e amigos do Programa de Pós-Graduação em Matemática da Universidade Federal de São Carlos, meu muito obrigado pelo apoio, pelas discussões enriquecedoras e pela camaradagem ao longo destes anos. A convivência e o aprendizado compartilhado com todos vocês tornaram esta jornada mais leve e prazerosa.

Um agradecimento especial à minha família, que sempre acreditou em mim e me deu forças nos momentos mais desafiadores. Aos meus pais, Jaider e Maria do Carmo, pela educação, pelo amor incondicional e por sempre estarem ao meu lado.

Gostaria também de expressar meu sincero agradecimento à CAPES pelo apoio financeiro, que foi fundamental para a execução desta pesquisa. Sem esse suporte, muitos dos recursos e oportunidades que me foram proporcionados n ao teriam sido possíveis.

Por fim, agradeço a todos que, direta ou indiretamente, contribuíram para a realização desta tese. A todos que me ofereceram uma palavra de encorajamento, um conselho ou simplesmente estiveram presentes, meu sincero muito obrigado.

Resumo

Neste trabalho, analisamos campos vetoriais planares suaves por partes, definidos em duas regiões, em que a variedade de comutação é uma curva que passa pela origem. Em uma dessas regiões, atua um campo vetorial suave com um equilíbrio do tipo sela-nó na origem, enquanto na outra, o campo vetorial é transversal à variedade de comutação. É bem conhecido que este campo vetorial suave por partes tem codimensão dois no conjunto de todos os campos vetoriais suaves por partes, e uma perturbação singular deste cenário é nova na literatura. Além disso, como o equilíbrio considerado está sobre a variedade de comutação, ele será chamado de equilíbrio de fronteira. Regularizamos o campo vetorial suave por partes usando o método conhecido como Sotomayor-Teixeira. Após essa etapa, adotamos uma abordagem de perturbação singular. Nesse processo, identificamos um ponto de equilíbrio não normalmente hiperbólico. Para uma compreensão completa da dinâmica em torno deste ponto, aplicamos a ele uma sequência de transformações, conhecidas como "blow-ups".

Palavras-chave: perturbações singulares; campo vetorial suave por partes; blow-up; bifurcação de equilíbrio de fronteira; regularização.

Abstract

In this work, we analyze piecewise smooth planar vector fields defined in two regions, where the switching manifold is a curve passing through the origin. In one of these regions, a smooth vector field acts with a saddle-node equilibrium at the origin, while in the other, the vector field is transversal to the switching manifold. It is well known that this piecewise smooth vector field has codimension two in the set of all piecewise smooth vector fields, and a singular perturbation in this scenario is new in the literature. Also, since the equilibrium considered is over the switching manifold, it will be called a boundary equilibrium. We regularized the piecewise smooth vector field using the method known as Sotomayor-Teixeira. After this step, we adopt a singular perturbation approach. In this process, we identify a non-normally hyperbolic equilibrium point. For a complete understanding of the dynamics around this point, we apply a sequence of transformations to it, known as "blow-ups".

Keywords: singular perturbations; piecewise smooth vector field; blow-up; boundary equilibrium bifurcation; regularization.

Contents

List of Figures

Introduction

Mathematical modeling is a field of study that aims to translate everyday life problems into mathematical problems, thus playing a crucial role in understanding and predicting complex phenomena in various domains of knowledge. Essentially, this area of study seeks to express the problematic situation in a set of equations in order to identify patterns that can predict future scenarios, analyze the temporal evolution of the problem, and possibly suggest optimized strategies for dealing with these situations.

Among the various modeling approaches, the use of Differential Equations stands out, capable of representing a wide variety of real-world phenomena (see [26]). In some of these phenomena, a sudden change in the dynamics governing the model may occur. In these cases, the use of nonsmooth differential equations is more suitable for describing the system, and thus, it is necessary to consider a piecewise smooth vector field (PSVFs, for short). Such systems basically consist of a set of differential equations that simulate the problem in different situations, which are activated or deactivated through previously established thresholds.

The medical field is full of problems that can be modeled using PSVFs. For example, viral behavior can be expressed in systems of differential equations that describe the interactions between infected cells, susceptible cells, and the infectious form of a virus, which typically behaves differently in patients with or without treatment. Such difference in behavior makes the mathematical modeling technique using PSVFs an excellent alternative for analyzing situations where treatments are activated or deactivated. This approach is even more promising when intermittent medication use is necessary, which is common due to side effects and the body's recovery time. The described scenario is perfectly suited to studying the dynamics of the human immunodeficiency virus (commonly known by the abbreviation HIV) as can be observed in [8].

The same logic can be applied to monitoring patients undergoing oncological therapies, which are typically administered intermittently (see [3]), or in containment protocols during the COVID-19 pandemic, as observed in [2], where a non-pharmacological alternative is presented to deal with the pandemic that has plagued humanity in recent years. In this latter model, the equations simulate

situations with (or without) social isolation of the infected, and the switch between vector fields is decided based on the number of contaminated individuals so that the healthcare system does not collapse.

Examples of models using PSVF are not limited solely to medical issues. In [34], a model describing energy supply availability in a specific region is presented, taking into account different investments in new infrastructure. Other works describing real-world phenomena using the same modeling strategy can be found in [5], [6], [7], [29], and [30]

Despite the potential for application, the exploration of piecewise smooth vector fields is a relatively recent field of study, whose mathematical formulation was substantially influenced by the works of Koslova (see [20]), and even more significantly by the studies of Filippov (see [14]), who proposed terminology and theoretical foundations for understanding these vector fields.

We will formally introduce the necessary concepts to understand this work in Section 1. To contextualize the reader now, let us consider a Piecewise Smooth Vector Field, denoted by $X = (X_+, X_-, \Sigma)$, defined in $U \subset \mathbb{R}^n$. It consists of a pair of vector fields $X_+, X_- \in \mathfrak{X}^r(U)$, whose respective domains are separated by a submanifold $\Sigma = f^{-1}(0)$, and described as follows:

$$X(p) = \begin{cases} X_+(p), & \text{if} \quad f(p) \geq 0 \\ X_-(p), & \text{if} \quad f(p) \leq 0 \end{cases}, \tag{1}$$

where $f : U \to \mathbb{R}$ is a C^r-class function with $0 \in \mathbb{R}$ as a regular value in the open set U, where $r \geq 1$ is sufficiently large for our purpose, and $\mathfrak{X}^r(U)$ is the space of C^r-class vector fields on U.

Unlike smooth vector fields, in general, the uniqueness of solutions for PSVFs cannot be guaranteed due to the loss of smoothness of X at points of Σ. Therefore, a careful analysis of these discontinuity points is essential for a comprehensive understanding of the dynamics of these systems. In this context, one of Filippov's most relevant contributions was the introduction of the convention bearing his name, which clarifies the dynamics of these fields in open and densely populated regions in the discontinuity region.

Although Filippov's convention is a classical approach in the process of understanding and familiarizing oneself with the theory of PSVFs, this convention is not the only way to study these systems. As an alternative, we can study the transition between the vector fields that compose the PSVF using the *Geometric Singular Perturbation Theory* (GSPT, for short), see [25, 28]. Basically, the process of transforming a PSVF into a singular perturbation problem involves subjecting the original PSVF to a *Sotomayor-Teixeira regularization* (see [31]), which naturally generates a *fast-slow system* that can be analyzed using Fenichel's Theory (see [13]); where results related to perturbations of invariant manifolds are applied to describe the dynamics of the fast-slow system near normally hyperbolic

points of the so-called *critical manifold*, which we will formally define in Section 1 (see also, [32]).

As we mentioned, Fenichel's Theory provides information around normally hyperbolic points. However, the regularization process can generate points that are non-normally hyperbolic, and in this scenario, other techniques are necessary for study, such as the method of geometric desingularization, known as the *blow-up method*, used by Dumortier and Roussarie in [12] and later by Krupa and Szmolyan in [21, 22]. The blow-up method offers a deeper understanding of the dynamics around non-hyperbolic points in fast-slow systems.

The essence of this technique is to "inflate" the degenerate point into a higher-dimensional structure, such as a line, a circle, or a sphere. This allows the dynamics to be transferred to the new structure and facilitates the recovery of crucial information about the original problem. During this process, new degenerate points may arise, and in such cases, the procedure can be reapplied. Notably, as long as the system satisfies the Lojasiewicz inequality, it is possible to understand the behavior around these points through a finite number of blow-ups, as highlighted in Remark 3 in Section 2.2. For complementary reading on this technique, we suggest consulting the reference [1]. In a more specific context involving fast-slow systems, we recommend reading [17] and Chapter 7 of [23].

This thesis conducts a comprehensive investigation that combines geometric singular perturbation theory with the Blow-up method to explore a planar piecewise smooth vector field $X = (X_+, X_-)$, where the second vector field X_- is transversal to the switching manifold at a point $p \in \Sigma$, while X_+ exhibits a classical saddle-node equilibrium at p. Since this equilibrium is located on Σ, it is referred to as a *boundary equilibrium*, and, in this specific case, a *boundary-saddle-node*, which, as discussed in [15], is of codimension two within the space of all planar PSVFs. The chapter structure is designed to guide the reader through a logical sequence, ensuring that the theoretical foundations consistently support the applications and results.

Chapter 1 is dedicated to the preliminary concepts, providing a solid foundation for subsequent exploration. We begin with a general discussion of the Blow-up method, illustrating its utility in analyzing the dynamics around non-hyperbolic singularities. Next, we introduce fast-slow systems, which enable the modeling of dynamics across different time scales. Following this, we address piecewise smooth vector fields, highlighting their characteristics and relevance in analyzing systems with abrupt behavioral transitions. To complement this theoretical foundation, we present the Sotomayor-Teixeira regularization, a technique that allows for the smoothing of discontinuities, offering a new perspective on the study of transitions in these systems.

Building on these theoretical foundations, Chapter 2 is dedicated to the application of the Blow-

up method to fast-slow systems, expanding its implications for the analysis of singular systems. The chapter begins with an explanation of how to generate a fast-slow system through the regularization of piecewise smooth vector fields. Next, it discusses the use of the Blow-up method in perturbed singular problems, emphasizing the relevance of the criteria for choosing appropriate weights. Additionally, the concepts of quasi-homogeneous vector fields are explored, as well as the determination of weights through the Newton polyhedron, establishing an analytical framework that enables the application of the method to these systems.

The practical exploration of the blow-up method is conducted in Chapter 3, where we investigate a PSVF X that exhibits a boundary-saddle-node type singularity, allowing for a comprehensive and detailed analysis of its dynamics. The chapter begins with the presentation of the model, followed by the construction of a fast-slow system associated with X, which is obtained through the Sotomayor-Teixeira regularization. Next, we proceed with the application of the blow-up method, employing a selection of weights that highlights specific aspects of the dynamics in question. The analysis progresses into the directional charts, exploring the behavior of the non-normally hyperbolic point in one of the local charts, necessitating the application of a new blow-up to fully desingularize the system.

Thus, the approach developed throughout this work provides a consistent framework for the analysis of singular dynamical systems, with steps that can be applied and adapted to other similar contexts. The systematic structure adopted here grants the method the advantage of reproducibility, serving as a promising foundation for future investigations and broadening research perspectives in analogous systems.

CHAPTER 1

Preliminaries

In this chapter, we will present the fundamental concepts and results that will serve as the basis for the development of this work. We will begin by introducing, in the first section, the idea of the blow-up method through an example involving a single time scale system. In the following three sections, we will discuss the concepts of fast-slow systems, piecewise smooth vector fields, and the Sotomayor-Teixeira regularization. Integrating these four sections will allow us to establish the method discussed in Chapter 2. The main references for this chapter are [14], [16], [17], [23], and [31].

1.1 Blow-up method

The Grobman-Hartman theorem represents a crucial milestone in the theory of dynamical systems and differential equations. Essentially, this theorem establishes that the qualitative behavior of a nonlinear system around a hyperbolic equilibrium point is locally equivalent to that of a linear system. Such correspondence significantly simplifies the analysis of the system's local behavior, enabling the deduction of fundamental properties from its linearized version.

However, it is important to emphasize that not all equilibrium points are characterized as hyperbolic, which makes the direct application of the Grobman-Hartman Theorem impossible. In this scenario, the desingularization technique, called Blow-up, becomes relevant. This technique, in essence, performs a transformation of coordinates with the purpose of analyzing the dynamics of the vector field in the vicinity of a non-hyperbolic singular point.

The blow-up method emerged as a technique developed separately from the geometric study of equations with multiple time scales. Although our main focus is to explore fast-slow systems (see Section 1.2), as in [23], we choose to introduce this technique through an example involving a single time scale system. This approach allows for a clearer and more accessible exposition of the type of

problem that the blow-up method aims to solve.

As an example, consider the ordinary differential equation:

$$\begin{cases} x' &= x^2 - 2xy, \\ y' &= y^2 - 2xy. \end{cases} \tag{1.1}$$

We observe that the origin $(x,y) = (0,0)$ is a non-hyperbolic equilibrium point since the linearization of System (1.1) at this point is given by the zero matrix, which prevents the direct application of the Grobman-Hartman theorem. To circumvent this issue, we will consider a special transformation $\varphi(\theta,r) : \mathbb{S}^1 \times I \to \mathbb{R}^2$ given by:

$$\varphi(\theta,r) = \big(r\ \cos(\theta),\ r\ \mathrm{sen}(\theta)\big) \tag{1.2}$$

where $\mathbb{S}^1$ denotes the unit circle, with $\theta \in [0,2\pi]$, and $I \subset \mathbb{R}$ is an interval that contains the origin. With this change, using the relation $(x,y) = \big(r\ \cos(\theta), r\ \mathrm{sen}(\theta)\big)$, we can rewrite the System (1.1) as follows:

$$\begin{cases} \theta' &= 3r\ \cos(\theta)\ \mathrm{sen}(\theta)\big(\mathrm{sen}(\theta) - \cos(\theta)\big), \\ r' &= r^2\left[\cos^3(\theta) - 2\mathrm{sen}(\theta)\ \cos(\theta)\left(\mathrm{sen}(\theta) + \cos(\theta)\right) + \mathrm{sen}^3(\theta)\right]. \end{cases} \tag{1.3}$$

Note that the mapping defined by φ maps the circle $\mathbb{S}^1 \times \{r = 0\}$ to the origin in the plane $\mathbb{R}^2$. Furthermore, since φ is a diffeomorphism for $r > 0$, the orbits of System (1.1) in a small neighborhood of the origin correspond to the orbits of (1.3) in a small neighborhood of $\mathbb{S}^1 \times \{r = 0\}$. However, observe that (1.3) vanishes along $\mathbb{S}^1 \times \{r = 0\}$. To overcome this, we can divide the right-hand side of (1.3) by r. This operation does not alter the qualitative properties of the orbits in the region $\mathbb{S}^1 \times \{r > 0\}$. Thus, it will be sufficient to study the desingularized system

$$\begin{cases} \theta' &= 3\ \cos(\theta)\ \mathrm{sen}(\theta)\big(\mathrm{sen}(\theta) - \cos(\theta)\big), \\ r' &= r\left[\cos^3(\theta) - \mathrm{sen}(2\theta)\left(\mathrm{sen}(\theta) + \cos(\theta)\right) + \mathrm{sen}^3(\theta)\right]. \end{cases} \tag{1.4}$$

which no longer vanishes along $\mathbb{S}^1 \times \{r = 0\}$. The most important fact is that the orbits of (1.4) near $\mathbb{S}^1 \times \{r = 0\}$ correspond to the orbits of (1.1) near the origin.

After doing that, by directly inspecting the vector field $\bar{F}(\theta,r)$ associated with the system (1.4), we obtain

$$J\bar{F}_{(\theta,r)} = \begin{bmatrix} \frac{3}{4}\big(3\mathrm{sen}(3\theta) - \cos(\theta) - 3\cos(3\theta) - \mathrm{sen}(\theta)\big) & 0 \\ \frac{r}{4}\big(\cos(\theta) - 9\cos(3\theta) - \mathrm{sen}(\theta) - 9\mathrm{sen}(3\theta)\big) & \cos^3(\theta) - \mathrm{sen}(2\theta)\big(\cos(\theta) + \mathrm{sen}(\theta)\big) + \mathrm{sen}^3(\theta) \end{bmatrix}.$$

Consequently, we can verify that the six equilibrium points on $\mathbb{S}^1 \times \{r = 0\}$, located at

$$\theta \in 0, \frac{\pi}{4}, \frac{\pi}{2}, \pi, \frac{5\pi}{4}, \frac{3\pi}{2}$$

are hyperbolic saddle-type, whose respective linearizations are given by:

$$J\bar{F}_{(0,0)} = \begin{bmatrix} -3 & 0 \\ 0 & 1 \end{bmatrix}, \qquad J\bar{F}_{(0,\frac{\pi}{4})} = \frac{\sqrt{2}}{2}\begin{bmatrix} 3 & 0 \\ 0 & -1 \end{bmatrix}, \qquad J\bar{F}_{(0,\frac{\pi}{2})} = \begin{bmatrix} -3 & 0 \\ 0 & 1 \end{bmatrix},$$
$$J\bar{F}_{(0,\pi)} = \begin{bmatrix} 3 & 0 \\ 0 & -1 \end{bmatrix}, \qquad J\bar{F}_{(0,\frac{5\pi}{4})} = \frac{\sqrt{2}}{2}\begin{bmatrix} -3 & 0 \\ 0 & 1 \end{bmatrix}, \qquad J\bar{F}_{(0,\frac{3\pi}{2})} = \begin{bmatrix} 3 & 0 \\ 0 & -1 \end{bmatrix}.$$

The procedure to which we have just subjected the System (1.1) is known as the blow-up method. As illustrated in Figure 1.1a, this method, in a sense, "blow-up" the non-hyperbolic equilibrium point of the System (1.1) to the circle $\mathbb{S}^1 \times \{r = 0\}$, containing six new hyperbolic points. These new points can be studied using the Grobman-Hartman Theorem and other techniques from dynamical systems. After this analysis, by "blows-down" the blow-up system, we can extract valuable information about the original system, as illustrated in Figure 1.1b. In general, the goal of the blow-up method is to obtain a new system that is simpler to analyze.

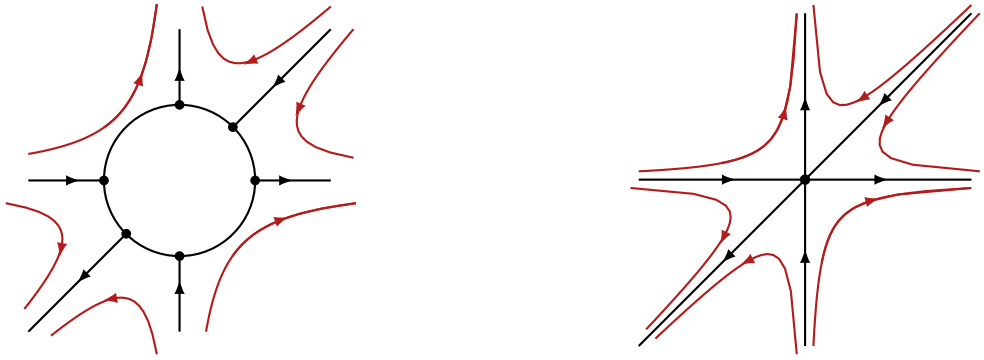

(a) Blow-up system. (b) Original system.

Figure 1.1: Phase portrait representation of systems (1.4) and (1.1), respectively. Once the expanded system is understood, we then "blows-down" the phase portrait of (1.4), resulting in a qualitative description of the original system (1.1).

In Chapter 2, we will formally define this method for problems involving fast-slow systems (see Section 1.2) arising from PSVFs (see Section 1.3).

1.2 Fast-slow systems

Fast-slow systems, as will be defined below, are extensively studied in the literature due to their relevance in real-world models and the challenging mathematical problems they present. The detailed understanding of the phase portrait of these systems is the primary objective of Geometric Singular Perturbation Theory (GSPT). In general terms, GSPT aims to investigate the limits of Equations (1.5) and (1.6) as $\varepsilon = 0$, analyze invariant objects in these limits, and subsequently use perturbation methods to describe the dynamics of Equations (1.5) and (1.6) for small values of ε. For an introduction to this topic, as well as more advanced applications and theoretical aspects, see [16] and [23].

Consider the functions $f : \mathbb{R}^m \times \mathbb{R}^n \times \mathbb{R} \to \mathbb{R}^m$ and $g : \mathbb{R}^m \times \mathbb{R}^n \times \mathbb{R} \to \mathbb{R}^n$ are C^k-functions, with k sufficiently large. A *Fast-slow system* is a singularly perturbed ordinary differential equation (ODE) of the form

$$\begin{cases} \varepsilon \dot{x} = & \varepsilon \frac{dx}{d\tau} & = & f(x,y,\varepsilon), \\ \dot{y} = & \frac{dy}{d\tau} & = & g(x,y,\varepsilon), \end{cases} \tag{1.5}$$

where the over-dot denotes differentiation with respect to the *Slow time* τ, $x \in \mathbb{R}^m$ and $y \in \mathbb{R}^n$ represent the *Fast* and *Slow variables*, respectively, and $0 < \varepsilon \ll 1$ is a small parameter accounting for the time scale separation. By defining the *Fast time* as $t := \frac{\tau}{\varepsilon}$, we can reformulate the system in Equation (1.5) as an $\varepsilon-$family of ODEs of the form:

$$\begin{cases} x' = & \frac{dx}{dt} & = & f(x,y,\varepsilon), \\ y' = & \frac{dy}{dt} & = & \varepsilon g(x,y,\varepsilon), \end{cases} \tag{1.6}$$

where the symbol $'$ denotes the derivative with respect to the fast time t.

Note that the systems described in Equations (1.5) and (1.6) are equivalent for $\varepsilon > 0$, differing only in the temporal parameterization of the corresponding trajectories. When setting $\varepsilon = 0$ in (1.5), we obtain the *Reduced problem*

$$\begin{cases} 0 & = & f(x,y,0), \\ \dot{y} & = & g(x,y,0), \end{cases} \tag{1.7}$$

also known as the *Slow subsystem*, whose flow is referred to as the *Slow flow*. Similarly, when taking $\varepsilon = 0$ in (1.6), we obtain the *Layer problem*

$$\begin{cases} x' & = & f(x,y,0), \\ y' & = & 0, \end{cases} \tag{1.8}$$

also known as the *Fast subsystem*, where the slow variables y are considered parameters. The two singular limit Systems (1.7) and (1.8) are no longer equivalent. However, we notice that the set of points where $f(x,y,0) = 0$ delineates the phase space of solutions for the slow subsystem and the equilibrium points for the Fast subsystem. This observation leads us to the following natural definition:

Definition 1. *The critical manifold of a fast-slow system* (1.5) *is defined by*

$$C_0 = \Big\{ (x,y) \in \mathbb{R}^m \times \mathbb{R}^n \ : \ f(x,y,0) = 0 \Big\}.$$

Although we are using the term manifold to describe C_0, it is crucial to emphasize that the solutions of the equation $f(x,y,0) = 0$ do not always strictly fit the definition of a manifold. However, as is common in fast-slow systems, we continue to refer to C_0 as a critical manifold by convention (see Example 6 and Remark 4 in Section 2.3) .

A fundamental property in the analysis of fast-slow systems dynamics is characterized by the normal hyperbolicity of points on the critical manifold, which we will define next.

Definition 2. *A subset $S \subset C_0$ is called normally hyperbolic if the $m \times m$ matrix $D_x f(p,0)$ of first partial derivatives with respect to the fast variables has no eigenvalues with zero real part for all $p \in S$. A normally hyperbolic subset $S \subset C_0$ is called attracting if all eigenvalues of $D_x f(p,0)$ have negative real part for $p \in S$. Similarly, S is called repelling if all eigenvalues have positive real part. If S is normally hyperbolic and neither attracting nor repelling, it is of saddle type.*

Example 1. *Consider the system*

$$\begin{cases} \varepsilon \dot{x} &= y - \frac{x^3}{3} + x, \\ \dot{y} &= -x. \end{cases} \tag{1.9}$$

Through direct calculation, we conclude that both the reduced and layer problems are described by

$$\begin{array}{rclcrcl} 0 &=& y - \frac{x^3}{3} + x, & & x' &=& y - \frac{x^3}{3} + x, \\ \dot{y} &=& -x, & & y' &=& 0, \end{array}$$

respectively, where the critical manifold is characterized by

$$C_0 = \left\{ (x,y) \in \mathbb{R}^2 \ : \ y = \frac{x^3}{3} - x \right\}.$$

Additionally, note that

$$D_x f(x,y,\varepsilon) = 1 - x^2,$$

where $f(x,y,\varepsilon) = y - \frac{x^3}{3} + x$. This expression indicates that C_0 loses its normal hyperbolicity at points $(1, -\frac{2}{3})$ and $(-1, \frac{2}{3})$, resulting in the division of the critical manifold into three connected components

$$\begin{aligned} C_0^{a_1} &= \left\{ (x,y) \in C_0 : \quad x < -1 \right\}, \\ C_0^{r} &= \left\{ (x,y) \in C_0 : -1 < x < 1 \right\}, \\ C_0^{a_2} &= \left\{ (x,y) \in C_0 : \quad x > -1 \right\}, \end{aligned}$$

all of which are normally hyperbolic; where $C_0^{a_1}$ and $C_0^{a_2}$ are attracting, while C_0^r is a repelling (see Figure 1.2).

The determination of normal hyperbolicity, or its absence, in a critical manifold plays a crucial role in defining the analytical strategies required to investigate the corresponding fast-slow system. If the critical manifold maintains normal hyperbolicity, we can apply Fenichel's theorem (see [13] and [18]), that we will present next. However, if there is a loss of this normality due to the presence of non-normally hyperbolic points, we can utilize the blow-up method, which will be discussed in the next chapter.

Fenichel's Theorem [13, 18] (see also [33]) provides geometric tools and techniques to analyze fast-slow systems containing hyperbolic points. To state it, we need to recall the notion of Hausdorff

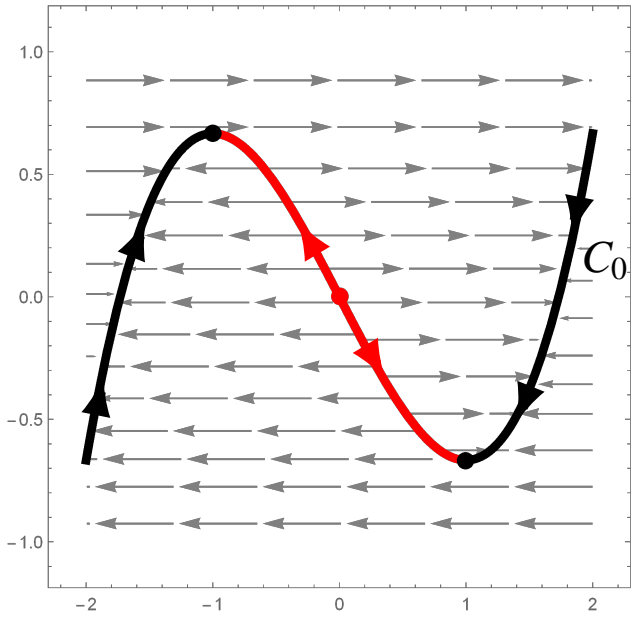

Figure 1.2: Representation of the singular limit of the Fast-slow system (1.9). The critical manifold C_0 has an equilibrium point depicted in red, located at the origin, and loses its normal hyperbolicity at the points $(x,y) = (\pm 1, \mp 2/3)$, marked in black. This results in the division of C_0 into three normally hyperbolic subsets, where C_0^r, highlighted in red, exhibits repulsive behavior, while $C_0^{a_1} \cup C_0^{a_2}$, highlighted in black, is attractive. Gray arrows indicate fast flow, while red and black arrows on C_0 represent slow flow.

distance between two nonempty sets $V, W \subset \mathbb{R}^{m+n}$, which is defined by

$$d_H(V,W) = max\left\{ \sup_{v\in V} \inf_{w\in W} \|v-w\|, \sup_{w\in W} \inf_{v\in V} \|v-w\| \right\}.$$

Theorem 1 (Fenichel's Theorem [13, 18])**.** *Suppose that $S_0 \subset C_0$ is a compact normally hyperbolic submanifold (possibly with boundary) of the critical manifold C_0 of* (1.5)*. Then, for $\varepsilon > 0$ sufficiently small, the following hold:*

1. *There exists a locally invariant manifold S_ε diffeomorphic to S_0.*
2. *S_ε has Hausdorff distance $\mathcal{O}(\varepsilon)$, as $\varepsilon \to 0$, from S_0.*
3. *The flow on S_ε converges to the slow flow as $\varepsilon \to 0$.*
4. *S_ε is C^k-smooth.*
5. *S_ε is normally hyperbolic and has the same stability properties, i.e., attracting, repelling or saddle-type, with respect to the fast variables as S_0.*
6. *S_ε is usually not unique. In regions that remain at a fixed distance from ∂S_ε, all manifolds satisfying Items 1 - 5 above lie at a Hausdorff distance of order $\mathcal{O}(\exp^{-\frac{K}{\varepsilon}})$ from each other for some $K > 0, K \in \mathcal{O}(1)$, as $\varepsilon \to 0$.*

Definition 3. *A manifold S_ε, as obtained in the conclusion of Theorem 1, is called a slow manifold.*

It is worth noting that, in some cases, fast-slow systems may not precisely conform to the formulation we present. For example, the Olsen model for the peroxidase-oxidase reaction, discussed in [24], does not follow this pattern. The advantage of the formulation presented in System (1.5), known as the Standard form of fast-slow systems, lies in our ability to clearly observe the differentiation of temporal scales between the slow and fast variables.

1.3 Piecewise Smooth Vector Fields

Let $f : U \subset \mathbb{R}^n \to \mathbb{R}$ be a function of class C^r having $0 \in \mathbb{R}$ as a regular value in the open set U, with $r \geq 1$ being sufficiently large for our purpose. Consider the codimension one submanifold $\Sigma = f^{-1}(0) = \{p \in U \mid f(p) = 0\}$, called *switching manifold*, that separates U into two regions that we will represent by $\Sigma^+ = \{p \in U \mid f(p) \geq 0\}$ and $\Sigma^- = \{p \in V \mid f(p) \leq 0\}$.

We will denote by $\mathfrak{X}^r(U)$ the space of vector fields of class C^r in U. A *piecewise smooth vector field* $X : U \to \mathbb{R}^n$ is written as

$$X(p) = \begin{cases} X_+(p), & \text{if } f(p) \geq 0, \\ X_-(p), & \text{if } f(p) \leq 0, \end{cases} \tag{1.10}$$

where $X_+, X_- \in \mathfrak{X}^r(U)$. As usual in the literature, System (1.10) is denoted by $X = (X_+, X_-, \Sigma)$ or simply by $X = (X_+, X_-)$, when Σ is well understood.

Observe that, over Σ, X is multi-valuated. So, we need to provide a rule for the transition of the orbits between Σ^+ and Σ^- across Σ. This can be obtained by following Filippov's convention (see [14]). During this analysis, it will be particularly relevant to understand the contact between the vector field X_+ (or X_-) and the switching manifold Σ. When convenient, by establishing concepts of the vector fields X_+ and X_- that can be associated through the indexing sign, we will do so simultaneously using notation related to $X_\pm$.

This will be done by using the derivative of f in the direction of the vector field $X_\pm$ (also known as the Lie derivative of f with respect to $X_\pm$), that is given by the expression

$$X_\pm f(p) = \langle \nabla f(p), X_\pm(p) \rangle ,$$

where $\langle ., . \rangle$ is the usual inner product in $\mathbb{R}^2$. For $i \geq 2$ the higher order Lie derivatives are defined, inductively, by

$$X_\pm^i f(p) = \left\langle \nabla X_\pm^{i-1} f(p), X_\pm(p) \right\rangle .$$

So, generically, it will appears the following regions on Σ:

- *Crossing region*: $\Sigma^c = \{p \in \Sigma : X_+f(p) \cdot X_-f(p) > 0\}$.
- *Escaping region*: $\Sigma^e = \{p \in \Sigma : X_+f(p) > 0 \text{ and } X_-f(p) < 0\}$.
- *Sliding region*: $\Sigma^s = \{p \in \Sigma : X_+f(p) < 0 \text{ and } X_-f(p) > 0\}$.

The *escaping* Σ^e or *sliding* Σ^s regions are respectively composed by points of Σ where both vector fields X_+ and X_- simultaneously point outwards or inwards from Σ while, generically, the interior of its complement in Σ defines the *crossing region* Σ^c, which can be subdivided into two regions defined by $\Sigma^{c+} = \{p \in \Sigma \mid X_\pm f(p) > 0\}$ and $\Sigma^{c-} = \{p \in \Sigma \mid X_\pm f(p) < 0\}$, as illustrated in the Figure 1.3.

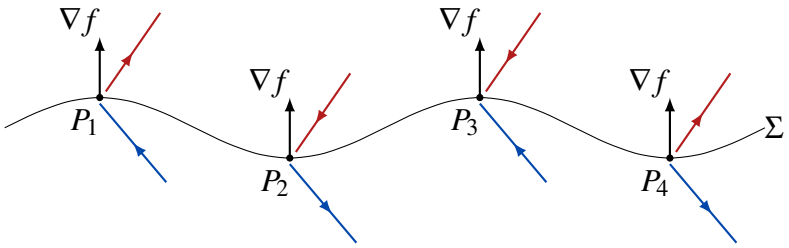

Figure 1.3: Dynamic behavior at points located in the Crossing, Sliding and Escaping region of the switching manifold Σ. In this representation, we have $P_1 \in \Sigma^{c+}$, $P_2 \in \Sigma^{c-}$, $P_3 \in \Sigma^s$, and $P_4 \in \Sigma^e$.

The complement of the union of these regions is the set consisting of the *tangency* points between $X_\pm$ and Σ, which we denote by $S_\pm$. In other words, a point $p \in \Sigma$ is called a *tangency point* of $X_\pm$ if it satisfies $X_\pm f(p) = 0$. A tangency point is called a *fold point* of $X_\pm$ if $X_\pm^2 f(p) \neq 0$. Moreover, $p \in \Sigma$ is a *visible* (resp. *invisible*) fold point of X_+ if $X_+^2 f(p) > 0$ (resp. $X_+^2 f(p) < 0$); analogously, $p \in \Sigma$ is a *visible* (resp. *invisible*) fold point of X_- if $X_-^2 f(p) < 0$ (resp. $X_-^2 f(p) > 0$). The vector fields $X_\pm$ have a cusp point at $p \in \Sigma$ if $X_\pm f(p) = 0, X_\pm^2 f(p) = 0$ and $X_\pm^3 f(p) \neq 0$ (see Figure 1.4).

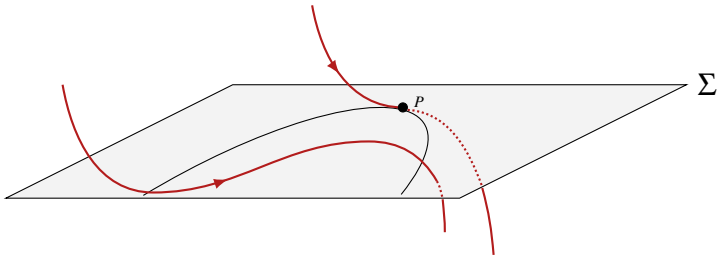

Figure 1.4: Representation of the tangency set S_+ filled with visible (respectively, invisible) fold points to the left (respectively, right) of the cusp point P. The remaining points are considered regular points.

Although Figures 1.4 and 1.3 are merely graphical representations, the visual concept established by them is essential for a proper understanding of the dynamics over Σ. To enhance our comprehension, let us examine a concrete example.

Example 2. *Consider the PSVF X*

$$X(x,y,z) = \begin{cases} X_+(x,y,z) = \begin{pmatrix} Sgn(\alpha)y \\ Sgn(\beta) \\ Sgn(\gamma)x \end{pmatrix}, & f(x,y,z) \geq 0 \\ X_-(x,y,z) = \begin{pmatrix} 0 \\ Sgn(\mu) \\ Sgn(\theta)y \end{pmatrix}, & f(x,y,z) \leq 0 \end{cases} \tag{1.11}$$

in $\mathbb{R}^3$*, where* $\alpha,\beta,\gamma,\mu,\theta \in \mathbb{R}\backslash\{0\}$ *and* $f(x,y,z) = z$*. A direct analysis shows that the Lie derivatives with respect to* X_+ *are given by:*

$$\begin{aligned} X_+f(x,y,z) &= Sgn(\gamma)x, \\ X_+^2f(x,y,z) &= Sgn(\alpha\gamma)y, \\ X_+^3f(x,y,z) &= Sgn(\alpha\beta\gamma). \end{aligned}$$

Since $X_+f(x,y,z) = 0$ *when* $x = 0$*, this indicates that* S_+ *corresponds to the y-axis. Furthermore, restricted to* S_+*,* $X_+^2f(x,y,z) = 0$ *only when* $y = 0$*. Given that* $X_+^3f(x,y,z) \neq 0$*, we conclude that the origin is a cusp point of* X_+*, dividing* S_+ *into two half-lines filled with fold points. Similarly, the Lie derivatives with respect to* X_- *are:*

$$\begin{aligned} X_-f(x,y,z) &= Sgn(\theta)y, \\ X_-^2f(x,y,z) &= Sgn(\mu\theta). \end{aligned}$$

Since $X_-f(x,y,z) = 0$ *when* $y = 0$*, this shows that* S_- *is the x-axis. Moreover,* $X_-^2f(x,y,z) \neq 0$ *on* S_-*, indicating that this region is entirely filled with fold points. It is worth noting that* $X_\pm f, X_\pm^2 f$*, and* $X_\pm^3 f$ *directly depend on the signs of the parameters* α,β,γ,μ*, and* θ*, which influence whether the fold points in* $S_\pm$ *are visible or invisible (see Figure 1.5).*

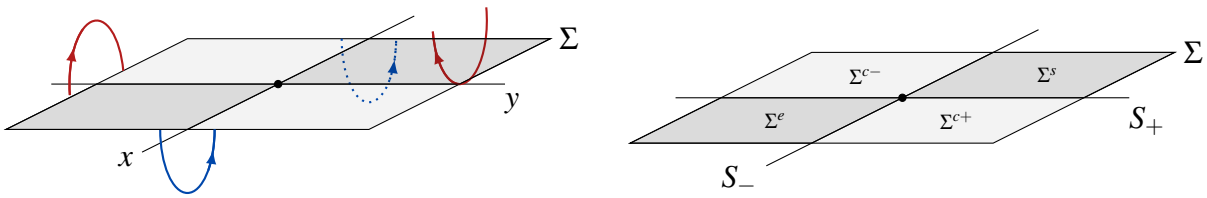

(a) Dynamic representation in Σ.

(b) Sets $S^\pm, \Sigma^{c\pm}, \Sigma^e$ and Σ^s.

Figure 1.5: Subsets of Σ and representation of the dynamics of the PSVF X presented in Equation (1.11) equipped with positive parameters. In this configuration, the x-axis is filled with invisible fold points of the vector field X_-. On the other hand, the y-axis is filled with invisible and visible fold points of the vector field X_+, respectively, to the left and right of the cusp point located at the origin.

Remark 1. *As we can observe, the origin in the previous system is actually a point of double tangency: it is a cusp for the vector field X_+ and a fold for X_-. Interestingly, this type of singularity, called Cusp-Fold, appears in various applied models, as exemplified in [3] and [8]. The PSVF presented in Equation* (1.11) *is explored in [4], where it provides* 32 *canonical forms for* 3*D piecewise smooth vector fields presenting the so called cusp-fold singularity. All these canonical forms are topologically distinct and collect the main topological aspects of the singularities described as kind of the tangencies involved and positions of the sliding, escaping and crossing regions.*

In order to define a trajectory of a PSVF passing through a crossing point, it is enough to concatenate the trajectories of X_+ and X_- through that point. However, in the sliding and escaping sets we need an auxiliary vector field, known as *Sliding vector field X^s* (see Figure 1.6), which is a convex linear combination of $X_+(p)$ and $X_-(p)$, given by:

$$X^s(p) = \alpha X_-(p) + (1-\alpha)X_+(p), \tag{1.12}$$

ensuring that X^s is tangent to Σ (see Figure 1.6). In other words, $\alpha \in [0,1]$ such that

$$\begin{aligned} & \langle \alpha X_-(p) + (1-\alpha)X_+(p), \nabla f(p)\rangle && = \quad 0 \\ \Rightarrow \quad & \alpha\left(\langle X_-(p), \nabla f(p)\rangle - \langle X_+(p), \nabla f(p)\rangle\right) && = -\langle X_+(p), \nabla f(p)\rangle. \end{aligned}$$

Therefore,

$$\alpha = \frac{-\langle X_+(p), \nabla f(p)\rangle}{\langle X_-(p), \nabla f(p)\rangle - \langle X_+(p), \nabla f(p)\rangle} = \frac{-X_+f(p)}{X_-f(p) - X_+f(p)}. \tag{1.13}$$

Using Equation (1.13), we can rewrite Equation (1.12) as follows:

$$X^s(p) = \frac{X_-f(p)X_+(p) - X_+f(p)X_-(p)}{X_-f(p) - X_+f(p)}, \tag{1.14}$$

for all $p \in \Sigma^s \cup \Sigma^e$. It is worth mentioning that X^s can be extended to $\partial(\Sigma^s \cup \Sigma^e)$ using the *normalized sliding vector field*

$$X^s_N(p) = X_-f(p)X_+(p) - X_+f(p)X_-(p). \tag{1.15}$$

In addition, an equilibrium of the sliding vector field is called pseudo-equilibrium. In this scenario the trajectories of X are considered as a concatenation of trajectories of X_+, X_- and X^s.

1.4 Sotomayor-Teixeira Regularization

The smoothing process of a piecewise smooth vector field X can be understood as the construction of a one-parameter family of smooth vector fields X^Φ_ε, which converges to X as the parameter ε

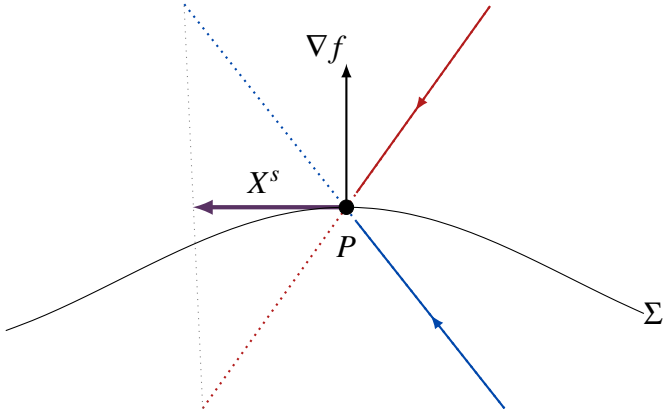

Figure 1.6: Representation of the Sliding vector field.

approaches zero. One of the widely used methods for this smoothing is the regularization proposed by Sotomayor and Teixeira in [31]. This approach approximates X by a family of smooth vector fields that coincides with the original field outside a band around the switching manifold Σ. By applying classical tools to the regularized system, it becomes possible to extract information about the behavior of the original field as the regularization parameter decreases.

The Sotomayor-Teixeira regularization is widely recognized in the literature, particularly due to its strong connection with Filippov's convention. In [32], it was shown that this regularization leads to singular perturbation problems, where the reduced dynamics is conjugated to the sliding dynamics.

To formalize this process, consider a function $\phi : \mathbb{R} \to \mathbb{R}$ of class C^∞ that satisfies $\phi(\pm 1) = \pm 1$, $\phi^{(i)}(\pm 1) = 0$ for $i = 1, 2, \ldots, n$, and $\phi'(s) > 0$ for $s \in (-1, 1)$. In this context, a C^n-Sotomayor-Teixeira regularization is given by the regularized vector field $X_\varepsilon^\Phi(p)$ as follows:

$$X_\varepsilon^\Phi(p) = \frac{1 + \Phi_\varepsilon(f(p))}{2} X_+(p) + \frac{1 - \Phi_\varepsilon(f(p))}{2} X_-(p),$$

where $\Phi_\varepsilon(f(p)) = \Phi(f(p)/\varepsilon)$, and the function $\Phi : \mathbb{R} \to \mathbb{R}$, of class C^n, is defined as:

$$\Phi(s) = \begin{cases} \phi(s) & \text{if } |s| \leq 1, \\ \text{sign}(s) & \text{if } |s| > 1. \end{cases} \tag{1.16}$$

Example 3. *Let us consider the function Φ defined as in Equation (1.16), with $\phi(t) = -\frac{1}{2}t^3 + \frac{3}{2}t$, whose graph is shown in Figure 1.8a. Through a direct analysis, we can observe that ϕ is of class C^∞ and satisfies the conditions $\phi(\pm 1) = \pm 1$, $\phi'(\pm 1) = 0$, and $\phi'(s) > 0$ for $s \in (-1, 1)$. Thus, the X_ε^Φ regularization of*

$$X(x,y) = \begin{cases} X_+(x,y) = \begin{pmatrix} 1 \\ 1 \end{pmatrix}, & y \geq 0 \\ X_-(x,y) = \begin{pmatrix} 0 \\ 1 \end{pmatrix}, & y \leq 0 \end{cases} \tag{1.17}$$

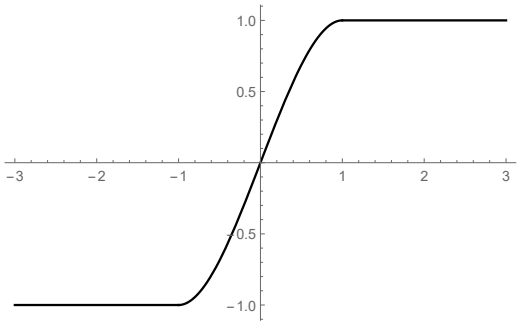

Figure 1.7: Graph of the Transition Function Φ.

is given by:

$$X_\varepsilon^\Phi(x,y) = \frac{1+\Phi(\frac{y}{\varepsilon})}{2}\begin{pmatrix}1\\1\end{pmatrix} + \frac{1-\Phi(\frac{y}{\varepsilon})}{2}\begin{pmatrix}0\\1\end{pmatrix}. \tag{1.18}$$

Thus, for $y \in (-\varepsilon,\varepsilon)$, X_ε^Φ can be expressed as

$$X_\varepsilon^\Phi(x,y) = \begin{pmatrix} -\frac{y^3}{4\varepsilon^3} + \frac{3y}{4\varepsilon} + \frac{1}{2} \\ 1 \end{pmatrix}.$$

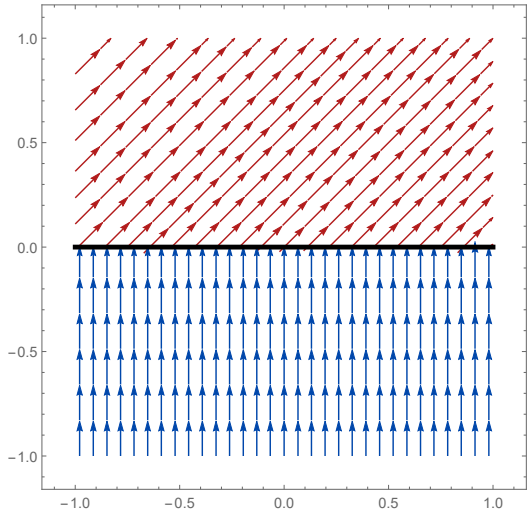

(a) The dynamics of X.

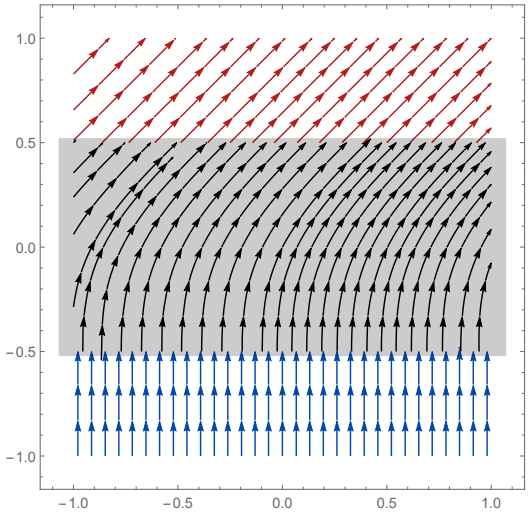

(b) The dynamics of X_ε^Φ.

Figure 1.8: The dynamics of the ε-regularization X_ε^Φ is influenced by the transition function Φ and the regularization parameter ε. As ε approaches zero, X_ε^Φ converges to X within the strip $\Sigma \times (-\varepsilon,\varepsilon)$, while remaining identical to X outside of this strip. The Figure 1.8b uses $\varepsilon = \frac{1}{2}$ for purely illustrative purposes.

Thus, Φ acts as a C^n-monotonic transition function. In regions away from Σ, $X_\varepsilon^\Phi(p)$ aligns with $X_+(p)$ or $X_-(p)$, depending on whether $f(p)$ is greater or smaller than ε. Within the band where $|f(p)| \leq \varepsilon$, the regularized field becomes a linear combination of both fields, smoothing the transition. This behavior can be observed in Figure 1.8 corresponding to Example 3. For a more in-depth analysis of this topic, the reference [27] is recommended.

CHAPTER 2

The blow-up method for fast-slow systems

In Section 1.1, we introduced the blow-up method using the coordinate change

$$(x,y) = (r\cos(\theta), r\,\mathrm{sen}(\theta)), \tag{2.1}$$

known as polar blow-up. However, this is not the only approach to handle non-hyperbolic equilibrium points. In this chapter, we will explore in more detail weighted directional and polar blow-ups in the context of fast-slow systems.

2.1 Generating a fast-slow system through the regularization of a PSVF

To initiate the process, we introduce a fast-slow system obtained by regularizing a PSVF. For this purpose, consider the PSVF X, as specified in Equation 1.10, in the case where $n = 2$ and the function defining the switching manifold is $h(x,y) = x$. This setup allows for a detailed analysis of how the system smoothly transitions between distinct dynamics, incorporating an interaction between fast and slow time scales - an essential feature of fast-slow systems.

As defined in Section 1.4, it is possible to describe the ε-regularization of X as:

$$X_\varepsilon^\Phi(x,y) = \frac{1+\Phi_\varepsilon(h(x,y))}{2}X_+(x,y) + \frac{1-\Phi_\varepsilon(h(x,y))}{2}X_-(x,y). \tag{2.2}$$

Thus, denoting the coordinate functions of $X_\pm(x,y)$ as $X_\pm^1(x,y)$ and $X_\pm^2(x,y)$, the differential system associated with X_ε^Φ can be described as:

$$\begin{cases} \dot{x} &= \frac{X_+^1(x,y)+X_-^1(x,y)}{2} + \frac{X_+^1(x,y)-X_-^1(x,y)}{2}\Phi\left(\frac{x}{\varepsilon}\right), \\ \dot{y} &= \frac{X_+^2(x,y)+X_-^2(x,y)}{2} + \frac{X_+^2(x,y)-X_-^2(x,y)}{2}\Phi\left(\frac{x}{\varepsilon}\right). \end{cases} \tag{2.3}$$

Now, through the change of variables $x := \bar{x}\varepsilon$, the previous system can be rewritten as:

$$\begin{cases} \varepsilon\dot{\bar{x}} &= \frac{X_+^1(\bar{x}\varepsilon,y)+X_-^1(\bar{x}\varepsilon,y)}{2} + \frac{X_+^1(\bar{x}\varepsilon,y)-X_-^1(\bar{x}\varepsilon,y)}{2}\Phi(\bar{x}) := f(\bar{x},y,\varepsilon), \\ \dot{y} &= \frac{X_+^2(\bar{x}\varepsilon,y)+X_-^2(\bar{x}\varepsilon,y)}{2} + \frac{X_+^2(\bar{x}\varepsilon,y)-X_-^2(\bar{x}\varepsilon,y)}{2}\Phi(\bar{x}) := g(\bar{x},y,\varepsilon). \end{cases} \tag{2.4}$$

Finally, we can perform the time rescaling as described in Section 1.2 to obtain the rescaled system:

$$\begin{cases} \bar{x}' &= f(\bar{x},y,\varepsilon) \\ y' &= \varepsilon g(\bar{x},y,\varepsilon) \end{cases}. \tag{2.5}$$

The obtained system exactly matches the standard form of fast-slow systems presented in Chapter 1. In Section 3.2, we will see a practical example of this construction, where we obtain a fast-slow system by regularizing a PSVF containing a saddle-node singularity.

2.2 Blow-up method for perturbed singular problems

For a better understanding of the relation between the blow-up method and fast-slow systems, we will start by reformulating the $\varepsilon-$family of vector fields, as presented in Equation (2.5), as a single vector field in $\mathbb{R}^3$ in the following form:

$$\begin{cases} x' &= f(x,y,\varepsilon) \\ y' &= \varepsilon g(x,y,\varepsilon) \\ \varepsilon' &= 0 \end{cases}. \tag{2.6}$$

System (2.6) is refered to as *extended vector field* (see [12]). Observe that the dynamics of System (2.5) is precisely the dynamics of (2.6) in invariant planes of the form $\{\varepsilon = \varepsilon_0\}$.

Furthermore, let us assume that the origin $(x,y,\varepsilon) = (0,0,0)$ is a non-normally hyperbolic point of the critical manifold, that is, it satisfies $f(0,0,0) = 0$ and $\frac{\partial f}{\partial x}(0,0,0) = 0$ (see Definition 2). The blow-up method can be adapted to desingularize the origin of the system presented in Equation (2.6).

Definition 4. *Let F be an analytic vector field defined in $\mathbb{R}^n$ such that $F(0) = 0$ and is described by Equation* (2.6)*. Consider the generalized polar transformation $\varphi : \mathbb{S}^{n-1} \times I \to \mathbb{R}^n$ defined by:*

$$\varphi(\bar{z}_1,\cdots,\bar{z}_n,r) = (r^{a_1}\bar{z}_1,\cdots,r^{a_n}\bar{z}_n), \tag{2.7}$$

where I is a real interval containing the origin, $a_i \in \mathbb{N}$ for $i \in \{1,\cdots,n\}$ and $\sum_{i=1}^{n} \bar{z}_i^2 = 1$. The ***weighted polar blow-up*** *of the vector field F, denoted as $\hat{F}$, is defined by*

$$\hat{F} = D\varphi^{-1}_{(\bar{z}_1,\cdots,\bar{z}_n,r)} \circ F \circ \varphi(\bar{z}_1,\cdots,\bar{z}_n,r) \tag{2.8}$$

for $r \neq 0$ and by the continuous extension of (2.8) *to $r = 0$. Suppose that $j_k(F) = 0$ and $j_{k+1}(F) \neq 0$, where $j_k(F)$ denote the k-jet of F at the origin, define the* ***(desingularized) weighted polar blow-up*** *by $\bar{F} = \frac{1}{r^k}\hat{F}$.*

Remark 2. *There is no standard terminology to distinguish between the vector fields $\hat{F}$ and $\bar{F}$ mentioned in the previous definition. For example, in [23], the term "desingularized" is replaced by "rescaled" to emphasize that multiplying F by $\frac{1}{r^k}$ (or rescaling) does not alter the qualitative structure of the vector field near the singularity at $r = 0$. This rescaling (or desingularization) is essential for the analysis of the blow-up system, as we will see in Subsection 3.3.2.*

We can observe that the function φ maps the sphere $B_0 := \mathbb{S}^{n-1} \times \{0\}$ to the origin in $\mathbb{R}^n$, while the inverse function φ^{-1} maps the point $0 \in \mathbb{R}^n$ to B_0. This characteristic suggests that the operation φ^{-1} can be called *blow-up*, while φ is called *blow-down*. The sets B_0 and $\{0\}$ are called *exceptional divisor* and *blow-up center*, respectively. The term "weighted" reflects the fact that the exponents that appear in (2.7) are not necessarily equal. However, when all exponents a_i are equal to 1, we can omit the term "weighted".

Thus, to understand the behavior of solutions near the origin of System (2.6), it is essential to examine the singular points on the exceptional divisor B_0. Some of these singular points may still remain degenerate. In such cases, it is necessary to investigate them through multiple blow-up operations.

Remark 3. *If a vector field F on $\mathbb{R}^n$ with $F(0) = 0$ satisfies the Lojasiewicz inequality, that is, there exist $k \in \mathbb{N}$ and $c > 0$ such that*

$$||F(z)|| \geq c||z||^k,$$

in some neighborhood of 0, then it is possible to understand the behavior of the solutions of F near the origin using a finite number of blow-ups. The interesting thing is that a vast number of vector fields comply with this inequality, which highlights the efficiency of the blow-up method. For example, analytical vector fields always obey a Lojasiewicz inequality at an isolated singularity. For more details, consult [9], [10] and [11].

When dealing with a dimension n greater than two, the use of polar coordinates can become a somewhat complicated task. To overcome this problem, we can use directional charts that cover the exceptional divisor (see Figure 2.1). In each of these charts, we define coordinates and a corresponding vector field that, in turn, induce vector fields in the euclidean space (see [19]). Once the analysis of the relevant projected vector fields is performed, it is possible to overlap suitable regions of the charts and match the flow on such charts via transition maps, and thus describe the dynamics all around the sphere $\mathbb{S}^{n-1}$.

As mentioned in [17], in practice, what we do to define coordinates in a chart is to fix one of the blow-up coordinates to ± 1. This approach is known as directional blow-up, which will be formalized through the next two definitions.

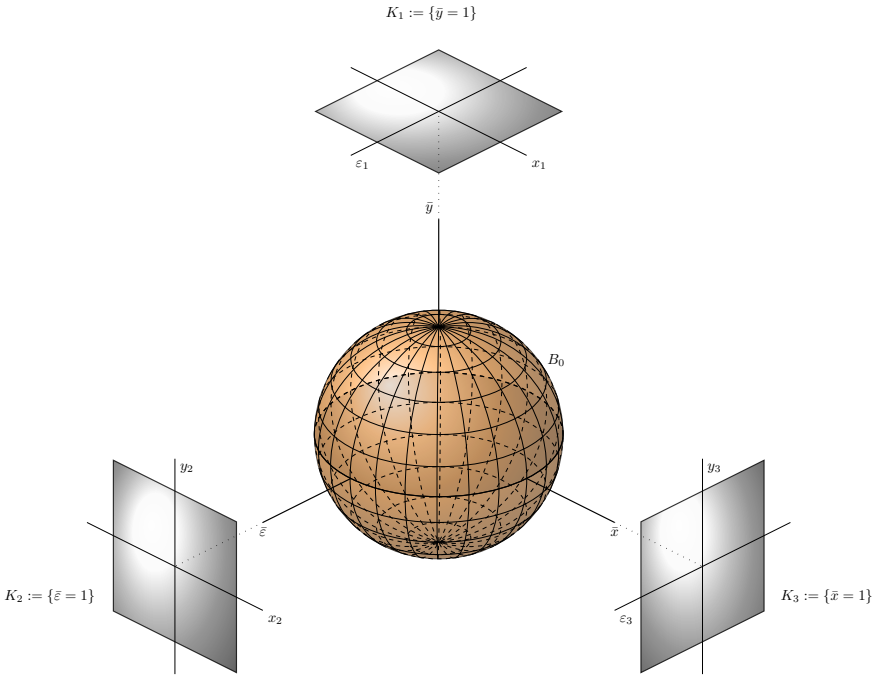

Figure 2.1: Charts for B_0.

Definition 5. *Let F be an analytic vector field defined in $\mathbb{R}^n$ such that $F(0) = 0, DF(0) = 0$ and, described by Equation* (2.6)*. Consider the directional blow-up map in the $i-$direction $\varphi_i : \mathbb{S}^{n-1} \times I \to \mathbb{R}^n$:*

$$\varphi_i(\bar{z}_1, \cdots, \bar{z}_n, r) = (r^{a_1}\bar{z}_1\bar{z}_i, \cdots, r^{a_{i-1}}\bar{z}_{i-1}\bar{z}_i, r^{a_i}\bar{z}_i, r^{a_{i+1}}\bar{z}_{i+1}\bar{z}_i, \cdots, r^{a_n}\bar{z}_n\bar{z}_i)$$

*where I is a real interval containing the origin, $a_i \in \mathbb{N}$ for $i \in \{1, \cdots, n\}$ and $\sum_{i=1}^{n} \bar{z}_i^2 = 1$. The **weighted directional blow-up** of the vector field F, denoted as $\hat{F}$, is defined by*

$$\hat{F} = D\varphi_i^{-1}{}_{(\bar{z}_1, \cdots, \bar{z}_n, r)} \circ F \circ \varphi_i(\bar{z}_1, \cdots, \bar{z}_n, r) \tag{2.9}$$

for $r \neq 0$ and by the continuous extension of (2.9) *to $r = 0$. Suppose that $j_k(F) = 0$ and $j_{k+1}(F) \neq 0$, where $j_k(F)$ denote the k-jet of F at the origin, define the **(desingularized) weighted directional blow-up** by $\bar{F} = \frac{1}{r^k}\hat{F}$.*

Definition 6. *Consider the setup of the previous definition. Let $k_a : \mathbb{S}^{n-1} \times I \to \mathbb{R}^n$ be a chart and use $\mu_a : \mathbb{R}^n \to \mathbb{R}^n$ to denote the blowup/coordinate change induced by the following commutative diagram:*

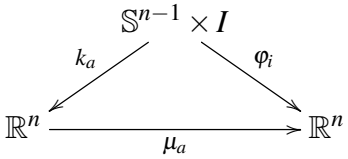

If K_a is a suitably chosen (weighted) affine chart for the ith coordinate given by

$$(\bar{z}_1,\cdots,\bar{z}_n,r)\mapsto\left(\frac{\bar{z}_1}{\bar{z}_i^{b_1}},\cdots,\frac{\bar{z}_{i-1}}{\bar{z}_i^{b_{i-1}}},\frac{\bar{z}_{i+1}}{\bar{z}_i^{b_{i+1}}},\cdots,\frac{\bar{z}_n}{\bar{z}_i^{b_n}},r\right)$$

then one may write the map μ_a as

$$\mu_a(w_1,\cdots,w_n,r):=(r^{a_1}w_1,\cdots,r^{a_{i-1}}w_{i-1},r^{a_i},r^{a_{i+1}}w_{i+1},\cdots,r^{a_n}w_n)$$

where $w=(w_1,\cdots,w_n)^\top\in\mathbb{R}^n$ denotes coordinates for the domain of μ_a and the range of k_a, i.e., for the space $\mathbb{R}^n$ in the lower left-hand corner of the diagram above. We also call μ_a the weighted directional blow-up in the direction i, since it is a local coordinate expression for the weighted directional blow-up given in Definition 5.

By integrating the expansion method with coordinate charts in the resulting space $\mathbb{S}^{n-1}\times I$, we can simplify the calculations required for weighted blow-ups, which are commonly represented by a mapping function from $\mathbb{S}^{n-1}\times I$ to $\mathbb{R}^n$. This approach reduces the problem to a coordinate transformation in $\mathbb{R}^n$, which will be explored in Chapter 3 and can be schematically visualized in Figure 2.2.

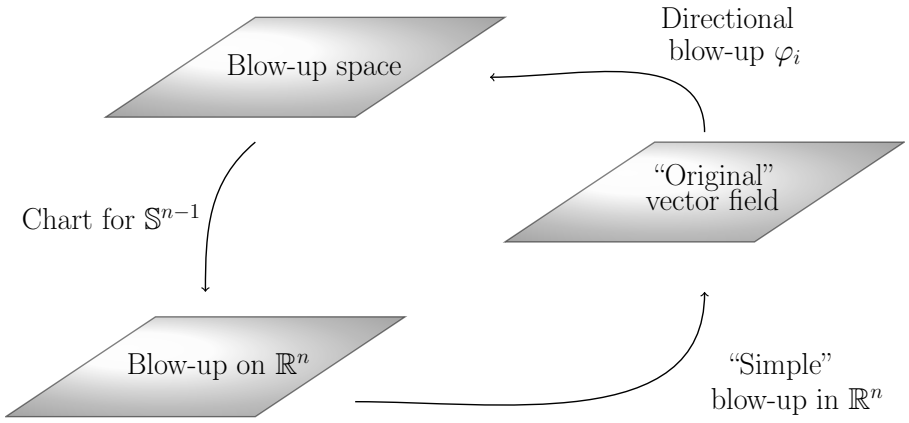

Figure 2.2: Blow-up method.

The blow-up method was first used in the study of fast-slow systems in the paper [12], which is a landmark in the investigation of the so-called "canard solutions". For a deeper understanding and examples illustrating the definitions surrounding the expansion method presented in this chapter, we recommend [17] and Chapter 7 of [23].

2.3 Choosing weights for the blow-up

In the previous section, we presented the Blow-up method through Definitions 4, 5, and 6. Although this method offers a computable approach to desingularization, it requires considerable effort,

making the appropriate selection of weights fundamental for its application. The challenge lies in the fact that the choice of weights is not always evident, and this decision directly impacts the computational effort needed to analyze the problem. Due to its relevance, this section is dedicated to exploring how to select the weights for the blow-up process in an objective and well-founded manner.

2.3.1 Quasi-homogeneous vector fields

To illustrate the influence of an appropriate choice of weights in the blow-up process and to motivate the definitions that will be presented next, we will start with an example.

Example 4. *Consider the following differential system:*

$$\begin{cases} \dot{x} &= y &= F_1(x,y), \\ \dot{y} &= -x^2 &= F_2(x,y). \end{cases} \tag{2.10}$$

Note that $F(0,0) = 0$ and that $DF(0,0)$ has two zero eigenvalues. Through a direct calculation, we obtain that the polar blow-up (see Definition 4) of the vector field $F = (F_1, F_2)$ associated with the map $\varphi(\theta, r) = (r\cos\theta, r\,\mathrm{sen}\,\theta)$ is given by:

$$\overline{F} = \hat{F}(\theta, r) = \left(r\cos^3(\theta) - \mathrm{sen}^2(\theta), \frac{r\cos(\theta)\mathrm{sen}(\theta)}{1 + r\cos(\theta)} \right)^\top,$$

which has two equilibrium points given by $p_1 = (0,0)$ and $p_2 = (\pi, 0)$. Both points are non-hyperbolic, with their respective linearizations $D\overline{F}_{p_i}$ having two zero eigenvalues. In this scenario, we would need to apply another blow-up to desingularize the system. Instead, let us modify the polar blow-up map and define:

$$\varphi(\theta, r) := (r^2\cos(\theta), r^3\mathrm{sen}(\theta)). \tag{2.11}$$

With this modification and another exercise in calculation, we obtain the vector field:

$$\overline{F} = \frac{1}{r}\hat{F}(\theta, r) = \left(\frac{6\mathrm{sen}^2(\theta) - 4\cos^3(\theta)}{\cos(2\theta) - 5}, -\frac{2r\cos(\theta)\mathrm{sen}(\theta)(1 + \cos(\theta))}{\cos(2\theta) - 5} \right). \tag{2.12}$$

Through another exercise in calculation, we can observe that now $\overline{F}$ has two equilibrium points $p_1 \approx (0.63, 0)$ and $p_2 \approx (-0.63, 0)$, given in polar coordinates in the blow-up space, which are found to be hyperbolic saddles. Therefore, F has been desingularized in just one step. The phase portrait of $\overline{F}$ presented in Equation (2.12) *is represented in Figure 2.3.*

As we anticipated, the previous example demonstrates the importance of a careful selection of the weights involved in the blow-up process. Next, we will see that the vector field F present in Example 4 belongs to a class of vector fields known as quasi-homogeneous vector fields. Interestingly,

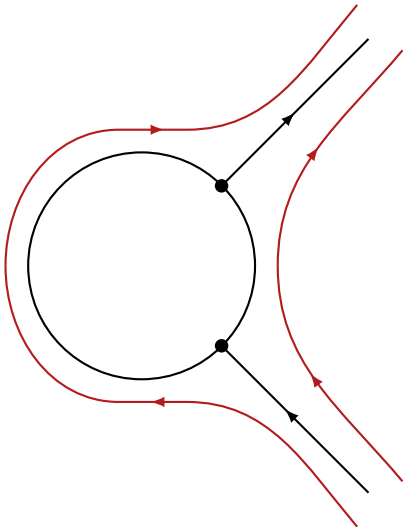

Figure 2.3: Representation of the phase portrait of the System (2.12) obtained by the blow-up of (2.10) around the origin.

the weights assigned in the blow-up method for such functions can be obtained through a direct calculation, considerably simplifying the application of the method.

Before further exploring Example 4 and understanding how the choice of weights occurs, it is useful to introduce some additional concepts to explain how the map φ described in Equation (2.11) is chosen.

Definition 7. *A function $f:\mathbb{R}^n\to\mathbb{R}$ is called quasi-homogeneous of type $(a_1,\cdots,a_n)\in\mathbb{N}^n$ and degree k if, for all $r\in\mathbb{R}$,*

$$f(r^{a_1}x_1,...,r^{a_n}x_n)=r^k f(x_1,...,x_n).$$

A vector field F is considered quasi-homogeneous of type $(a_1,\cdots,a_n)$ and degree $k+1$ if all its $j-th$ components $F_j(x_1,\cdots,x_n)$ are quasi-homogeneous of type $(a_1,\cdots,a_n)$ and degree $k+a_j$.

Based on this definition, let us revisit Example 4 considering the vector field $F(x,y)=(y,x^2)^T$. Writing the conditions for quasi-homogeneity, we obtain:

$$F_1(r^{a_1}x,r^{a_2}y)=r^{a_2}y=r^{k+a_1}y=r^{k+a_1}F_1(x,y),$$

$$F_2(r^{a_1}x,r^{a_2}y)=r^{2a_1}x^2=r^{k+a_2}x^2=r^{k+a_2}F_2(x,y).$$

Solving the previous equations, we obtain $3a_1=2a_2$. By selecting a_1 and a_2 with the smallest possible values, we find that F is quasi-homogeneous of type $(2,3)$ and degree 2. This special property of F explains why $\varphi(\theta,r)=(r^2\cos\theta,r^3\text{sen}\theta)$ is an appropriate choice for the blow-up map presented in Example 4.

2.3.2 Determination of blow-up weights via newton polyhedron

In Subsection 2.3.1, we highlight how the blow-up method significantly simplifies if we consider a quasi-homogeneous vector field. Interestingly, even in the absence of such quasi-homogeneity (as illustrated in Example 7), we can resort to weights to facilitate the blow-up process, focusing exclusively on the quasi-homogeneous components. For more information, refer to [1], [11], and Chapter 12 of [23]. This approach establishes a direct connection between the Newton polygon and the blow-up method, as the Newton polygon leads us to identify the quasi-homogeneous components.

A comprehensive analysis of Newton polygon techniques exceeds the scope of this text. Therefore, in this subsection, we will begin with the fundamental definitions related to the Newton polyhedron and then present a practical approach for determining the weights needed in the blow-up method.

2.3.2.1 Newton polygon

Consider the set $\mathfrak{D} \subset \mathbb{Z}^2$, where $\mathbb{Z}^2$ denotes the lattice of integer numbers. Although the literature does not provide an unanimous definition for the Newton polygon associated with $\mathfrak{D}$ (as discussed in [23]), it is essential to recognize that the convex hull, $\text{conv}(\mathfrak{D})$, is the smallest convex set in $\mathbb{R}^2$ that completely contains $\mathfrak{D}$. This understanding is fundamental before we proceed to the three proposed definitions for the Newton polygon.

Definition 8. *The Newton polygon Γ associated with $\mathfrak{D}$ can be defined in three distinct ways:*

(N_1) *Just the convex hull of $\mathfrak{D}$.*

(N_2) *The convex hull of $\mathfrak{D} \oplus \mathbb{Z}^2_+$, where $\oplus$ denotes the Minkowski sum[1] of two sets and $\mathbb{Z}^2_+$ denotes the lattice of non-negative integers.*

(N_3) *The convex hull of $\mathfrak{D} \cup \{(0,k),(k,0)\} \oplus \mathbb{Z}^2_+$, where $k := \max\{q_1+q_2 \mid (q_1,q_2) \in \mathfrak{D}\}$.*

Before we proceed, let's understand the differences between $(N_1)-(N_3)$ through a simple and purely illustrative example.

Example 5. *Consider the set $\mathfrak{D}$ defined as follows:*

$$\mathfrak{D} := \{(2,0),(1,1),(1,2),(3,1)\}.$$

The graphical representations for the Newton polygon in each of the versions presented in Definition 8 are described in Figure 2.4. It is evident that each definition leads to a different result. However,

[1] The Minkowski sum of sets A and B is defined as the set of all possible sums of an element from A with an element from B.

it is important to note that all forms of the Newton polygon Γ *presented in Example 5 share the edge connecting* $(2,0)$ *to* $(1,1)$ *on their boundary.*

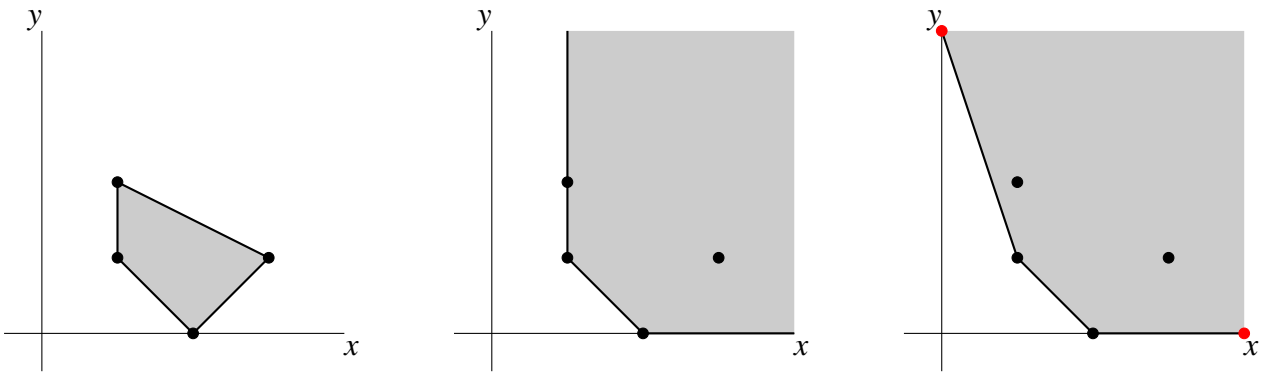

(a) Γ with respect to (N_1). (b) Γ with respect to (N_2). (c) Γ with respect to (N_3).

Figure 2.4: The polygonal figure $conv(\mathfrak{D})$, shown in Figure 2.4a, represents the Newton polygon regarding version (N_1). In Figure 2.4b, we have the visualization of definition (N_2), where the Minkowski addition with $\mathbb{Z}^2_+$ results in a Newton polygon without defined boundaries. In Figure 2.4c, we highlight definition (N_3), in which the calculation of $k=4$ is obtained by summing the components of the vector $(3,1)$, promoting the construction of the points $(4,0)$ and $(0,4)$, highlighted in red.

To facilitate understanding and structure what we are going to present, we will introduce some additional notations. Considering j varying over $\{1,2,\ldots,n\}$, we define $\Gamma^{(0)}_j$ as the vertices of the Newton polygon that lie on $\partial\Gamma$, and $\Gamma_{j_1 j_2}$ as the finite edges on $\partial\Gamma$ connecting the vertices $\Gamma^{(0)}_{j_1}$ and $\Gamma^{(0)}_{j_2}$. To simplify notation, we will denote the segment between $\Gamma^{(0)}_i$ and $\Gamma^{(0)}_{i+1}$ simply as Γ_i.

The Newton polygon arises as an essential tool in the search for the local roots of an analytic function $f:\mathbb{R}^2\to\mathbb{R}$, as described in Chapter 12 of [23]. By focusing on solutions near the origin $(x,y)=(0,0)$, we can use the Taylor expansion:

$$f(x,y)=\sum_{q_1,q_2\geq 0} f_{q_1q_2}x^{q_1}y^{q_2}, \tag{2.13}$$

which converges absolutely on a set $U=\{(x,y)\in\mathbb{R}^2 : |x|<\delta, |y|<\delta\}$ for some $\delta>0$. The Newton polygon $\Gamma(f)$, associated with f, is constructed from the set:

$$\mathfrak{D}=\left\{(q_1,q_2)\in\mathbb{Z}^2 : f_{q_1q_2}\neq 0\right\}.$$

Definition 9. *Let* $\Gamma_{j_1j_2}$ *be an edge in the Newton polygon with vertices*

$$\Gamma^{(0)}_{j_1}=(q_{11},q_{12}) \qquad \textit{and} \qquad \Gamma^{(0)}_{j_2}=(q_{21},q_{22}).$$

Then we define the truncation $\hat{f}$ *of* (2.13) *with respect to* $\Gamma_{j_1j_2}$ *by*

$$\hat{f}(x,y):=f_{q_{11}q_{12}}x^{q_{11}}y^{q_{12}}+f_{q_{21}q_{22}}x^{q_{21}}y^{q_{22}}.$$

Although Definitions 8 and 9 may initially seem disconnected from the earlier chapters of this text, the upcoming subsections will explore their relevance in the application of the blow-up method. Before that, we can introduce the Newton polygon within the context of fast-slow systems, as illustrated in the following example.

Example 6. *Consider the fast-slow system given by:*

$$\begin{aligned} \varepsilon \dot{x} &= x^3 + y^3 - 2xy, \\ \dot{y} &= g(x,y). \end{aligned} \tag{2.14}$$

Note that the critical manifold C_0 can be characterized by

$$C_0 = \{(x,y) \in \mathbb{R}^2 : x^3 + y^3 - 2xy = 0\},$$

whose graphical representation is presented in Figure 2.5a. The presence of a self-intersection in

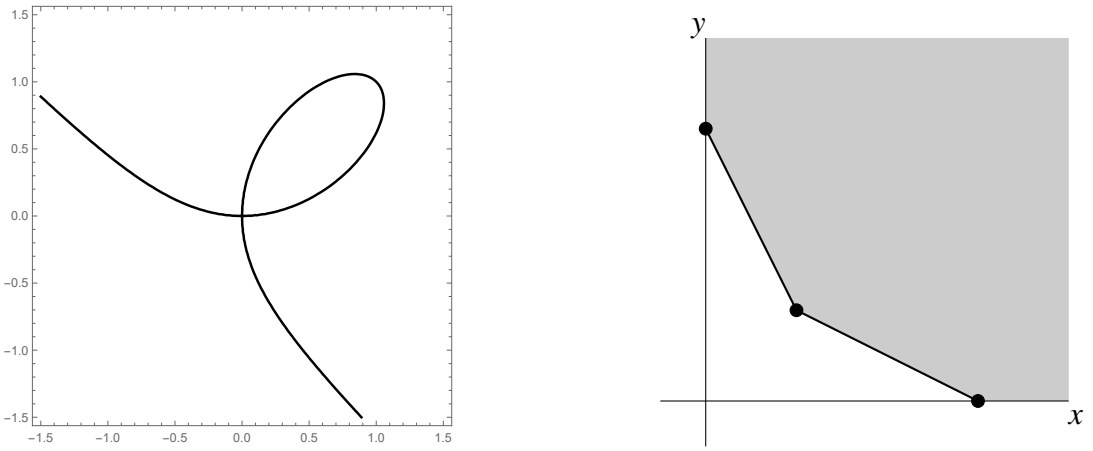

(a) Critical manifold C_0.

(b) Newton polygon associated with $f(x,y)$.

Figure 2.5: Visualization of the critical manifold C_0, defined as the set of solutions of the equation $f(x,y) = x^3 + y^3 - 2xy = 0$ for the Fast-slow system (2.14), along with the Newton polygon Γ associated with the function $f(x,y)$.

C_0 poses a significant challenge in the analysis of the System (2.14)*, as we do not have a clear local description of the critical manifold C_0 in the vicinity of the origin. In Chapter 12 of [23], an analysis of C_0 is found using the Newton polyhedron as a tool to investigate this critical manifold. In this example, we limit ourselves to determining the Newton polyhedron Γ for the map $f(x,y) = x^3 + y^3 - 2xy$, as illustrated in Figure 2.5a. We observe that versions (N_2) and (N_3) of Definition 8 coincide in this example, since*

$$\mathfrak{D} = \{(q_1,q_2) \in \mathbb{Z}^2 : f_{q_1 q_2} \neq 0\} = \{(3,0),(1,1),(0,3)\}.$$

Remark 4. *Note that C_0 cannot be considered a manifold due to its self-intersection at the origin. Therefore, the previous example not only demonstrates the process of obtaining the Newton polygon*

associated with the function $f(x,y) = x^3 + y^3 - 2xy$, but also highlights the improper use of notation, as mentioned in Section 1.2, where by convention we refer to the set C_0 as a manifold. Despite this obvious abuse of notation, we will continue to follow this convention.

2.3.2.2 Newton polygon of differential systems

In Subsection 2.3.2.1, we addressed the definition of the Newton polygon for analytic functions. In this section, we will expand this approach to include vector fields and understand how these structures can be related to the blow-up method.

Consider the planar vector field represented by:

$$\begin{cases} x' = F_1(x,y), \\ y' = F_2(x,y). \end{cases} \tag{2.15}$$

Suppose that $(x,y) = (0,0)$ is an equilibrium point, and that $F = (F_1, F_2)$ is analytic, with $F_1(x,y)$ and $F_2(x,y)$ expressed as power series:

$$F_1(x,y) = \sum_{q_x,q_y \geq 0} F^{(1)}_{q_x,q_y} x^{q_x} y^{q_y}, \qquad F_2(x,y) = \sum_{q_x,q_y \geq 0} F^{(2)}_{q_x,q_y} x^{q_x} y^{q_y}.$$

Similarly to what we explored in Subsection 2.3.2.1, we can use Definition 8 to establish that the Newton polygon $\Gamma(F)$ corresponding to the vector field F, associated with the differential system (2.15), is constructed from the set:

$$\mathfrak{D}(F) := \left\{ (q_x - 1, q_y) \in \mathbb{Z}^2 : F^{(1)}_{q_x,q_y} \neq 0 \right\} \cup \left\{ (q_x, q_y - 1) \in \mathbb{Z}^2 : F^{(2)}_{q_x,q_y} \neq 0 \right\}. \tag{2.16}$$

Note that the point $(-1, q_y)$ is associated with the monomial $F^{(1)}_{0,q_y} y^{q_y}$, the point $(q_x, -1)$ is associated with the monomial $F^{(2)}_{q_x,0} x^{q_x}$, and in general, the point (i,j) is associated with the leading terms $F^{(1)}_{i+1,j} x^{i+1} y^j$ and $F^{(2)}_{i,j+1} x^i y^{j+1}$. It us worth noting that $(0,0)$ is associated with the monomials $F_{1,10}x$ and $F_{2,01}y$, consequently if the origin of System (2.15) is degenerate, then $(0,0) \notin \mathfrak{D}$.

Example 7. *Consider the vector field*

$$\begin{cases} x' &= xy + y^2 &= F_1(x,y), \\ y' &= x^4 &= F_2(x,y). \end{cases} \tag{2.17}$$

It is relatively easy to find the Newton polygon (see Figure 2.6) since

$$\mathfrak{D}(F) = \{\Gamma^{(0)}_0 = (-1,2), \Gamma^{(0)}_1 = (0,1), \Gamma^{(2)}_3 = (4,-1)\}.$$

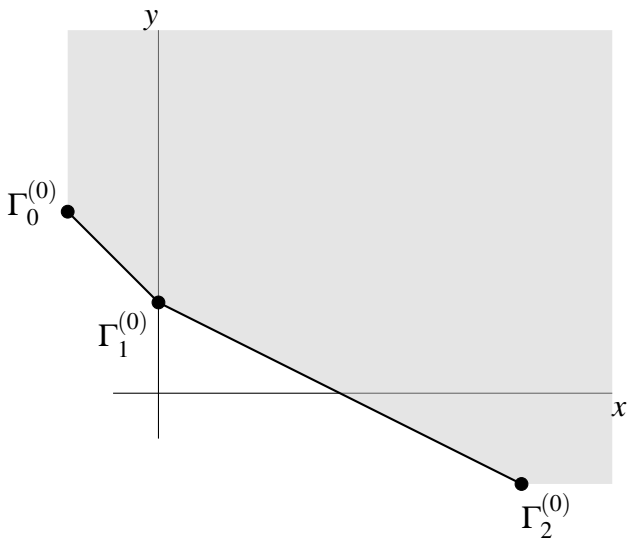

Figure 2.6: Newton polygon associated with the differential system (2.17).

Note that the vector field $F = (F_1, F_2)$ associated with the System (2.17) in the previous example is not quasi-homogeneous of type (α, β) and degree k according to Definition 7; this can be verified by direct calculation, as the quasi-homogeneity conditions

$$\begin{aligned} r^{\alpha+\beta}xy + r^{2\beta}y^2 = F_1(r^\alpha x, r^\beta y) &\stackrel{!}{=} r^{\alpha+k}F_1(x,y) = r^{\alpha+k}(xy+y^2), \\ r^{4\alpha}x^4 = F_2(r^\alpha x, r^\beta y) &\stackrel{!}{=} r^{\beta+k}F_2(x,y) = r^{\beta+k}x^4, \end{aligned} \tag{2.18}$$

would imply $\alpha = \beta$ and also $2\alpha = \beta$, which is a contradiction. However, if we consider truncation with respect to Γ_1 (see Definition 9), we find that $\hat{F}(x,y) = (xy, x^4)^T$ is quasi-homogeneous of type $(1,2)$ and degree 3, since the quasi-homogeneity conditions would be satisfied

$$\begin{aligned} r^{\alpha+\beta}xy = \hat{F}_1(r^\alpha x, r^\beta y) &= r^{\alpha+k}\hat{F}_1(x,y) = r^{\alpha+k}xy, \\ r^{4\alpha}x^4 = F_2(r^\alpha x, r^\beta y) &= r^{\beta+k}F_2(x,y) = r^{\beta+k}x^4, \end{aligned} \tag{2.19}$$

result in $2\alpha = \beta = k$. Selecting α and β as the smallest possible values, we find that F is quasi-homogeneous of type $(1,2)$ and degree 3. This happens because the Newton polygon can be used as a tool to obtain quasi-homogeneous components through truncation with respect to its edges.

Remark 5. *As discussed in Subsection 2.3.2.1, the literature also does not offer a unanimous construction for the set $\mathfrak{D}$ defined in* (2.16)*. For example, in [11] and [23], two different versions are proposed from what we are presenting in this text. Nonetheless, it is important to emphasize that regardless of the version adopted, the property of the Newton polygon identifying quasi-homogeneous components prevails. The set $\mathfrak{D}$ introduced in* (2.16) *follows the same construction presented in [1], which we consider the most appropriate for our purpose.*

2.3.2.3 Finding the weights

In general, when performing blow-up on the System (2.15) using the mapping

$$(r,\theta) \mapsto (r^{\alpha}\cos(\theta), r^{\beta}\operatorname{sen}(\theta)) = (x,y),$$

with $r \in \mathbb{R}$, $\theta \in [0, 2\pi)$, we obtain a new system

$$\begin{cases} r' = \dfrac{r^{\beta}F_1\cos(\theta) + r^{\alpha}F_2\operatorname{sen}(\theta)}{r^{\alpha+\beta-1}\left(\alpha\cos^2(\theta) + \beta\operatorname{sen}^2(\theta)\right)}, \\ \theta' = \dfrac{\alpha r^{\alpha}F_2\cos(\theta) - \beta r^{\beta}F_1\operatorname{sen}(\theta)}{r^{\alpha+\beta}\left(\alpha\cos^2(\theta) + \beta\operatorname{sen}^2(\theta)\right)}, \end{cases} \tag{2.20}$$

where F_1 and F_2 are evaluated at $(r^{\alpha}\cos(\theta), r^{\beta}\operatorname{sen}(\theta))$. Conveniently, we can divide the right-hand side of the previous system by a common factor r^{δ} and obtain the "weighted polar blow-up" (see Definition 4), which in this case can also be termed (α,β)-polar blow-up. Therefore, our challenge consists of finding suitable α, β and δ, which we will do using the Newton polygon.

Using version (N_2) of Definition 8, we obtain that the Newton polygon Γ associated with the System (2.15) is given by the convex hull of $\mathfrak{D}(F) \oplus \mathbb{Z}^2_+$. Let us denote by Γ_k the finite segments of this polygon. If one of these segments is entirely contained in the half-plane $i \leq 0$ (or $j \leq 0$), it is labeled as Γ_0 (or Γ_{n+1}). The remaining segments, organized from left to right, are designated as $\Gamma_1, \Gamma_2, \cdots, \Gamma_n$, which by construction, have at least one vertex situated in the first quadrant. For each $k = 1, 2, \cdots, n$, the segment Γ_k is contained in a line with equation

$$\Gamma_k : \alpha_k x + \beta_k y = \delta_k, \tag{2.21}$$

where α_k and β_k are coprime integers. We anticipate that the appropriate parameters α, β, and δ are then chosen from the α_k, β_k, and δ_k provided by the segments $\Gamma_1, \Gamma_2, \cdots, \Gamma_n$.

If $(i,j) \in \mathfrak{D}(F)$, then either $F^{(1)}_{i+1,j}x^{i+1}y^j$ is a monomial of F_1 or $F^{(2)}_{i,j+1}x^i y^{j+1}$ is a monomial of F_2. We define $\delta = \alpha i + \beta j$ as the quasi-degree of type (α,β) of these monomials. Thus, monomials with quasi-degree $\delta = \alpha i + \beta j$ can be grouped to form the quasi-homogeneous components of type (α,β). Therefore, the vector field $F = (F_1, F_2)$ can be constructively decomposed into its quasi-homogeneous components of type (α,β), which can be identified through the Newton polygon. In practice, we are only interested in the values of α and β, which can be obtained by observing Equation (2.21). More systematically, it follows that

$$(\alpha,\beta) = \nabla(\alpha x + \beta y - \delta).$$

Thus, we can obtain the weights for the blow-up by calculating the gradient of the equation of the line containing the segment.

Example 8. *Let us revisit the system*

$$\begin{array}{rcl} x' & = & xy+y^2 \\ y' & = & x^4 \end{array} \begin{array}{l} = F_1(x,y), \\ = F_2(x,y). \end{array}$$

present in Example 7 whose Newton polygon is illustrated by Figure 2.6. By direct calculation, we obtain that the line containing the segment Γ_1 *lies on the line with equation*

$$x+2y=2,$$

whose gradient is the vector $(1,2)$*. Thus, we directly obtain that* $\alpha=1$ *and* $\beta=2$*. These values are identical to those obtained when we explored Equation* (2.19) *in Subsection 2.3.2.2 where we analyzed the quasi-homogeneous component of* F *obtained by truncating with respect to* Γ_1*.*

The practicality of computing the Newton polygon is a computational facilitator in applying the blow-up method and is widely used in dimension two, as observed in [1]. Unfortunately, we do not know of a definitive treatment of all the relationships between the blow-up method and the Newton polygon (or Newton polyhedron) in an arbitrary dimension n. Therefore, we will restrict ourselves to examples.

That said, we can adapt Definition 8 to obtain the Newton polyhedron in higher dimensions and use the same ideas that we have presented so far.

Example 9. *Consider the differential system*

$$\begin{cases} x' &= \varepsilon \cdot F(x,\hat{y},\varepsilon) \\ \hat{y}' &= G(x,\hat{y},\varepsilon) \end{cases}, \tag{2.22}$$

which will be thoroughly analyzed in Section 3.3, where

$$\begin{aligned} F(x,\hat{y},\varepsilon) &:= x^2 = L(x,\hat{y},\varepsilon), \\ G(x,\hat{y},\varepsilon) &:= \varepsilon+\varepsilon\hat{y}-x+x^2-\frac{\hat{y}^n\Phi^{(n)}(1)}{2\cdot n!}. \end{aligned}$$

The Newton polyhedron associated with the vector field $(\varepsilon L, G)^T$*, linked to system* (3.10)*, can be systematically constructed using a three-dimensional version of Definition 8 (as illustrated in Figure 2.7). This is because the set* $\mathfrak{D}$ *associated with this vector field is given by:*

$$\mathfrak{D}=\left\{\Gamma_1^{(0)}=(1,0,0),\Gamma_2^{(0)}=(0,-1,1),\Gamma_3^{(0)}=(0,0,1),\Gamma_4^{(0)}=(1,-1,0),\Gamma_5^{(0)}=(2,-1,0),\Gamma_6^{(0)}=(0,n-1,0)\right\}.$$

Notice that the face Γ_{246} (highlighted in red in Figure 2.7) is common in all $(N_1)-(N_3)$ versions of Definition 5 when adapted to the three-dimensional case. Furthermore, this face is contained in the plane with equation

$$nx+\hat{y}+n\varepsilon=n-1 \tag{2.23}$$

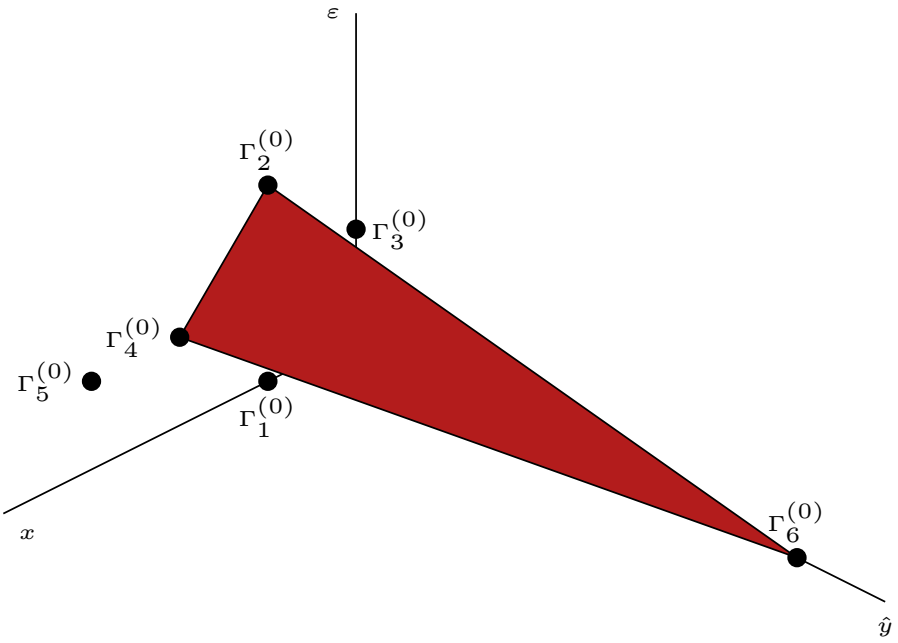

Figure 2.7: Representation of the face Γ_{246} of the Newton polyhedron Γ obtained in Example 9.

which, in turn, has the gradient vector given by $n_{246} = (n, 1, n)$.

Thus, following a procedure analogous to the one carried out in Example 8, it follows that the truncation with respect to Γ_{246} (see Definition 9) produces a nearly homogeneous component of $(\varepsilon L, G)^T$, and consequently, the weights for the application of the blow-up method are $(a, b, c) = (n, 1, n)$. We will revisit the analysis of the weights obtained for the system in Example 9 in Subsection 3.3.1.

CHAPTER 3

The blow-up method applied to the boundary-saddle-node

3.1 Boundary-saddle-node model

In this study, we analyze a PSVF in which $p \in \Sigma$ constitutes a classical saddle-node singularity for X_+, while X_- intersects the discontinuity surface Σ transversally at p. This configuration is known as a boundary-saddle-node. One possible form of this bifurcation is given by

$$X(x,y) = \begin{cases} X_+(x,y) &= (x^2, -y), & \text{if } x-y \geq 0; \\ X_-(x,y) &= (a,b), & \text{if } x-y \leq 0. \end{cases}$$

For a detailed discussion on the boundary-saddle-node and other types of boundary singularities, refer to [15].

Before to starting the regularization process let us apply a linear coordinate transformation of the form

$$\tilde{x} = x, \qquad \tilde{y} = x - y;$$

and assume $a = 0$ and $b = 1$. Then we obtain the PSVF (dropping the tildes in order to simplify the notation)

$$X(x,y) = \begin{cases} X_+(x,y) &= (x^2, -x+y+x^2), & \text{if } y \geq 0; \\ X_-(x,y) &= (0,1), & \text{if } y \leq 0. \end{cases} \tag{3.1}$$

and the PSVF (3.1) will be the main model that we will consider along this thesis.

The dynamics of (3.1) outside the switching manifold $\Sigma = \{(x,y) \,|\, y = 0\}$ can be determined using the classical theory of dynamical systems (see Figure 3.1). However, trajectories that intersect Σ require special attention.

By means of Fenichel's theory and blow up methods we get the following main result.

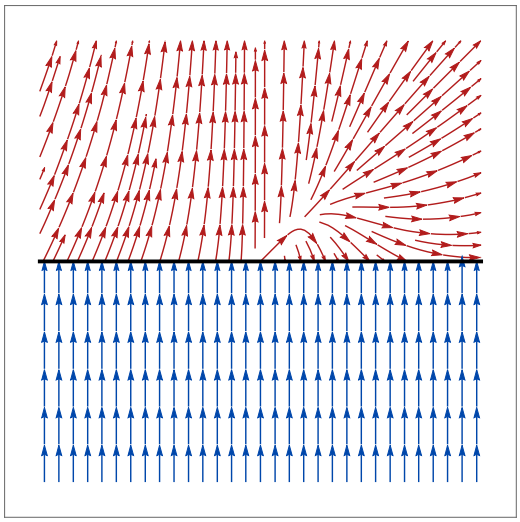

Figure 3.1: Phase portrait of PSVF X.

Theorem 2. *Take X_ε^Φ a $\mathscr{C}^n$-Sotomayor-Teixeira regularized vector field associated to* (3.1).

Consider the horizontal segments

$$H_- = [-\varepsilon, 1+\varepsilon] \times \{-\varepsilon\} \text{ and } H_+ = [R(-\varepsilon), R(\varepsilon)] \times \left\{\frac{1}{4}+\varepsilon\right\},$$

where the points $(R(-\varepsilon), \frac{1}{4}+\varepsilon)$ and $(R(\varepsilon), \frac{1}{4}+\varepsilon)$ are the iterated of $(-\varepsilon, -\varepsilon)$ and $(-\varepsilon, 1+\varepsilon)$, respectively, following the flow of the regularized vector field X_ε^Φ. Then, it happens:

(a) H_- and H_+ are transversal sections for X_ε^Φ;

(b) After the desingularization using the parameters ε, ρ and λ, the flow of X_ε^Φ defines a map U_ε between the transversal sections H_- and H_+.

The map $U_\varepsilon : H_- \to H_+$ is called the transition map of X_ε^Φ (see Figure 3.2).

Our goal is to thoroughly study the dynamics of X using singular perturbation techniques along with desingularization via blow-up, structuring the process into stages described in the following sections. The proof of the previous theorem, with all necessary details, will be presented in Section 3.5.

3.2 Obtaining a fast-slow system

Let Φ be a $\mathscr{C}^n$ transition function. The ε-regularization X_ε^Φ of X is given by:

$$X_\varepsilon^\Phi = \frac{1}{2}\left(1+\Phi\left(\frac{y}{\varepsilon}\right)\right)X_+ + \frac{1}{2}\left(1-\Phi\left(\frac{y}{\varepsilon}\right)\right)X_-, \tag{3.2}$$

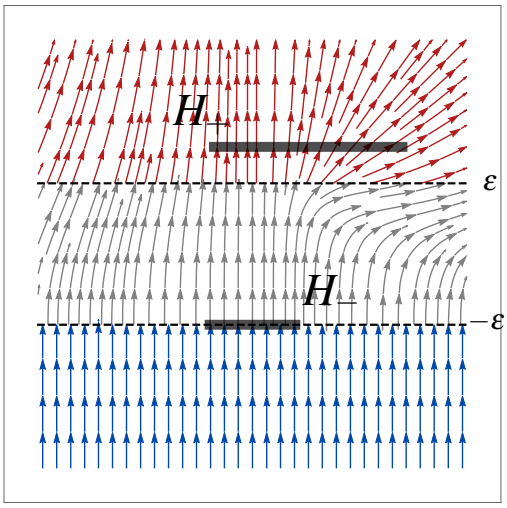

Figure 3.2: Phase portrait of the regularized vector field X_ε^Φ associated to (3.1), highlighting the regularization strip $\Sigma \times [-\varepsilon, \varepsilon]$, along with the transversal sections H_+ and H_- that define the transition map U_ε.

whose trajectories verify the system of ordinary differential equations

$$\begin{cases} \dot{x} &= \frac{1}{2}x^2\left(\Phi\left(\frac{y}{\varepsilon}\right)+1\right), \\ \dot{y} &= \frac{1}{2}\left(\left((x-1)x+y-1\right)\Phi\left(\frac{y}{\varepsilon}\right)+(x-1)x+y+1\right). \end{cases} \tag{3.3}$$

Taking the coordinate change $y = \varepsilon\tilde{y}$, we can rewrite System (3.3) as

$$\begin{cases} \dot{x} &= \frac{1}{2}x^2\left(\Phi(\tilde{y})+1\right), \\ \varepsilon\dot{\tilde{y}} &= \frac{1}{2}\left(\left(\Phi(\tilde{y})+1\right)\left(\varepsilon\tilde{y}+(x-1)x\right)-\Phi(\tilde{y})+1\right). \end{cases} \tag{3.4}$$

We will see throughout the text that we are interested in studying such a system near the point $(x,\tilde{y},\varepsilon) = (0,1,0)$. Since $1+\Phi(\tilde{y}) > 0$ for $\tilde{y}$ close enough to 1, let us divide the right side of the equations of the system (3.4) by $\frac{1}{2}(1+\Phi(\tilde{y}))$ and we get a new system

$$\begin{cases} \dot{x} &= x^2 &&= l(x,\tilde{y},\varepsilon), \\ \varepsilon\dot{\tilde{y}} &= \varepsilon\tilde{y}+(x-1)x-1+\frac{2}{\Phi(\tilde{y})+1} &&= m(x,\tilde{y},\varepsilon). \end{cases} \tag{3.5}$$

By introducing the new time rescaling $t = \tau\varepsilon$, we obtain the system

$$\begin{cases} x' &= \varepsilon x^2 &&= \varepsilon l(x,\tilde{y},\varepsilon), \\ \tilde{y}' &= \varepsilon\tilde{y}+(x-1)x-1+\frac{2}{\Phi(\tilde{y})+1} &&= m(x,\tilde{y},\varepsilon), \end{cases} \tag{3.6}$$

which is equivalent to the previous one (for $\varepsilon \neq 0$). Taking $\varepsilon = 0$ in System (3.5), we get the reduced problem

$$\begin{cases} \dot{x} &= x^2 &&= l(x,\tilde{y},0), \\ 0 &= (x-1)x-1+\frac{2}{\Phi(\tilde{y})+1} &&= m(x,\tilde{y},0), \end{cases} \tag{3.7}$$

thus the critical manifold C_0 is characterized by:

$$C_0 = \left\{ (x,\tilde{y}) \mid 0 \leq x \leq 1 \text{ and } \Phi(\tilde{y}) = \frac{2}{-x^2+x+1} - 1 \right\} . \tag{3.8}$$

and the slow dynamics, confined to C_0, are described by $\dot{x} = x^2$. Similarly, by setting $\varepsilon = 0$ in System (3.6), the fast dynamics are governed by $\tilde{y}' = (x-1)x - 1 + \frac{2}{\Phi(\tilde{y})+1}$.

Note that, restricted to C_0, we have

$$\frac{\partial m}{\partial \tilde{y}}(x,\tilde{y},0) = \frac{-2\Phi'(\tilde{y})}{(\Phi(\tilde{y})+1)^2} = 0$$

if and only if $\Phi'(\tilde{y}) = 0$ (that is, $\tilde{y} = \pm 1$). As $\Phi(1) = 1$, the unique points that verify the previous equation are $P_1 = (0,1)$ and $P_2 = (1,1)$, which shows that such points are non-normally hyperbolic. Furthermore, the subset $S = C_0 \setminus \{P_1, P_2\}$ is normally hyperbolic attracting (see Definition 2).

A detailed analysis of the dynamics around a singularity similar to that located at P_2 can be found in [27].Since we are interested in the dynamics in a neighborhood of the boundary-saddle-node singularity, let us explore the point $P_1 = (x,\tilde{y}) = (0,1)$. The Figure 3.3 illustrates the dynamics in the limit case, considering $\varepsilon = 0$ in (3.5) and (3.6).

Taking $\hat{y} = \tilde{y} - 1$, we can rewrite Systems (3.5) and (3.6) as follows

$$\begin{cases} \dot{x} &=& x^2 &=& L(x,\hat{y},\varepsilon), \\ \varepsilon\dot{\hat{y}} &=& \varepsilon(\hat{y}+1) + (x-1)x - 1 + \frac{2}{\Phi(\hat{y}+1)+1} &=& M(x,\hat{y},\varepsilon), \end{cases}$$

and

$$\begin{cases} x' &=& \varepsilon x^2 &=& \varepsilon L(x,\hat{y},\varepsilon), \\ \hat{y}' &=& \varepsilon(\hat{y}+1) + (x-1)x - 1 + \frac{2}{\Phi(\hat{y}+1)+1} &=& M(x,\hat{y},\varepsilon), \end{cases}$$

that is, $L(x,\hat{y},\varepsilon) := l(x,\hat{y}+1,\varepsilon)$ and $M(x,\hat{y},\varepsilon) := m(x,\hat{y}+1,\varepsilon)$. This modification translates the point P_1 at coordinates $(x,\tilde{y},\varepsilon)$ to the origin at coordinates $(x,\hat{y},\varepsilon)$.

The Fenichel's theory (see Chapter 1) does not provide information about the dynamics at non-normally hyperbolic points (as in the case of point P_1). To get around this problem, the next step in our analysis consists of "explode" the point P_1 to obtain information about its dynamics.

3.3 Application of the blow-up method.

Consider the blow-up

$$\begin{array}{rccc} \overline{\varphi}: & \mathbb{S}^2 \times \mathbb{R}_+ & \to & \mathbb{R}^3 \\ & (\bar{x},\bar{y},\bar{\varepsilon},r) & \mapsto & (r^a\bar{x}, r^b\bar{y}, r^c\bar{\varepsilon}) \end{array} \tag{3.9}$$

applied to the system

$$\begin{cases} x' &=& \varepsilon \cdot F(x,\hat{y},\varepsilon) \\ \hat{y}' &=& G(x,\hat{y},\varepsilon) \\ \varepsilon' &=& 0 \end{cases} \tag{3.10}$$

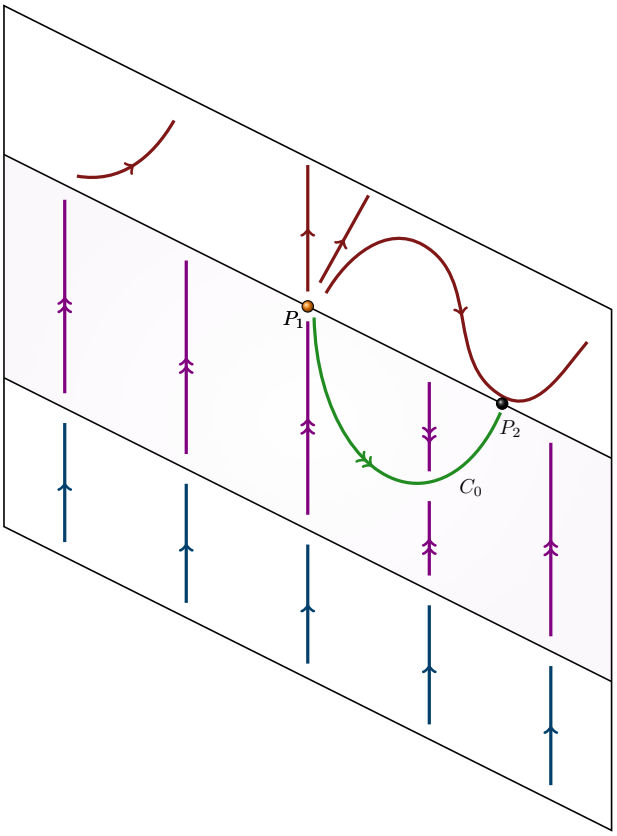

Figure 3.3: Dynamics in the limit case, i.e. take $\varepsilon = 0$ in (3.5) and (3.6). It is important to remark that the vector field X_+ has a tangential point at $x = 1$. However we will be only interested in the local dynamics around the boundary saddle-node equilibrium placed at the origin. A singular perturbation analysis of this kind of visible fold point was studied in [27].

which has the same format of System (2.6), where

$$F(x,\hat{y},\varepsilon) := x^2 = L(x,\hat{y},\varepsilon),$$
$$G(x,\hat{y},\varepsilon) := \varepsilon + \varepsilon\hat{y} - x + x^2 - \frac{\hat{y}^n \Phi^{(n)}(1)}{2\cdot n!} \approx M(x,\hat{y},\varepsilon).$$

Observe that $G(x,\hat{y},\varepsilon)$ is an approximation using the Taylor polynomial around $\hat{y} = 0$, to $M(x,\hat{y},\varepsilon)$, where n is the smallest positive integer such that $\Phi^{(n)}(1) \neq 0$.

In our context, ε is not negative. So, five charts are enough to cover the representative part of $\mathbb{S}^2$ where we are interested in the dynamics. Let $\mathscr{B}^+_{\bar{\varepsilon}} := \mathscr{B} \cap \{\bar{\varepsilon} \geq 0\}$ be a submanifold of the exceptional divisor $\mathscr{B} := \mathbb{S}^2 \times \mathbb{R}$; similarly, introduce $\mathscr{B}^{\pm}_{\bar{x}}$ and $\mathscr{B}^{\pm}_{\bar{y}}$. Now let us define five charts for $\mathscr{B}$:

- $\mathscr{K}_1 : \mathscr{B}^-_{\bar{x}} \to \mathbb{R}^3$ given by $\bar{x} = -r_1^a, \bar{y} = r_1^b y_1$ and $\bar{\varepsilon} = r_1^c \varepsilon_1$.
- $\mathscr{K}_2 : \mathscr{B}^+_{\bar{\varepsilon}} \to \mathbb{R}^3$ given by $\bar{x} = r_2^a x_2, \bar{y} = r_2^b y_2$ and $\bar{\varepsilon} = r_2^c$.
- $\mathscr{K}_3 : \mathscr{B}^-_{\bar{y}} \to \mathbb{R}^3$ given by $\bar{x} = r_3^a x_3, \bar{y} = -r_3^b$ and $\bar{\varepsilon} = r_3^c \varepsilon_3$.
- $\mathscr{K}_4 : \mathscr{B}^+_{\bar{x}} \to \mathbb{R}^3$ given by $\bar{x} = r_4^a, \bar{y} = r_4^b y_4$ and $\bar{\varepsilon} = r_4^c \varepsilon_4$.

- $\mathscr{K}_5 : \mathscr{B}^+_{\bar{y}} \to \mathbb{R}^3$ given by $\bar{x} = r_5^a x_5, \bar{y} = r_5^b$ and $\bar{\varepsilon} = r_5^c \varepsilon_5$.

In a simplified way, the maps $\mathscr{K}_1, \mathscr{K}_2, \mathscr{K}_3, \mathscr{K}_4$ and $\mathscr{K}_5$ can be seen as the projections, respectively, of the sets $\mathscr{B}^-_{\bar{y}}, \mathscr{B}^+_{\bar{\varepsilon}}, \mathscr{B}^+_{\bar{y}}, \mathscr{B}^+_{\bar{x}}$ and $\mathscr{B}^-_{\bar{x}}$ on the planes $\bar{y} = -1, \bar{\varepsilon} = 1, \bar{y} = 1, \bar{x} = 1$ and $\bar{x} = -1$, respectively. Geometrically, this means that we want to cover the exceptional divisor $\mathscr{B}$ with graphs using rectangular coordinate systems positioned in specific directions. In Figure 2.1, we can imagine moving the rectangular coordinate systems along the dotted lines in the direction of the sphere and adjusting them to it (see Figure 3.4).

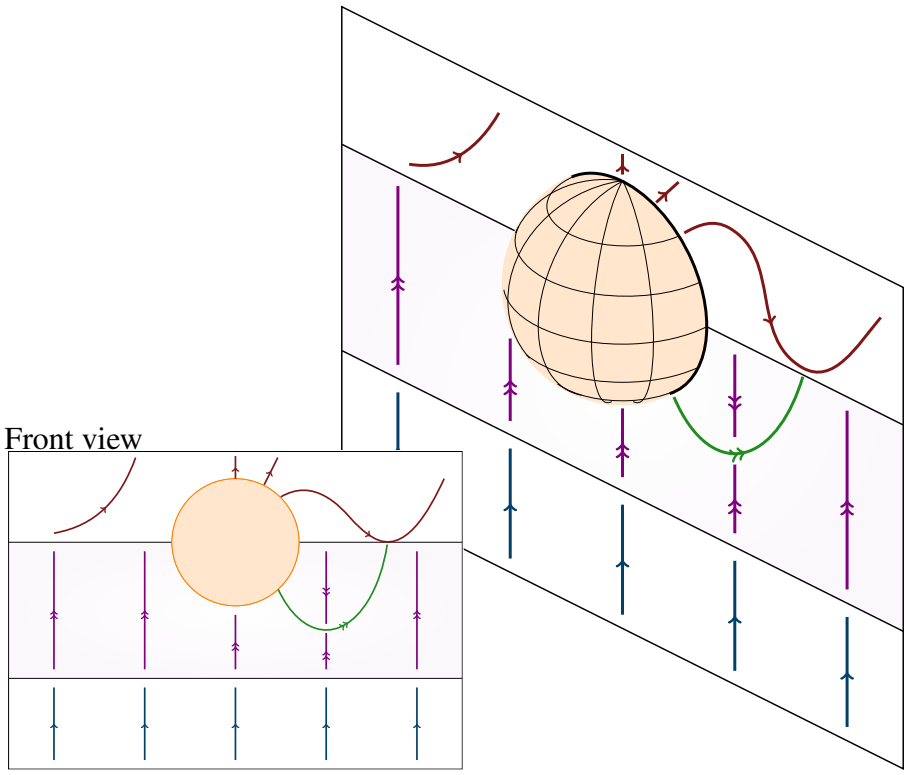

Figure 3.4: Representation of the exceptional divisor $\mathscr{B}_0$ after the blow-up of the point P_1.

3.3.1 Choosing weights for the blow-up

As discussed in Section 2.3, the appropriate choice of weights (a,b,c) for the blow-up is crucial for the method's implementation (see Example 4 in Subsection 2.3.1). To explore the possibilities for these weights, we will analyze the change of coordinates defined in the chart $\mathscr{K}_3$. Specifically, consider the following transformation: $x = r^{a_3} x_3$, $y = -r^{b_3}$, and $\varepsilon = r^{c_3}\varepsilon_3$. With this, we have: Thus, we have:

$$\begin{cases} x &= r_3^a x_3 \\ y &= -r_3^b \\ \varepsilon &= r_3^c \varepsilon_3 \end{cases} \quad \overset{\frac{d}{dt}}{\Longrightarrow} \quad \begin{cases} x' &= a r_3^{a-1} x_3 r_3' + r_3^a x_3' \\ y' &= -b r_3^{b-1} r_3' \\ \varepsilon' &= c r_3^{c-1} \varepsilon_3 r_3' + r_3^c \varepsilon_3' \end{cases}. \tag{3.11}$$

Using Equation (3.10) we can rewrite System (3.11) as follows:

$$\begin{cases} x_3' &= r_3^{c-a}\varepsilon_3 F + ab^{-1}r_3^{-b}x_3 G \\ r_3' &= -b^{-1}r_3^{1-b}G \\ \varepsilon_3' &= cb^{-1}r_3^{-b}\varepsilon_3 G \end{cases} \tag{3.12}$$

Note that the expression for the vector field in the chart has powers of r_3 that depend on a, b, and c. By expanding the expression for x_3', we obtain:

$$x_3' = ab^{-1}\left[\left(\varepsilon_3 r_3^{-b+c} - \varepsilon_3 r_3^{c}\right)x_3 - r_3^{a-b}x_3^2 + r_3^{2a-b}x_3^3 + (-1)^{n+1}\omega_n r_3^{-b+nb}\right] + \varepsilon_3 x_3^2 r_3^{a+c}, \tag{3.13}$$

where

$$\omega_n = \frac{\Phi^{(n)}(1)}{2n!}.$$

The idea is to determine suitable values for a, b, and c to facilitate the desingularization of the system (see Definition 5); this choice can be refined to highlight r raised to the highest possible exponent, enabling a more robust desingularization. Thus, we consider

$$c - b = a - b = bn - b,$$

which can be verified by taking $b = 1$ and $a = c = n$. Consequently, substituting $(a,b,c) = (n,1,n)$ into Equation (3.13), we obtain:

$$x_3' = \left[r_3^{n+1}x_3^2\varepsilon_3 + nx_3\left(\Lambda_3 + r_3\Upsilon_3\right)\right]r_3^{n-1}, \tag{3.14}$$

where $\Lambda_3 = -x_3 + \varepsilon_3 - (-1)^n\omega_n$ and $\Upsilon_3 = r_3^n x_3^2 - \varepsilon_3$.

Note that, not by chance, the weights used in obtaining Equation (3.14) are the same as those employed in the analysis of System (2.22) in Example 9. The difference lies in the fact that the construction of the Newton polyhedron in the aforementioned example provides a computational advantage, allowing the weights to be obtained simply by analyzing the exponents.

It is clear from that the dynamics depend on the parity of n and on the sign of ω_n. In other words, the dynamics strongly depend on the transition function Φ adopted. However, since Φ is monotonic, the following Lemma assures that there are only two cases to consider.

Lemma 1. *If $\Phi : \mathbb{R} \to [-1,1]$ is a monotonic transition function such that*

$$\Phi(1) = 1; \qquad \Phi'(1) = \cdots = \Phi^{(n-1)}(1) = 0; \qquad \Phi^{(n)}(1) \neq 0;$$

then the following statements hold:

1. *n is even if, and only if, $\omega_n < 0$;*

2. *n is odd if, and only if, $\omega_n > 0$.*

Proof. Since Φ is an analytic function, then its Taylor expansion near $x = 1$ is given by

$$\Phi(x) = 1 + \frac{\Phi^{(n)}(1)(x-1)^n}{n!}.$$

Due to the fact that Φ is an increasing function in $(-1,1)$ and $\Phi(1) = 1$, given $\varepsilon > 0$ there is $c^* \in (1-\varepsilon, 1)$ such that

$$\begin{aligned} 1 - \varphi(c^*) > 0 \iff 1 - \left(1 + \frac{\varphi^{(n)}(1)(c^*-1)^n}{n!}\right) &> 0 \\ \iff -\frac{\varphi^{(n)}(1)(c^*-1)^n}{n!} &> 0 \\ \iff -\varphi^{(n)}(1)(c^*-1)^n &> 0 \end{aligned}$$

From the last inequality, it follows that:

1. n is even if, and only if, $\Phi^{(n)}(1) < 0$;

2. n is odd if, and only if, $\Phi^{(n)}(1) > 0$;

and therefore the conclusion holds. □

In [27, Proposition 10] were given examples of polynomial monotonic transition function given by

$$\Phi_n(x) = (-1)^n \frac{(2n+1)!}{2^{2n}(n!)^2} \int_0^x (s-1)^n (s+1)^n ds.$$

However, if one wants to consider *analytic* transition functions, it can be considered

$$\Phi(x) = \begin{cases} -1, & x \le -1, \\ \operatorname{sen}\left(\frac{\pi x}{2}\right), & -1 \le x \le 1, \\ 1, & x \ge 1, \end{cases}$$

for n even and $\Phi^{(n)}(1) < 0$, and

$$\Phi(x) = \begin{cases} -1, & x \le -1, \\ \dfrac{\operatorname{sen}(\pi x) + \pi x}{\pi}, & -1 \le x \le 1, \\ 1, & x \ge 1, \end{cases}$$

for the case n odd and $\Phi^{(n)}(1) > 0$.

3.3.2 Dynamics in the directional charts

By applying the same procedure used to obtain x_3' in (3.14), to find ε_3' and r_3', we can rewrite the system (3.12) as:

$$\hat{\mathscr{K}_3}: \begin{cases} x_3' &= \left[r_3^{n+1}x_3^2\varepsilon_3 + nx_3\left(\Lambda_3 + r_3\Upsilon_3\right)\right] r_3^{n-1}, \\ \varepsilon_3' &= n\varepsilon_3\left(\Lambda_3 + r_3\Upsilon_3\right)r_3^{n-1}, \\ r_3' &= -r_3\left(\Lambda_3 + r_3\Upsilon_3\right)r_3^{n-1}. \end{cases} \tag{3.15}$$

Next, by dividing the right-hand side of System (3.15) by r_3^{n-1}, we obtain the desingularized blow-up $\overline{\mathscr{K}_3} = \frac{1}{r_3^{n-1}}\hat{\mathscr{K}_3}$ corresponding to the chart $\mathscr{K}_3$ (see Definitions 4, 5, and 6). Repeating this process for the remaining charts, we find that the desingularized blow-ups for the five charts of interest are given by:

$$\overline{\mathscr{K}}_1: \begin{cases} r_1' &= -\frac{r_1^{n+2}\varepsilon_1}{n} \\ y_1' &= 1 + \varepsilon_1 - y_1^n\omega_n + r_1\left(y_1\varepsilon_1 + r_1^{n-1} + \dfrac{y_1\varepsilon_1 r_1^n}{n}\right) \\ \varepsilon_1' &= r_1^{n+1}\varepsilon_1^2 \end{cases}$$

$$\overline{\mathscr{K}}_2: \begin{cases} x_2' &= r_2^{n+1}x_2^2 \\ y_2' &= 1 - x_2 - \omega_n y_2^n + r_2\left(y_2 + r_2^{n-1}x_2^2\right) \\ r_2' &= 0 \end{cases}$$

$$\overline{\mathscr{K}}_3: \begin{cases} x_3' &= nx_3\left(\Lambda_3 + r_3\Upsilon_3\right) + r_3^{n+1}x_3^2\varepsilon_3 \\ r_3' &= -r_3\left(\Lambda_3 + r_3\Upsilon_3\right) \\ \varepsilon_3' &= n\varepsilon_3\left(\Lambda_3 + r_3\Upsilon_3\right) \end{cases}$$

$$\overline{\mathscr{K}}_4: \begin{cases} r_4' &= \frac{r_4^{n+2}\varepsilon_4}{n} \\ y_4' &= -1 + \varepsilon_4 - y_4^n\omega_n + r_4\left(y_4\varepsilon_4 + r_4^{n-1} - \dfrac{y_4\varepsilon_4 r_4^n}{n}\right) \\ \varepsilon_4' &= -r_4^{n+1}\varepsilon_4^2 \end{cases}$$

$$\overline{\mathscr{K}}_5: \begin{cases} x_5' &= nx_5\left(\Lambda_5 - r_5\Upsilon_5\right) + r_5^{n+1}x_5^2\varepsilon_5 \\ r_5' &= -r_5\left(\Lambda_5 - r_5\Upsilon_5\right) \\ \varepsilon_5' &= n\varepsilon_5\left(\Lambda_5 - r_5\Upsilon_5\right) \end{cases}$$

where

$$\begin{array}{rclcl} \Lambda_3 &=& \Lambda_3(x_3,\varepsilon_3) &=& -x_3 + \varepsilon_3 - (-1)^n\omega_n \\ \Upsilon_3 &=& \Upsilon_3(\varepsilon_3,r_3) &=& r_3^{n-1}x_3^2 - \varepsilon_3 \\ \Lambda_5 &=& \Lambda_5(x_5,\varepsilon_5) &=& x_5 - \varepsilon_5 + \omega_n \\ \Upsilon_5 &=& \Upsilon_5(\varepsilon_5,r_5) &=& \varepsilon_5 + r_5^{n-1}x_5^2 \end{array}$$

From the blow-up method, our aim is to study the limit as r approaches 0. Since we are utilizing directional charts, we need to examine the limiting cases where r_i tends to 0.

Proposition 1. *The systems*

$$\mathscr{K}_1^0: \begin{cases} y_1' &= 1 + \varepsilon_1 - y_1^n\omega_n \\ \varepsilon_1' &= 0 \end{cases} \qquad \mathscr{K}_4^0: \begin{cases} y_4' &= -1 + \varepsilon_4 - y_4^n\omega_n \\ \varepsilon_4' &= 0 \end{cases}$$

$$\mathscr{K}_3^0: \begin{cases} x_3' &= nx_3\left[\varepsilon_3 - x_3 - (-1)^n\omega_n\right] \\ \varepsilon_3' &= n\varepsilon_3\left[\varepsilon_3 - x_3 - (-1)^n\omega_n\right] \end{cases} \qquad \mathscr{K}_5^0: \begin{cases} x_5' &= nx_5\left[x_5 - \varepsilon_5 + \omega_n\right] \\ \varepsilon_5' &= n\varepsilon_5\left[x_5 - \varepsilon_5 + \omega_n\right] \end{cases}$$

where $\mathscr{K}_i^0$ denotes the systems $\overline{\mathscr{K}}_i$ restricted to $r_i = 0$, have the following properties:

1. *The line characterized by $x_3 = \varepsilon_3 - (-1)^n \omega_n$ is filled with equilibrium points of $\mathscr{K}_3^0$, while the line characterized by $\varepsilon_5 = x_5 + \omega_n$ is filled with equilibrium points of $\mathscr{K}_5^0$. Additionally, the origin is a hyperbolic node of the systems $\mathscr{K}_3^0$ and $\mathscr{K}_5^0$ whose stability depends on the parity of n.When n is odd, the origin is a repelling star node for both systems. In the case where n is even, the origin is a repelling star node for $\mathscr{K}_3^0$ and an attracting star node for $\mathscr{K}_5^0$.*

2. *The curve characterized by $\varepsilon_1 = -1 + y_1^n \omega_n$ (respectively, $\varepsilon_4 = 1 + y_4^n \omega_n$) is filled with singularities of the system $\mathscr{K}_1^0$ (respectively, $\mathscr{K}_4^0$), whose stability in the direction of y_1 (respectively, y_4) also depends on the parity of n. If n is odd, the singularities of the system $\mathscr{K}_1^0$ (respectively, $\mathscr{K}_4^0$) are attracting. On the other hand, if n is even, such singularities are repelling for $y_1 > 0$ (respectively, $y_4 > 0$) and attracting for $y_1 < 0$ (respectively, $y_4 < 0$).*

Proof. By performing a direct calculation, we can observe that the origin is a singularity of the systems $\mathscr{K}_3^0$ and $\mathscr{K}_5^0$, and the corresponding Jacobian matrices, evaluated at the origin, are given by:

$$JK_3^0 = \begin{bmatrix} (-1)^{1+n} n\omega_n & 0 \\ 0 & (-1)^{1+n} n\omega_n \end{bmatrix} \quad \text{e} \quad JK_5^0 = \begin{bmatrix} n\omega_n & 0 \\ 0 & n\omega_n \end{bmatrix}.$$

This shows that both matrices have equal eigenvalues, ensuring that the origin is a attracting (respectively, repelling) star node when the eigenvalues are negative (respectively, positive). The sign of $(-1)^{1+n} n\omega_n$ and $n\omega_n$ depends on the parity of n and the sign of ω_n, which, in our context, can be summarized solely by the parity of n (see Lemma 1). Explicitly,

- If n is even, we have $\omega_n < 0$ and, consequently $(-1)^{1+n} n\omega_n > 0$ and $n\omega_n < 0$,
- If n is odd, we have $\omega_n > 0$ and, consequently: $(-1)^{1+n} n\omega_n > 0$ and $n\omega_n > 0$,

which guarantees the configuration presented in Item (i) of the Proposition 1. Also note that the sign of $\frac{\partial}{\partial y_1}(1 + \varepsilon_1 - y_1^n \omega_n) = -n y_1^{n-1} \omega_n$ (respectively, $\frac{\partial}{\partial y_4}(-1 + \varepsilon_4 - y_4^n \omega_n) = -n y_4^{n-1} \omega_n$), which determines the stability of the singularities present in $1 + \varepsilon_1 - y_1^n \omega_n = 0$ (respectively, $-1 + \varepsilon_4 - y_4^n \omega_n = 0$) in the direction of y_1 (respectively, y_4), also depends on the parity of n and the sign of ω_n. By analyzing the possibilities of n and ω_n, analogous to the previous paragraph, we ensure the configuration presented in Item (ii). □

The previous proposition (see Figure 3.5) provides sufficient information to describe the dynamics of $\mathscr{K}_1, \mathscr{K}_3, \mathscr{K}_4$ and $\mathscr{K}_5$ in the limiting cases where $r_i \to 0$. In order to analyze $\mathscr{K}_2$, we need to explore the system $\overline{\mathscr{K}}_2$, which is actually a fast-slow system (see Equation (2.6)).

Proposition 2. *The fast-slow system $\overline{\mathscr{K}}_2$ has the following properties:*

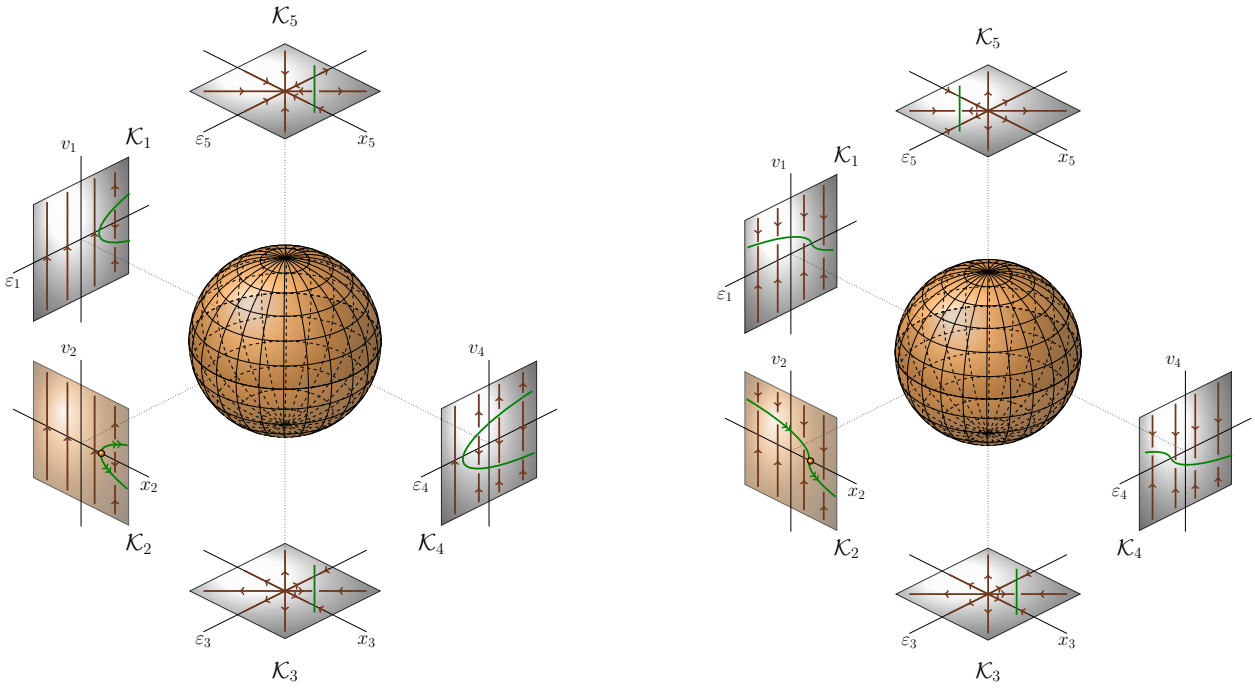

(a) Case where n is even.

(b) Case where n is odd.

Figure 3.5: Overview of the two possible configurations for the phase portraits in the local charts.

1. *The slow dynamics, restricted to the critical manifold*

$$S_0 = \{(x_2, y_2, 0) \ : \quad x_2 = 1 - \omega_n y_2^n\},$$

is given by $\dot{x}_2 = x_2^2$. *Furthermore,* S_0 *loses normal hyperbolicity at the point* $(x_2, y_2) = (1, 0)$.

2. *If n is odd, the critical manifold* S_0 *is filled with stable equilibrium points of the fast dynamics. On the other hand, if n is even,* S_0 *is filled with stable (respectively, unstable) equilibrium points of the fast dynamics when* $y_2 < 0$ *(respectively,* $y_2 > 0$*).*

Proof. Taking $r_2 = 0$ in System $\overline{\mathscr{K}}_2$, we get the layer problem

$$\begin{cases} x_2' &= 0, \\ y_2' &= 1 - x_2 - \omega_n y_2^n \end{cases}, \tag{3.16}$$

thus the critical manifold S_0 is characterized by:

$$S_0 = \{(x_2, y_2) \ : \quad x_2 = 1 - \omega_n y_2^n\}.$$

Note also that the sign of $\frac{\partial}{\partial y_2}(1 - x_2 - y_2^n \omega_n) = -n\omega_n y_2^{n-1}$, which determines the stability of the singularities in fast dynamics, again depends on the parity of n and the sign of ω_n. By analyzing the possibilities of n and ω_n, exactly as in the proof of Item (ii) of Proposition 1, we ensure the

configuration presented in items (ii) of Proposition 2. On the other hand, when we perform the temporal rescheduling $\tau = \varepsilon t$ on the system $\overline{\mathscr{K}}_2$ and then set $r_2 = 0$, we obtain the reduced problem

$$\begin{cases} \dot{x}_2 &= x_2^2, \\ 0 &= 1 - x_2 - \omega_n y_2^n, \end{cases} \tag{3.17}$$

whose slow dynamics, restricted to S_0, is given by $\dot{x} = x_2^2$ (see Section 1.2). Furthermore, note that

$$\frac{\partial}{\partial y_2}(1 - x_2 - \omega_n y_2^n) = -n\omega_n v_2^{n-1} = 0$$

if and only if $y_2 = 0$. This shows that S_0 loses normality hyperbolic at the point $(x_2, y_2) = (1,0)$ and, therefore, we finish the proof of Item (i). □

In Figure 3.6, we depict the phase portrait on the exceptional divisor $\mathscr{B}_0$, synthesizing all the information from Propositions 1 and 2. We highlight in black the point where S_0 loses normal hyperbolicity, where we will apply a new blow-up in the next section.

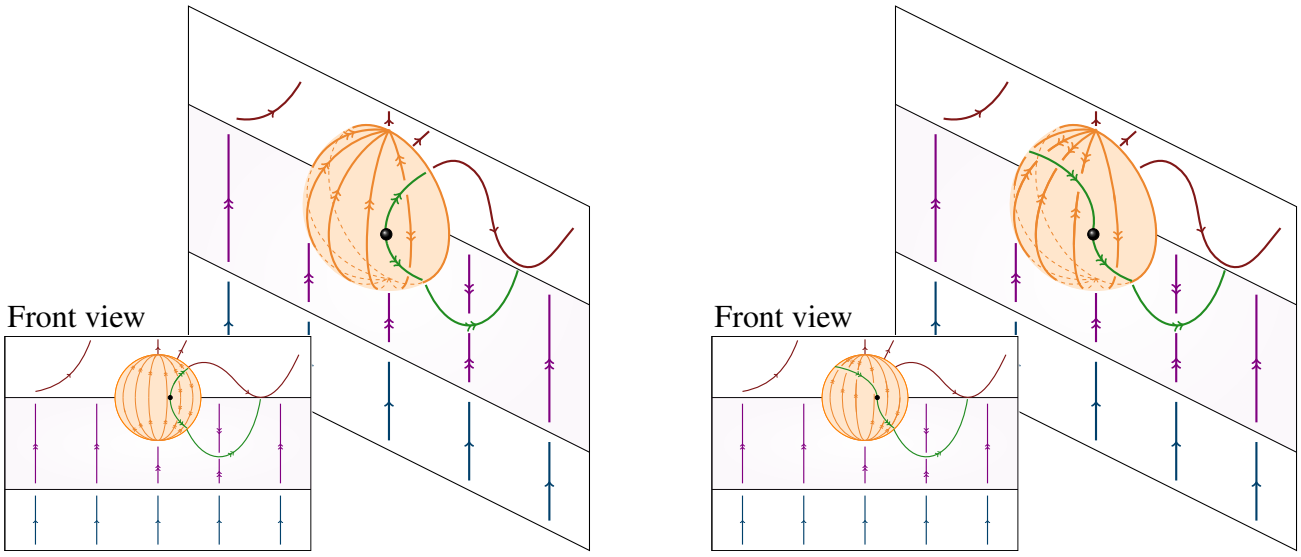

(a) Case where n is even.

(b) Case where n is odd.

Figure 3.6: Overview of the two possible configurations for the phase portraits after the blow-up of point P_1.

3.4 Blow-up of the non-normally hyperbolic point in the chart $\mathscr{K}_2$

As discussed in the previous sections, the point $(1,0,0)$ in the chart $\mathscr{K}_2$ is a non-normally hyperbolic point, for every $n \geq 2$ and $\omega_n \neq 0$. This section is devoted to carefully study the dynamics near

such a singularity. Firstly, the non-normally hyperbolic point $(1,0,0)$ must be translated to the origin. In order to simplify the notation, we rewrite the variables as

$$x_2 = u+1,\ \ y_2 = v,\ \ r_2 = \lambda.$$

The system obtained after translation and change of notation is given by the equation:

$$\left\{\begin{array}{rcl} u' &=& \lambda^{n+1}(u+1)^2, \\ v' &=& 1-(u+1)-\omega_n v^n + \lambda(v-\omega_{n+1}v^{n+1}) + \lambda^n(u+1)^2, \\ \lambda' &=& 0, \end{array}\right. \tag{3.18}$$

which is a fast-slow system. The next step is to find suitable weights for the blow-up. Following the approach used in the first blow-up, we get the weight vector $(a,b,c) = (n,n-1,1)$. Denote by $\mathscr{D}$ the exceptional divisor obtained from the second weighted blow-up

$$\begin{array}{rccc} \overline{\phi}: & \mathbb{S}^2\times\mathbb{R}_+ & \to & \mathbb{R}^3 \\ & (\bar{u},\bar{v},\bar{\lambda},s) & \mapsto & (s^n\bar{u}, s^{n-1}\bar{v}, s\bar{\lambda}) \end{array} \tag{3.19}$$

applied to the System (3.18). As in Section 3.3, by performing this new blow-up, we must analyze the dynamics in the hemisphere where $\bar{\lambda}\geq 0$ of the new exceptional divisor $\mathscr{D}$ (see Figure 3.7). We will do this by examining the five directional charts:

- $\mathscr{A}_1 : \mathscr{D}_v^- \to \mathbb{R}^3$ given by $u = s_1^n u_1,\ v = -s_1^{n-1}$ and $\lambda = s_1\lambda_1$;
- $\mathscr{A}_2 : \mathscr{D}_{\bar{\lambda}}^+ \to \mathbb{R}^3$ given by $u = s_2^n u_2,\ v = s_2^{n-1}v_2$ and $\lambda = s_2$;
- $\mathscr{A}_3 : \mathscr{D}_v^+ \to \mathbb{R}^3$ given by $u = s_3^n u_3,\ v = s_3^{n-1}$ and $\lambda = s_3\lambda_3$;
- $\mathscr{A}_4 : \mathscr{D}_u^+ \to \mathbb{R}^3$ given by $u = s_4^n,\ v = s_4^{n-1}v_4$ and $\lambda = s_4\lambda_4$;
- $\mathscr{A}_5 : \mathscr{D}_u^- \to \mathbb{R}^3$ given by $u = -s_5^n,\ v = s_5^{n-1}v_5$ and $\lambda = s_5\lambda_5$.

The chart $\mathscr{A}_2$ refers to the dynamics in the hemisphere where $\lambda > 0$ of the exceptional divisor $\mathscr{D}$, while the charts $\mathscr{A}_1, \mathscr{A}_3, \mathscr{A}_4$ and $\mathscr{A}_5$ are used to study the circle $\{\lambda = 0\}$. The notation used for $\mathscr{D}_{\bar{\lambda}}^+, \mathscr{D}_{\bar{u}}^\pm$, and $\mathscr{D}_{\bar{v}}^\pm$ follows the same idea as the notation adopted in Section 3.3. Thus, in a simplified way, the maps $\mathscr{A}_1, \mathscr{A}_2, \mathscr{A}_3, \mathscr{A}_4$, and $\mathscr{A}_5$ can be seen as the projections of the sets $\mathscr{D}_{\bar{\lambda}}^+, \mathscr{D}_{\bar{u}}^\pm$, and $\mathscr{D}_{\bar{v}}^\pm$ onto the planes $\bar{\lambda} = 1, \bar{u} = \pm 1$, and $\bar{v} = \pm 1$, respectively. We emphasize that in this new blow-up, the variables u_i and s_i have different meanings from the previous blow-up for $i = 1, \cdots, 5$.

The analysis is divided in two cases: $n > 2$ and $n = 2$. The first one depends neither on the parity of n nor on the sign of ω_n. On the other hand, the second one depends on the sign of ω_2. However, in both cases, we do not obtain a fast-slow system in any chart.

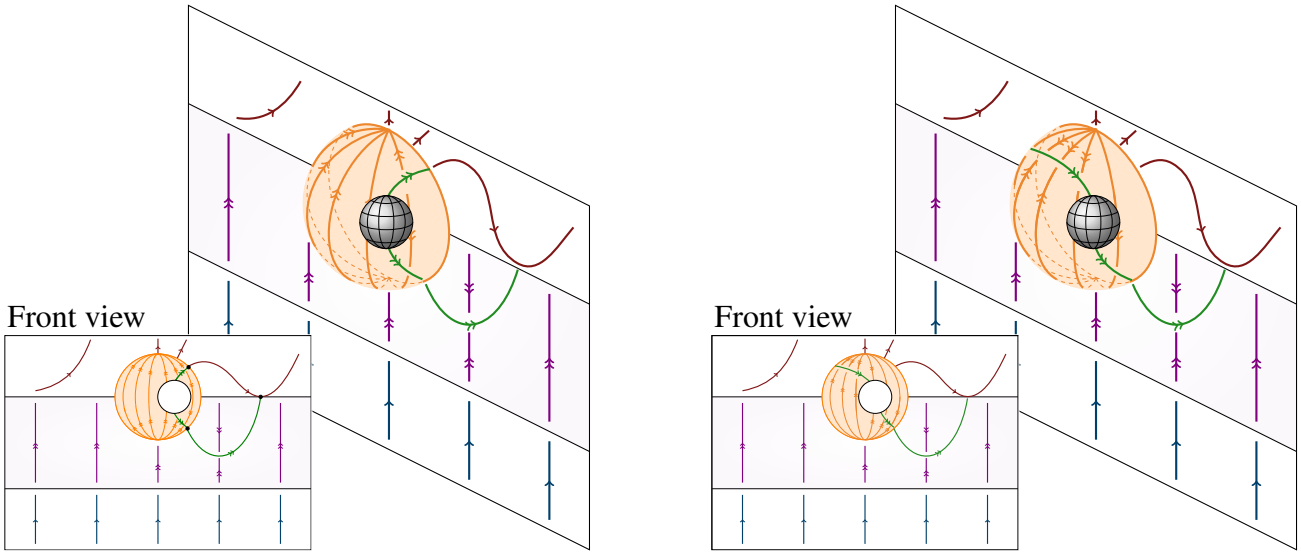

(a) Case where n is even.

(b) Case where n is odd.

Figure 3.7: Overview of the two possible configurations for the exceptional divisor $\mathscr{D}$ after the blow-Up of the non-normally hyperbolic point $(x_2, y_2, 0) = (1, 0, 0)$ identified in chart $\mathscr{K}_2$.

3.4.1 Case $n > 2$

Let us describe the dynamics after a weighted blow-up in System (3.18). In what follows we describe the dynamics in the charts $\mathscr{A}_1, \mathscr{A}_2$ and $\mathscr{A}_3$. It will be checked that the charts $\mathscr{A}_4$ and $\mathscr{A}_5$ do not present any equilibrium point. We remark that this analysis does not depends on the parity of n.

3.4.1.1 Chart $\mathscr{A}_2$

Considering System (3.18), after a blow-up of the form

$$u = s_2^n u_2, \quad v = s_2^{n-1} v_2, \quad \lambda = s_2;$$

the system obtained in $\mathscr{A}_2$ is

$$\begin{cases} u_2' &= 1 + s_2^n\left(2u_2 + s_2^n u_2^2\right), \\ v_2' &= 1 - u_2 + v_2 - \left(s_2^{n^2-2n}\omega_n v_2^n + s_2^{n^2-n}\omega_{n+1} v_2^{n+1}\right) + s_2^n\left(2u_2 + s_2^n u_2^2\right), \\ s_2' &= 0. \end{cases} \tag{3.20}$$

Since $n > 2$, the dynamics in the exceptional divisor $\{s_2 = 0\}$ is given by

$$u_2' = 1, \qquad v_2' = 1 - u_2 + v_2. \tag{3.21}$$

The following proposition summarizes important features of (3.21).

Proposition 3. *System* (3.21) *does not have equilibria and the line* $l_2 = \{u_2 = v_2\}$ *is an invariant set of such system. See Figure 3.8.*

Proof. Denote by Y_2 the vector field associated to System (3.21). It is straightforward to see that Y_2 does not have equilibria. Observe that the tangent vector of the line $l_2 = \{u_2 = v_2\}$ is given by $Y_2(u_2, v_2) = (1,1)$, and therefore l_2 is an invariant set of Y_2. □

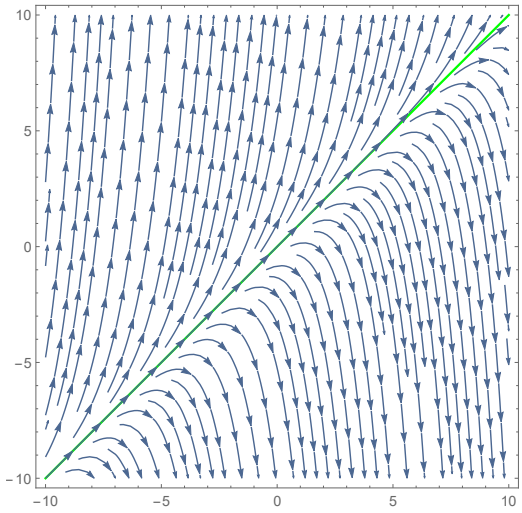

Figure 3.8: Phase portrait of System (3.21). The invariant line $l_2 = \{\alpha_2 = \beta_2\}$ is highlighted.

Remark 6. *Observe that, for $s_2 \neq 0$, it holds that*

$$\{u_2 = v_2\} = \{s_2^{-n} u = s_2^{-n+1} v\} = \{u = 0\},$$

which implies that the curve l_2 intersects the origin of the charts $\mathscr{A}_1$ and $\mathscr{A}_3$.

3.4.1.2 Charts $\mathscr{A}_4$ and $\mathscr{A}_5$

Recall that in our context we must study the system in $\mathscr{A}_4$ and $\mathscr{A}_5$ for $\lambda_{4,5} \geq 0$. In order to obtain the dynamics in $\mathscr{A}_4$ and $\mathscr{A}_5$, we peform, respectively, the weighted blow-ups

$$\begin{cases} u &= s_4^n, \\ v &= s_4^{n-1} v_4, \\ \lambda &= s_4 \lambda_4, \end{cases} \qquad \begin{cases} u &= -s_5^n, \\ v &= s_5^{n-1} v_5, \\ \lambda &= s_5 \lambda_5; \end{cases}$$

and the systems obtained are, respectively,

$$\begin{cases} s_4' &= \dfrac{s_4 \lambda_4^{n+1}}{n} \Gamma_4, \\ v_4' &= -1 + v_4 \lambda_4 - \Delta_4 + \left(\lambda_4^n - v_4 \lambda_4^{n+1} + \dfrac{v_4 \lambda_4^{n+1}}{n} \right) \Gamma_4, \\ \lambda_4' &= -\dfrac{\lambda_4^{n+2}}{n} \Gamma_4; \end{cases} \tag{3.22}$$

and

$$\begin{cases} s_5' &= \dfrac{s_5\lambda_5^{n+1}}{n}\Gamma_5, \\ v_5' &= 1+v_5\lambda_5-\Delta_5-\left(\lambda_5^n+v_5\lambda_5^{n+1}-\frac{v_5\lambda_5^{n+1}}{n}\right)\Gamma_5, \\ \lambda_5' &= -\dfrac{\lambda_5^{n+2}}{n}\Gamma_5. \end{cases} \tag{3.23}$$

where

$$\Gamma_4=\Gamma_4(s_4)=1+2s_4^n+s_4^{2n}, \qquad \Gamma_5=\Gamma_5(s_5)=-1+2s_5^n-s_5^{2n}.$$

$$\Delta_i=\Delta_i(s_i,v_i)=s_i^{n^2-2n}\omega_n v_i^n+s_i^{n^2-n}\omega_{n+1}v_i^{n+1}\lambda_i, \qquad \text{for } i=4,5.$$

For simplicity sake, we denote the sets $\{s_4=0\}$ and $\{s_5=0\}$ by $\{s_{4,5}=0\}$. In such sets, we obtain the systems

$$\begin{cases} v_4' &= -1+v_4\lambda_4+\left(\lambda_4^n-v_4\lambda_4^{n+1}+\frac{v_4\lambda_4^{n+1}}{n}\right), \\ \lambda_4' &= -\dfrac{\lambda_4^{n+2}}{n}; \end{cases} \tag{3.24}$$

and

$$\begin{cases} v_5' &= 1+v_5\lambda_5+\left(\lambda_5^n+v_5\lambda_5^{n+1}-\frac{v_5\lambda_5^{n+1}}{n}\right), \\ \lambda_5' &= \dfrac{\lambda_5^{n+2}}{n}. \end{cases} \tag{3.25}$$

The following proposition summarizes important features of Systems (3.24) and (3.25). Its proof is given by straightforward computations.

Proposition 4. *Consider Systems* (3.24) *and* (3.25). *If* $\lambda_{4,5}\geq 0$*, both systems do not have equilibria and the sets* $\{\lambda_{4,5}=0\}$ *are invariant, for all integer* $n>2$ *and* $\omega_n\neq 0$*. See Figure 3.9.*

3.4.1.3 Charts $\mathscr{A}_1$ and $\mathscr{A}_3$

Since we have already studied the charts $\mathscr{A}_2, \mathscr{A}_4$ and $\mathscr{A}_5$, it is sufficient to study the origin of $\mathscr{A}_1$ and $\mathscr{A}_3$. In order to obtain the dynamics in such charts, we perform, respectively, the weighted blow-ups

$$\begin{cases} u &= s_1^n u_1, \\ v &= -s_1^{n-1}, \\ \lambda &= s_1\lambda_1, \end{cases} \qquad \begin{cases} u &= s_3^n u_3, \\ v &= s_3^{n-1}, \\ \lambda &= s_3\lambda_3, \end{cases}$$

and the systems obtained are, respectively,

$$\begin{cases} u_1' &= -\dfrac{nu_1}{n-1}\Delta_1+\lambda_1^{n+1}\Gamma_1, \\ s_1' &= \dfrac{s_1}{n-1}\Delta_1, \\ \lambda_1' &= -\dfrac{\lambda_1}{n-1}\Delta_1, \end{cases} \tag{3.26}$$

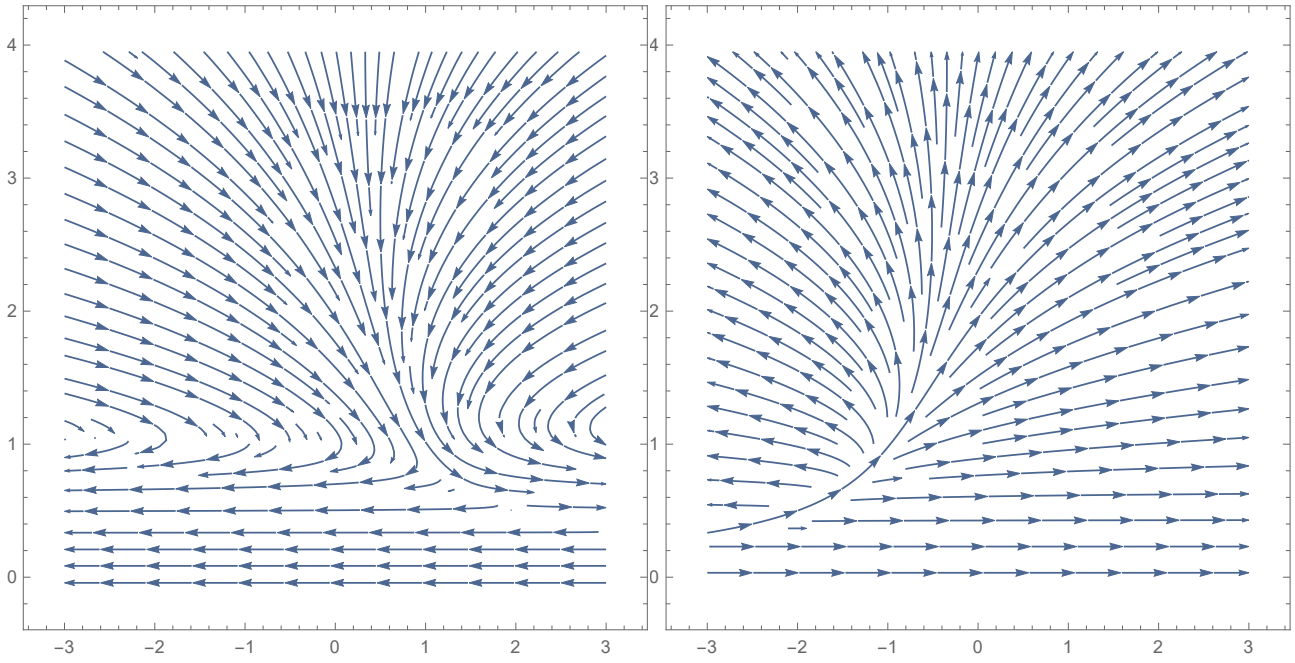

Figure 3.9: Phase portrait of Systems (3.24) (left) and (3.25) (right).

and

$$\begin{cases} u_3' &= \dfrac{nu_3}{n-1}\Delta_3 + \lambda_3^{n+1}\Gamma_3, \\ s_3' &= -\dfrac{s_3}{n-1}\Delta_3, \\ \lambda_3' &= \dfrac{\lambda_3}{n-1}\Delta_3, \end{cases} \tag{3.27}$$

where

$$\Gamma_i = \Gamma_i(u_i, s_i) = 1 + 2u_i s_i^n + u_i^2 s_i^{2n},$$
$$\Delta_1 = \Delta_1(u_1, s_1, \lambda_1) = u_1 + \lambda_1 - \lambda_1^n\Gamma_1 + (-1)^n\left(s_1^{n^2-2n}\omega_n - s_1^{n^2-n}\lambda_1\omega_{n+1}\right),$$
$$\Delta_3 = \Delta_3(u_3, s_3, \lambda_3) = u_3 - \lambda_3 - \lambda_3^n\Gamma_3 + \left(s_3^{n^2-2n}\omega_n + s_3^{n^2-n}\lambda_3\omega_{n+1}\right).$$

For $\{s_{1,3} = 0\}$, Systems (3.27) and (3.26) take the form

$$u_1' = -\frac{nu_1}{n-1}\left(u_1 + \lambda_1 - \lambda_1^n\right) + \lambda_1^{n+1}, \qquad \lambda_1' = -\frac{\lambda_1}{n-1}\left(u_1 + \lambda_1 - \lambda_1^n\right); \tag{3.28}$$

and

$$u_3' = \frac{nu_3}{n-1}\left(u_3 - \lambda_3 - \lambda_3^n\right) + \lambda_3^{n+1}, \qquad \lambda_3' = \frac{\lambda_3}{n-1}\left(u_3 - \lambda_3 - \lambda_3^n\right), \tag{3.29}$$

whose phase portraits are shown in Figures 3.10 and 3.11, respectively.

Straightforward computations proves the following proposition.

Proposition 5. *Consider Systems* (3.28) *and* (3.29) *in the half-plane* $\lambda_1 \geq 0$ *and* $\lambda_3 \geq 0$*, respectively. Then, for both systems, the origin is the only equilibrium point. Moreover, the Jacobian matrices of the vector fields associated to such systems is identically zero when computed at the origin. See Figures 3.10 and 3.11.*

Once the Jacobian matrices of (3.28) and (3.29) are zero when computed at the origin, we must blow-up such a singularity in order to study the dynamics of the systems near $(0,0)$. We emphasize that this blow-up consider only the variables u_1 and λ_1 (concerning System (3.28)) and u_3 and λ_3 (concerning System (3.29)). Details on the blow-up technique for planar analytic vector fields can be found in [1].

Performing a homogeneous polar blow-up

$$\left\{\begin{array}{rcl} u_1 &=& \rho_1\cos\theta_1,\\ \lambda_1 &=& \rho_1 \mathrm{sen}\theta_1, \end{array}\right. \qquad \left\{\begin{array}{rcl} u_3 &=& \rho_3\cos\theta_3,\\ \lambda_3 &=& \rho_3 \mathrm{sen}\theta_3, \end{array}\right.$$

in systems (3.28) and (3.29), we obtain, respectively,

$$\left\{\begin{array}{rcl} \rho_1' &=& \dfrac{-\rho_1\left(\mathrm{sen}\theta_1+\cos\theta_1\right)\left(n\cos^2\theta_1+\mathrm{sen}^2\theta_1\right)+\rho_1^n\mathrm{sen}^n\theta_1\left[(n-1)\cos\theta_1\left(\mathrm{sen}\theta_1+\cos\theta_1\right)+1\right]}{n-1},\\ \theta_1' &=& \mathrm{sen}\theta_1\cos^2\theta_1+\mathrm{sen}^2\theta_1\cos\theta_1-\rho_1^{n-1}\mathrm{sen}^{n+1}\theta_1\left(\mathrm{sen}\theta_1+\cos\theta_1\right) \end{array}\right. \tag{3.30}$$

and

$$\left\{\begin{array}{rcl} \rho_3' &=& \dfrac{-\rho_3\left(\mathrm{sen}\theta_3-\cos\theta_3\right)\left(\mathrm{sen}^2\theta_3-n\cos^2\theta_3\right)+\rho_3^n\mathrm{sen}^n\theta_3\left[(n-1)\cos\theta_1\left(\mathrm{sen}\theta_1-\cos\theta_1\right)-1\right]}{n-1},\\ \theta_3' &=& \mathrm{sen}^2\theta_3\cos\theta_3-\mathrm{sen}\theta_3\cos^2\theta_3+\rho_3^{n-1}\mathrm{sen}^{n+1}\theta_3\Big(\cos\theta_3-\mathrm{sen}\theta_3\Big) \end{array}\right. \tag{3.31}$$

The following propositions summarize the important features of Systems (3.30) and (3.31).

Remark 7. *We recall that a* semi-hyperbolic equilibrium point *of a planar vector field X is an equilibrium point p such that the Jacobian matrix of X at p has only one eigenvalue with non zero real part.*

Proposition 6. *Consider System* (3.30)*, which is obtained from* (3.28) *after a homogeneous polar blow-up. See Figure 3.10. Then the point $(0,\frac{\pi}{2})$ is a hyperbolic attracting node; and the point $(0,\frac{3\pi}{4})$ is a semi-hyperbolic repelling node.*

Proof. Direct computations shows that $(0,\frac{\pi}{2})$ and $(0,\frac{3\pi}{4})$ are equilibrium points of System (3.30). Moreover, the eigenvalues of the Jacobian matrix of (3.30) at $(0,\frac{\pi}{2})$ assure that such a point is a hyperbolic attracting node. Concerning the equilibrium $(0,\frac{3\pi}{4})$, straightforward computations assures that it is a semi-hyperbolic point, which is repelling at the exceptional divisor. Setting $\theta=\frac{3\pi}{4}$ in the component ρ_1' of (3.30), we have $\rho_1'=\frac{\rho_1^n}{2^{\frac{n}{2}}(n-1)}$, which is positive for $\rho_1>0$ sufficiently small. Therefore $(0,\frac{3\pi}{4})$ is a semi hyperbolic repelling node.

□

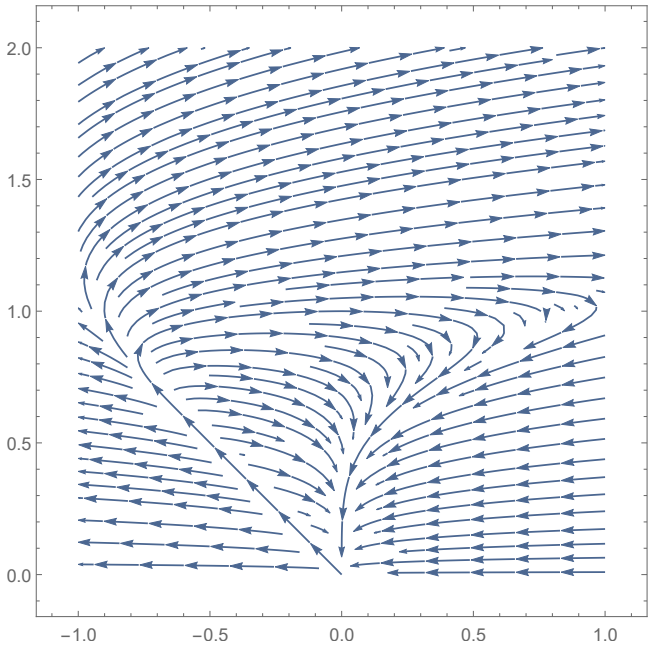

Figure 3.10: Phase portrait of System (3.28) in the region $\lambda_1 \geq 0$.

Proposition 7. *Consider System* (3.31)*, which is obtained from* (3.29) *after a blow-up in the positive* λ_3 *direction. See Figure 3.11. Then the point* $(0, \frac{\pi}{2})$ *is a hyperbolic attracting node; and the point* $(0, \frac{\pi}{4})$ *is a semi-hyperbolic saddle.*

Proof. Direct computations shows that $(0, \frac{\pi}{4})$ and $(0, \frac{\pi}{2})$ are equilibrium points of System (3.31). Moreover, the eigenvalues of the Jacobian matrix of (3.31) at $(0, \frac{\pi}{2})$ assure that such a point is a hyperbolic attracting node. Concerning the equilibrium $(0, \frac{\pi}{4})$, straightforward computations assures that it is a semi-hyperbolic point, which is repelling at the exceptional divisor. Setting $\theta = \frac{\pi}{4}$ in the component ρ_3' of (3.31), we have $\rho_1' = -\frac{\rho_1^n}{2^{\frac{n}{2}}(n-1)}$, which is negative for $\rho_1 > 0$ sufficiently small. Therefore $(0, \frac{\pi}{4})$ is a semi hyperbolic repelling node. □

3.4.1.4 Complete description of the dynamics on the sphere

Now we gather the information obtained in Propositions 3, 4, 5, 6 and 7 in order to completely describe the dynamics on $\mathscr{D}$ given by the half-sphere obtained from the blow-up of System (3.18). Denote by $c_4 = \{\lambda_4 = 0\}$ and $c_5 = \{\lambda_5 = 0\}$ the half circles of the equator of $\mathscr{D}$. Denote by P_1 and P_3 the equilibrium points positioned at the origin of the charts $\mathscr{A}_1$ and $\mathscr{A}_3$, respectively. Finally, denote by l_2 the invariant line of chart $\mathscr{A}_2$. See Figure 3.12.

Proposition 8. *Consider System* (3.18) *and suppose* $n > 2$*. After a weighted blow-up in which* $(a,b,c) = (n, n-1, 1)$*, the dynamics in the exceptional divisor* $\mathscr{D}$ *is given as follows:*

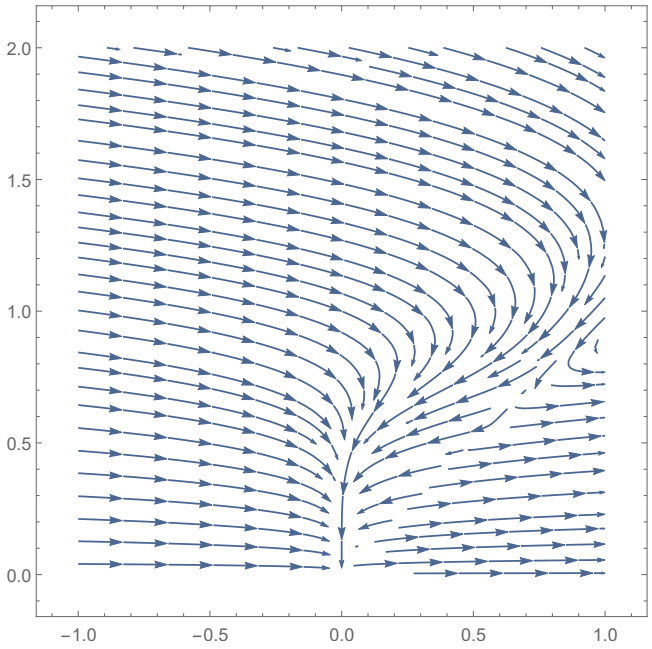

Figure 3.11: Phase portrait of System (3.29) in the region $\lambda_3 \geq 0$.

1. *In the compact set limited by the curves c_5 and l_2, all the trajectories have P_1 as α-limit and P_3 as ω-limit (including the trajectories in the invariant curves c_5 and l_2).*

2. *In the open region limited by the curves l_2 and c_4, all the trajectories have P_1 as α-limit and ω-limit. Therefore, this region is filled with homoclinic orbits.*

3. *The trajectory contained in the invariant curve c_4 has P_3 as α-limit and P_1 as ω-limit (see Figure 3.12).*

3.4.2 Case $n = 2$

In this case, System (3.18) takes the form

$$\begin{cases} u' &= \lambda^3(u+1)^2, \\ v' &= 1-(u+1)-\omega_2 v^2+\lambda(v-\omega_3 v^3)+\lambda^2(u+1)^2, \\ \lambda' &= 0, \end{cases} \tag{3.32}$$

and the weight vector is $(a,b,c) = (2,1,1)$. Differently from the case $n > 2$, the constant ω_2 plays an important role. Indeed, the charts $\mathscr{A}_4$ and $\mathscr{A}_5$ may present equilibria, depending on the sign of ω_2. As it is evident that $n = 2$ is even, we carefully analyze the situation where ω_2 is negative, which is the only relevant one in our context (see Lemma 1). Observe that, for $n = 2$, we have

$$\omega_2 = \frac{\varphi''(1)}{2\cdot 2!}, \qquad \omega_3 = \frac{\varphi'''(1)}{2\cdot 3!}.$$

We start our analysis by studying the dynamics in the charts $\mathscr{A}_1$, $\mathscr{A}_2$ and $\mathscr{A}_3$. More degenerate singularities will appear in the charts $\mathscr{A}_4$ or $\mathscr{A}_5$.

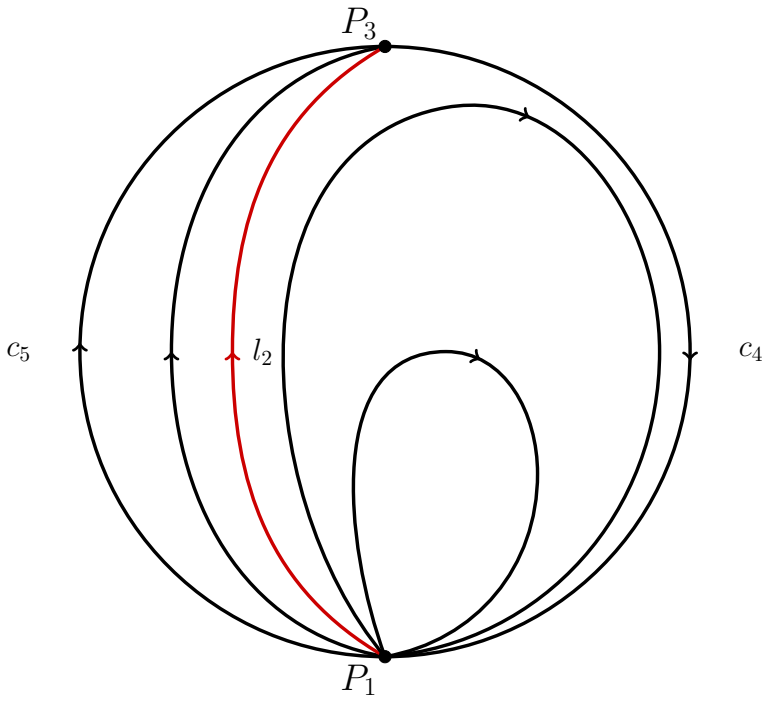

Figure 3.12: Phase portrait of System (3.18) in the exceptional divisor $\mathscr{D}$.

3.4.2.1 Chart $\mathscr{A}_2$

Considering System (3.32), after a blow-up of the form

$$u = s_2^2 u_2, \;\; v = s_2 v_2, \;\; \lambda = s_2;$$

the system obtained in $\mathscr{A}_2$ is

$$\left\{ \begin{array}{rcl} u_2' &=& 1 + s_2^2\Big(2u_2 + s_2^2 u_2^2\Big), \\ v_2' &=& 1 - u_2 + v_2 - \omega_2 v_2^2 + s_2^2\Big(2u_2 + s_2^2 u_2^2 - \omega_3 v_2^3\Big), \\ s_2' &=& 0, \end{array} \right. \tag{3.33}$$

and the dynamics in the exceptional divisor $\{s_2 = 0\}$ is given by

$$u_2' = 1, \qquad v_2' = 1 - u_2 + v_2 - \omega_2 v_2^2. \tag{3.34}$$

Observe that (3.34) does not present any equilibrium point. The phase portrait of (3.34) is given in Figure 3.13.

Once we studied the dynamics in chart $\mathscr{A}_2$, the next step is to study the charts $\mathscr{A}_1$ and $\mathscr{A}_3$.

3.4.2.2 Charts $\mathscr{A}_1$ and $\mathscr{A}_3$

In the charts $\mathscr{A}_1$ and $\mathscr{A}_3$, we analyze the singularities positioned at the origin. Other singularities will be studied in the charts $\mathscr{A}_4$ and $\mathscr{A}_5$.

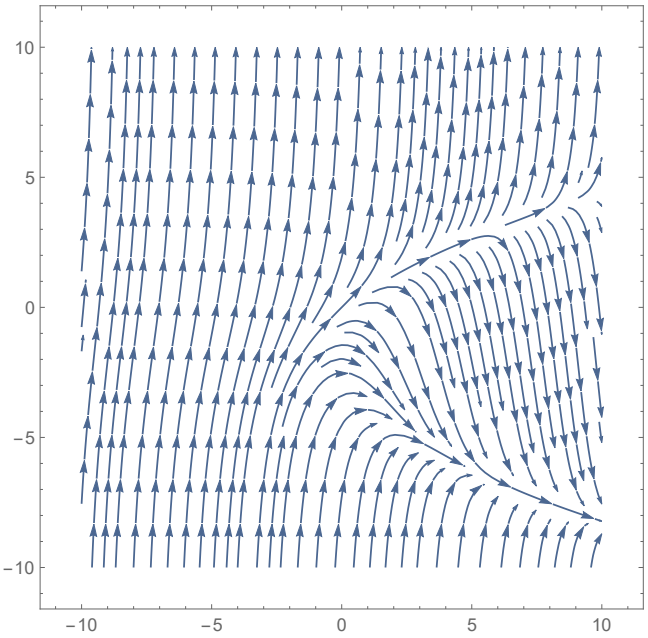

Figure 3.13: Phase portrait of System (3.34) for $\omega_2 < 0$.

In order to obtain the dynamics in $\mathscr{A}_1$ and $\mathscr{A}_3$, we perform, respectively, the weighted blow-ups

$$\left\{\begin{array}{rcl} u &=& s_1^2 u_1, \\ v &=& -s_1, \\ \lambda &=& s_1\lambda_1, \end{array}\right. \qquad \left\{\begin{array}{rcl} u &=& s_3^2 u_3, \\ v &=& s_3, \\ \lambda &=& s_3\lambda_3, \end{array}\right.$$

and the systems obtained are, respectively,

$$\left\{\begin{array}{rcl} u_1' &=& -2u_1\Delta_1 + \lambda_1^3\Gamma_1, \\ s_1' &=& s_1\Delta_1, \\ \lambda_1' &=& -\lambda_1\Delta_1, \end{array}\right. \tag{3.35}$$

and

$$\left\{\begin{array}{rcl} u_3' &=& 2u_3\Delta_3 + \lambda_3^3\Gamma_3, \\ s_3' &=& -s_3\Delta_3, \\ \lambda_3' &=& \lambda_3\Delta_3, \end{array}\right. \tag{3.36}$$

where

$$\Gamma_i = \Gamma_i(u_i, s_i) = 1 + 2u_i s_i^2 + u_i^2 s_i^4,$$

$$\Delta_1 = \Delta_1(u_1, s_1, \lambda_1) = \omega_2 + u_1 + \lambda_1 - \lambda_1^2\Gamma_1 - s_1^2\lambda_1\omega_3,$$

$$\Delta_3 = \Delta_3(u_3, s_3, \lambda_3) = \omega_2 + u_3 - \lambda_3 - \lambda_3^2\Gamma_3 + s_3^2\lambda_3\omega_3.$$

For $\{s_1 = 0\}$ and $\{s_3 = 0\}$, Systems (3.35) and (3.36) take the form

$$u_1' = -2u_1\left(\omega_2 + u_1 + \lambda_1 - \lambda_1^2\right) + \lambda_1^3, \qquad \lambda_1' = -\lambda_1\left(\omega_2 + u_1 + \lambda_1 - \lambda_1^2\right), \tag{3.37}$$

and

$$u_3' = 2u_3\left(\omega_2 + u_3 - \lambda_3 - \lambda_3^2\right) + \lambda_3^3, \qquad \lambda_3' = \lambda_3\left(\omega_2 + u_3 - \lambda_3 - u_3^2\right). \tag{3.38}$$

Both charts $\mathscr{A}_1$ and $\mathscr{A}_3$ present $(0,0)$ and $(-\omega_2,0)$ as equilibrium points. The equilibrium points given by $(-\omega_2,0)$ will be studied in the charts $\mathscr{A}_4$ and $\mathscr{A}_5$. For now, the relevant features in $\mathscr{A}_{1,3}$ are summarized in the following proposition, which is given by direct computations.

Proposition 9. *Consider Systems* (3.37) *and* (3.38)*, which were obtained after blow-up from System* (3.32)*. Denote the origin of $\mathscr{A}_1$ by P_1 and the origin of $\mathscr{A}_3$ by P_3. If $\omega_2 < 0$, then P_3 is an attracting hyperbolic node, whereas P_1 is a repelling hyperbolic node.*

3.4.2.3 Charts $\mathscr{A}_4$ and $\mathscr{A}_5$

In order to obtain the dynamics in $\mathscr{A}_4$ and $\mathscr{A}_5$, we peform, respectively, the weighted blow-ups

$$\begin{cases} u &= s_4^2, \\ v &= s_4 v_4, \\ \lambda &= s_4\lambda_4, \end{cases} \qquad \begin{cases} u &= -s_5^2, \\ v &= s_5 v_5, \\ \lambda &= s_5\lambda_5; \end{cases}$$

and the systems obtained in $\mathscr{A}_4$ and $\mathscr{A}_5$ are, respectively,

$$\begin{cases} s_4' &= \dfrac{s_4\lambda_4^3}{2}\Gamma_4, \\ v_4' &= -1 + v_4\lambda_4 - \omega_2 v_4^2 - \omega_3 s_4^2 v_4^3\lambda_4 + \left(\lambda_4^2 - \frac{v_4\lambda_4^3}{2}\right)\Gamma_4, \\ \lambda_4' &= -\dfrac{\lambda_4^4}{2}\Gamma_4; \end{cases} \tag{3.39}$$

and

$$\begin{cases} s_5' &= \dfrac{s_5\lambda_5^3}{2}\Gamma_5, \\ v_5' &= 1 + v_5\lambda_5 - \omega_2 v_5^2 - \omega_3 s_5^2 v_5^3\lambda_5 - \left(\lambda_5^2 + \frac{v_5\lambda_5^3}{2}\right)\Gamma_5, \\ \lambda_5' &= -\dfrac{\lambda_5^4}{2}\Gamma_5. \end{cases} \tag{3.40}$$

where

$$\Gamma_4 = \Gamma_4(s_4) = 1 + 2s_4^2 + s_4^4; \qquad \Gamma_5 = \Gamma_5(s_5) = -1 + 2s_5^2 - s_5^4.$$

In the exceptional divisor $\{s_{4,5} = 0\}$, Systems (3.39) and (3.40) take form

$$v_4' = -1 + v_4\lambda_4 - \omega_2 v_4^2 + \left(\lambda_4^2 - \frac{v_4\lambda_4^3}{2}\right), \qquad \lambda_4' = -\frac{\lambda_4^4}{2}; \tag{3.41}$$

and

$$v_5' = 1 + v_5\lambda_5 - \omega_2 v_5^2 + \left(\lambda_5^2 + \frac{v_5\lambda_5^3}{2}\right), \qquad \lambda_5' = \frac{\lambda_5^4}{2}. \tag{3.42}$$

We assume $\omega_2 < 0$, and this implies that there are two equilibria in $\mathscr{A}_4$, and there are none in $\mathscr{A}_5$.

The following proposition gathers important features of Systems (3.41) and (3.42). See Figure 3.14.

Proposition 10. *Consider Systems* (3.41) *and* (3.42). *If* $\omega_2 < 0$, *System* (3.42) *does not present any singularity and System* (3.41) *presents two semi-hyperbolic equilibria given by*

$$q_4^{\pm} = \Big(\pm \frac{1}{\sqrt{-\omega_2}}, 0 \Big).$$

Moreover, q_4^- *is a topological attracting node and* q_4^+ *is a topological saddle point.*

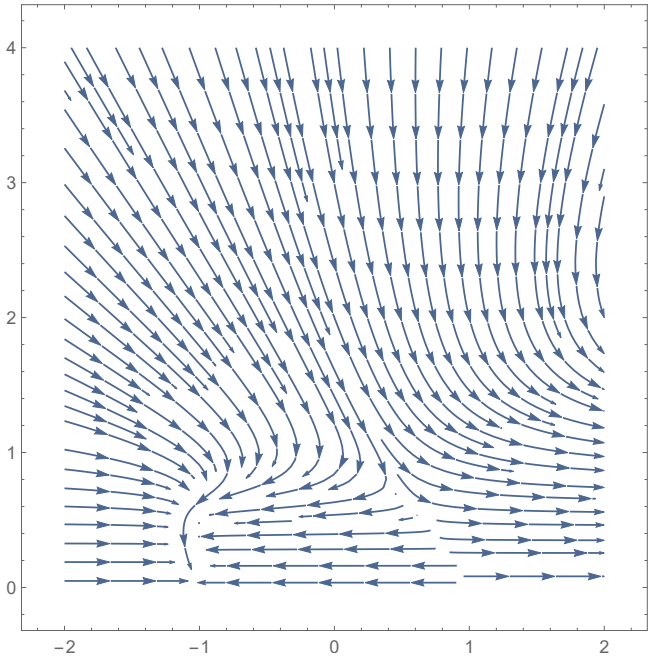

Figure 3.14: Phase portrait of System (3.41) for $\omega_2 < 0$ in the chart $\mathscr{A}_4$.

3.4.2.4 Complete description of the dynamics in $\mathscr{D}$ for $n = 2$

Now we recall the notation introduced in the analysis for $n = 2$. Let P_1 and P_3 be the origin of $\mathscr{A}_1$ and $\mathscr{A}_3$, respectively. Let $q_4^{\pm}$ be the equilibria in $\mathscr{A}_4$ for $\omega_2 < 0$. The stable separatrix of the saddle point q_4^+ will be denoted by S_4.

Denote by c_4 and c_5, respectively, the half circles in $\{\lambda_4 = 0\}$ and $\{\lambda_5 = 0\}$ connecting P_1 and P_3. Denote by $c_{3,4}$ and $c_{1,4}$ the arcs in $\mathscr{A}_4$ connecting q_4^+ to P_3 and P_1 to q_4^-, respectively. See Figure 3.15.

Proposition 11. *Consider System* (3.18) *and suppose that* $n = 2$ *and* $\omega_2 < 0$. *After a weighted blow-up in which* $(a,b,c) = (2,1,1)$, *the dynamics in the exceptional divisor* $\mathscr{D}$ *is given as follows:*

1. P_1 *is a repelling hyperbolic node, which is the* α*-limit for all orbits in* $\mathscr{D} \cap \{\lambda > 0\}$.

2. P_3 *is an attracting hyperbolic node, which is the* ω*-limit for all orbits in the open set limited by the curves* c_5, S_4 *and* $c_{3,4}$.

3. *q_4^- is an attracting node, which is the ω-limit for all orbits in the open set limited by the curves $c_{1,4}$, S_4 and $\{\lambda > 0\}$.*

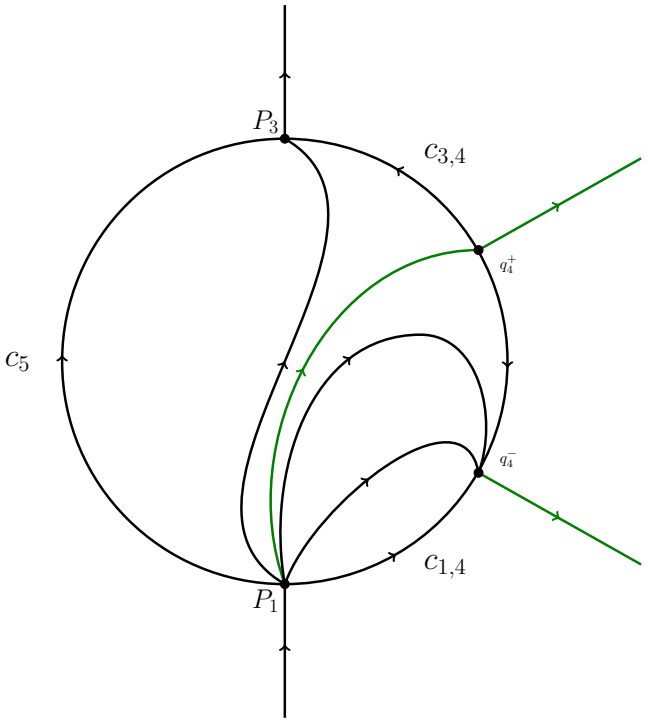

Figure 3.15: Phase portrait of the vector field after the second blow-up in the cases $\omega_2 < 0$.

3.5 Proof of Theorem 2

3.5.1 Item (a) of Theorem 2

Consider the segments

$$H_- = [-\varepsilon, 1+\varepsilon] \times \{-\varepsilon\} \text{ and } H_+ = [R(-\varepsilon), R(\varepsilon)] \times \left\{\frac{1}{4} + \varepsilon\right\},$$

and let $\overrightarrow{v}_1 = (0,1)$ a orthogonal vector to H_- and H_+. As usual, denote the regularized vector field (3.2) by Z_ε^Φ. Then

$$\left\langle \overrightarrow{v}_1; Z_\varepsilon^\Phi \right\rangle = \frac{1}{2}\left(\left((x-1)x + y - 1\right)\phi\left(\frac{y}{\varepsilon}\right) + (x-1)x + y + 1 \right);$$

in which $\langle ; \rangle$ denotes the usual inner product. Taking $y = -\varepsilon$, we obtain $\Phi_\varepsilon(-\varepsilon) = -1$ and so

$$\left\langle \overrightarrow{v}_1; Z_\varepsilon^\Phi(x, -\varepsilon) \right\rangle = 1 \neq 0.$$

As a consequence, H_- is transversal to the Z_ε-flow.

Analogously, taking $y = 1/4 + \varepsilon$, we obtain $\Phi_\varepsilon(\varepsilon) = 1$ and so

$$\left\langle \overrightarrow{v}_1; Z_\varepsilon^\Phi(x, -\varepsilon) \right\rangle = (x-1)x + 1/4 + \varepsilon \neq 0.$$

As a consequence, H_- is transversal to the Z_ε-flow.

3.5.2 Item (b) of Theorem 2

3.5.2.1 Case where n is greater than two

Initially, consider the case where n is an even number greater than two. To aid in understanding the configuration of the trajectories, we will use Figure 3.16, in which we distinguish some objects:

- C_0^ε the slow manifold obtained in Equation (3.8) (see also Figure 3.3);
- T_0^ε a vertical segment that is transversal to C_0^ε and it is contained in the open rectangle $(-\frac{1}{2}, 1) \times (-\varepsilon, \varepsilon)$;
- $B_0^{\varepsilon,\rho}$ the ball described in Figure 3.5-(A);
- $C_0^{\varepsilon,\rho,1}$ the lower branch of the slow manifold described in the charts $\mathscr{K}_2$ and $\mathscr{K}_4$. See Figure 3.5-(A);
- $P^{\varepsilon,\rho,1}$ the point at $C_0^\varepsilon \cap C_0^{\varepsilon,\rho,1}$;
- $C_0^{\varepsilon,\rho,2}$ the upper branch of the slow manifold described in the charts $\mathscr{K}_2$ and $\mathscr{K}_4$. See Figure 3.5-(A);
- $B_0^{\varepsilon,\rho,\lambda}$ the ball with a elliptic sector described in Figure 3.12 (also, consider the points P_1 and P_3 and the trajectory l_2 of this figure);
- $T_{P^{\varepsilon,\rho,1}}$, a vertical segment in the regularization band that is sufficiently close to $P^{\varepsilon,\rho,1}$ and that is transversal to C_0^ε.

For $0 \neq \varepsilon << 1$, the flow passing through a point $p = (x, y, \varepsilon)$ of T_0^ε, sufficiently close to C_0^ε, will reach a transversal section $T_{P^{\varepsilon,\rho,1}}$, passing through $P^{\varepsilon,\rho,1}$, in a finite negative time.

For $0 \neq \rho, \lambda << 1$, let us consider the following arcs and transversal sections:

- W_0^ε the arc of the fast system obtained in Equation (3.6) with $\varepsilon = 0$ that converges to the south pole SP_0^ρ of the sphere $B_0^{\varepsilon,\rho}$ in positive time (see Figure 3.16);

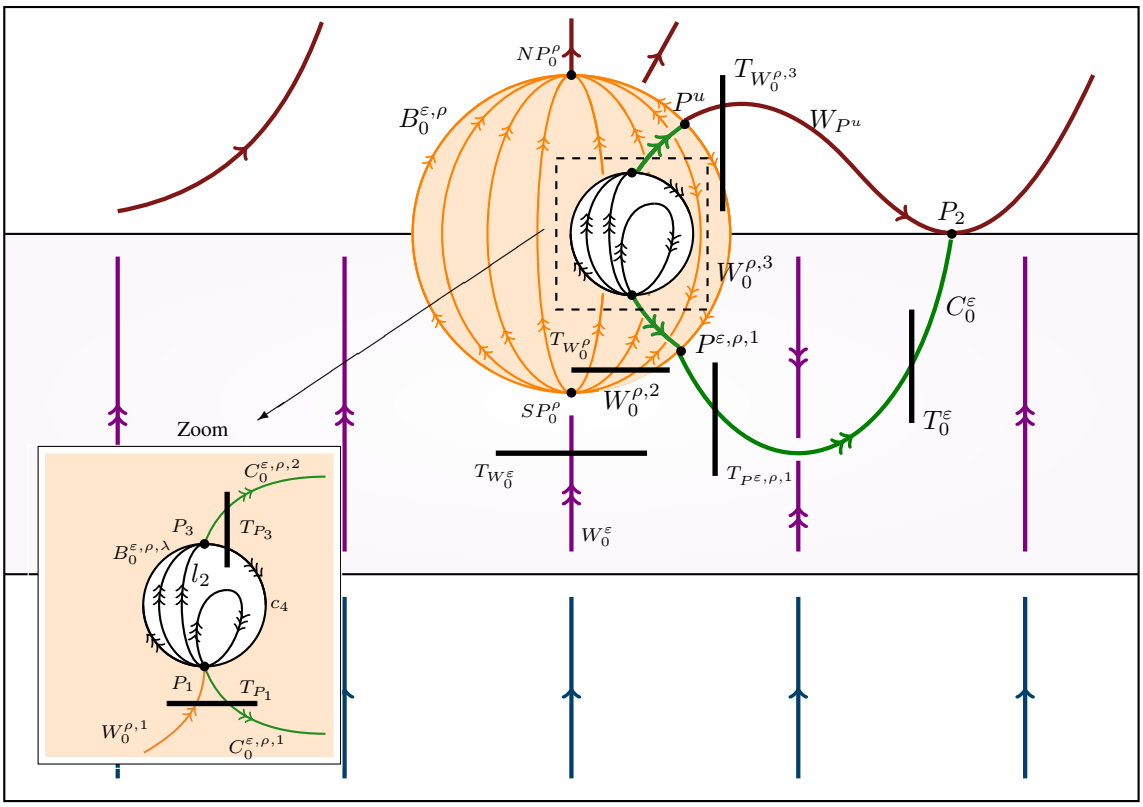

Figure 3.16: Frontal view of the phase portrait after the blow-up processes in the case where n is even and different from two.

- $T_{W_0^\varepsilon}$ a horizontal segment that is transversal to W_0^ε;
- The sphere $B_0^{\varepsilon,\rho,\lambda}$, which is obtained from the second blowing up (see also Figure 3.7);
- $W_0^{\rho,1}$ the arc of the fast system (highlighted in orange in Figure 3.16) in the chart $\mathscr{K}_2$ that converges to the south pole P_1 of the sphere $B_0^{\varepsilon,\rho,\lambda}$;
- $W_0^{\rho,2}$ the arc of the fast system and connecting SP_0^ρ and $P^{\varepsilon,\rho,1}$;
- $T_{W_0^\rho}$ a horizontal segment close to SP_0^ρ that is (simultaneously) transversal section to $W_0^{\rho,1}$ and $W_0^{\rho,2}$;
- c_4 the arc of the fast system connecting P_3 and P_1 (see Figure 3.12);
- W_{P^u} is the trajectory that tangentially touches point P_2 discussed in section 3.2;
- P^u the equilibrium point in the sphere $B_0^{\varepsilon,\rho}$ that is the intersection of $C_0^{\varepsilon,\rho,2}$ and W_{P^u};
- $W_0^{\rho,3}$ the arc of the fast system connecting $P^{\varepsilon,\rho,1}$ and P^u;
- $T_{W_0^{\rho,3}}$ a vertical segment close to P^u that is a (simultaneously) transversal section to $W_0^{\rho,3}$ and the unstable manifold W_{P^u} departing from P^u;

- T_{P_3} a vertical segment close to P_3 that is a (simultaneously) transversal section to c_4 and $C_0^{\varepsilon,\rho,2}$;
- T_{P_1} a vertical segment close to P_1 that is a (simultaneously) transversal section to $W_0^{\rho,1}$ and $C_0^{\varepsilon,\rho,1}$;

For negative time, the flow passing through a point in $T_{P^{\varepsilon,\rho,1}}$ will:

- be close to $W_0^{\rho,2}$. So, it came from $T_{W_0^\varepsilon}$ passing through $T_{W_0^\rho}$ for positive time. The same happens if it is close to $C_0^{\varepsilon,\rho,1}$ and does not touch T_{P_1}.
- be close to $W_0^{\rho,3}$. So, it came from T_{P_3} (in this case, before reaches T_{P_3}, the trajectory can passes through $T_{W_0^{\rho,3}}$). So, in negative time, the flow passes through T_{P_1} and $T_{W_0^\rho}$, going to $T_{W_0^\varepsilon}$.

We have to analyze the case when the trajectory is close to $C_0^{\varepsilon,\rho,1}$ and touches T_{P_1}. In this case, the trajectory (in negative time) will either touches T_{P_3} and goes to $T_{W_0^\varepsilon}$ as before; or it goes directly to T_{P_1} and so it, again, goes to $T_{W_0^\varepsilon}$.

The case where n is odd is similar to the case where n is even and greater than two, as the dynamics in $B_0^{\varepsilon,\rho,\lambda}$ are identical in both scenarios (see Subsection 3.4.1). As in the previous case, we can use Figure 3.17 to aid in understanding the configuration of the trajectories.

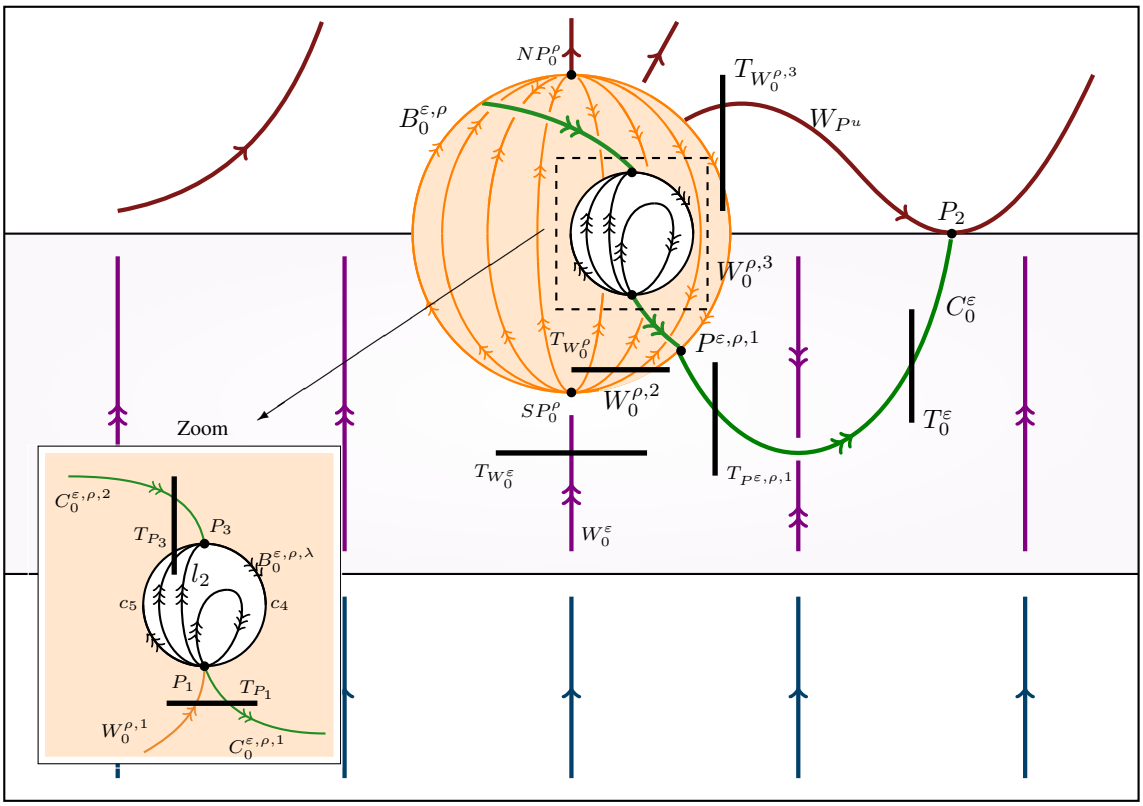

Figure 3.17: Frontal view of the phase portrait after the blow-up processes in the case where n is odd.

The main difference between these two subcases, which cover situations where n is greater than two, lies in the fact that the components $C_0^{\varepsilon,\rho,2}$ and $C_0^{\varepsilon,\rho,1}$ are attractive for the slow dynamics, and the point NP_0^ρ, equivalent to the origin in the chart $\mathscr{K}_3$, becomes a repulsive star node (see Proposition 2).

With this new configuration, for $0 \neq \varepsilon \ll 1$, the flow passing through a point $p = (x, y, \varepsilon)$ of T_0^ε, sufficiently close to C_0^ε, continues to reach a transversal section $T_{P^{\varepsilon,\rho,1}}$, close to $P^{\varepsilon,\rho,1}$, in a finite negative time, as in the previous case.

For $0 \neq \rho, \lambda \ll 1$, let us consider the following arcs and transversal sections:

- c_5: the arc to the left of the fast system that connects the points P_3 and P_1 (see Figure 3.12);
- T_{P_3}: now a vertical segment close to P_3 that is simultaneously a transversal section to c_5 and $C_0^{\varepsilon,\rho,2}$, as illustrated in Figure 3.17.

The other elements are exactly the same as those previously presented in Figure 3.16.

For negative time, the flow passing through a point in $T_{P^{\varepsilon,\rho,1}}$ will:

- be close to $W_0^{\rho,2}$. In this case, it came from $T_{W_0^\varepsilon}$, passing through $T_{W_0^\rho}$ in positive time. The same occurs if it is close to $C_0^{\varepsilon,\rho,1}$ and does not touch T_{P_1}.
- be close to $W_0^{\rho,3}$. Then, it passes close to the unstable manifold originating from NP_0^ρ (in this case, before reaching $T_P^{\varepsilon,\rho,1}$, the flow may pass through T_{P_3}); or it came from $T_{W_0^{\rho,3}}$.

As in the case where n is even and different from two, we need to analyze the case where the trajectory is close to $C_0^{\varepsilon,\rho,1}$ and touches T_{P_1}. In this case, the trajectory (in negative time) either touches T_{P_3} and goes to $T_{W_0^\varepsilon}$ as before, or goes directly to T_{P_1} and, again, goes to $T_{W_0^\varepsilon}$.

So, in negative time, the flow in a point of T_0^ε in a neighborhood of the critical manifold C_0^ε is completely determined and, in all cases where n is greater than two,, such a trajectory depart from $T_{W_0^\varepsilon}$. Note that there are other trajectories departing from $T_{W_0^\varepsilon}$ that does not goes to T_0^ε. Indeed, such a trajectories can goes nearby either the unstable manifold departing from NP_0^ρ, the north pole of $B_0^{\varepsilon,\rho}$ or W_{P^u}.

3.5.2.2 Case where n is equal to two

The case where $n = 2$ can be addressed similarly to the case where n is even and greater than two. The primary difference lies in the change in the dynamics within $B_0^{\varepsilon,\rho,\lambda}$, as described in Proposition 11 (see also Figure 3.15).

Despite this difference, for $0 \neq \varepsilon \ll 1$, the flow passing through a point $p = (x, y, \varepsilon)$ of T_0^ε, sufficiently close to C_0^ε, continues to reach a transverse section $T_{P^{\varepsilon,\rho,1}}$ in finite negative time.

The Figure 3.18 illustrates the behavior of the trajectories in the case where $n = 2$, such that $T_{q_4^+}$ and $T_{q_4^-}$ correspond to the transverse sections T_{P_3} and T_{P_1}, respectively, as described in the previous case.

For negative time, the flow passing through a point in $T_{P^{\varepsilon,\rho,1}}$ will:

- be close to $W_0^{\rho,2}$, indicating that the trajectory came from $T_{W_0^\varepsilon}$, passing through $T_{W_0^\rho}$ for positive time. The same occurs if the trajectory is close to $C_0^{\varepsilon,\rho,1}$.
- be close to $W_0^{\rho,3}$, indicating that the trajectory came from T_{P_3} (in this case, before reaching T_{P_3}, the trajectory may pass through $T_{W_0^{\rho,3}}$). Then, in negative time, the flow passes through T_{P_1} and $T_{W_0^\rho}$, heading towards $T_{W_0^\varepsilon}$.

Therefore, in negative time, the flow at a point of T_0^ε in a neighborhood of the critical manifold C_0^ε is completely determined, and in all cases, such a trajectory originates from $T_{W_0^\varepsilon}$.

As in the previous case, note that there are other trajectories originating from $T_{W_0^\varepsilon}$ that do not go to T_0^ε. In fact, in negative time, such trajectories may pass near the unstable manifold $C^{\varepsilon,\rho,2}$, originating from NP_0^ρ (the north pole of $B_0^{\varepsilon,\rho}$) or from W_{P^u}.

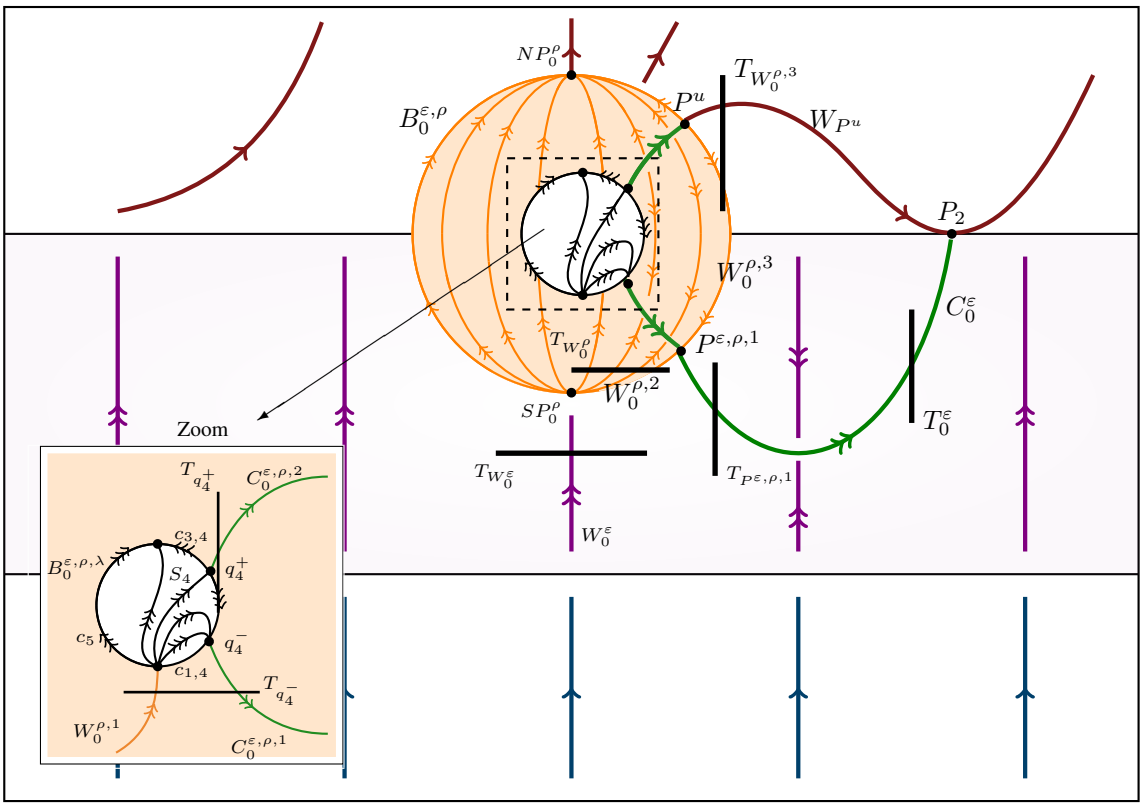

Figure 3.18: Frontal view of the phase portrait after the blow-up processes in the case where n is equal to two.

Concluding remarks

In this work, we conducted a thorough analysis of System (3.1) in a neighborhood of the origin, employing a set of techniques that involve the regularization process using a $\mathscr{C}^n$-Sotomayor-Teixeira regularization, together with the singular perturbations theory and the desingularization technique known as the blow-up.

We paid special attention to the process of desingularization of non-normally hyperbolic points, utilizing local charts to deepen our understanding of the dynamics. In this context, we observed that the choice of the regularization function generally has a significant influence on the dynamics of the charts. Particularly, based on Lemma 1, we found that the dynamics in these charts heavily depend on the parity of n related to the $\mathscr{C}^n$-Sotomayor-Teixeira regularization.

It is relevant to highlight that the sequence of figures presented here provides an overview of all the steps that we used to analyze the system under consideration. This strategy can be adapted and applied to analyze similar systems. This confers the method the advantage of being reproducible and useful for future investigations in similar systems.

Bibliography

[1] M. J. Alvarez, A. Ferragut, and X. Jarque. A survey on the Blow-up technique. *International Journal of Bifurcation and Chaos*, 21(11):3103–3118, 2011.

[2] T. Carvalho, R. Cristiano, D. S. Rodrigues, and D. J. Tonon. Global analysis of a piecewise smooth epidemiological model of COVID-19. *Nonlinear Dynamics*, 105(4):3763–3773, 2021.

[3] T. Carvalho, R. Cristiano, D. S. Rodrigues, and D. J. Tonon. Global analysis of the dynamics of a piecewise linear vector field model for prostate cancer treatment. *Journal of Dynamical and Control Systems*, 28(2):375–398, 2021.

[4] T. Carvalho, J. Cunha, and B. R. Freitas. Canonical forms of 3D cusp-fold singularities and its unfoldings. 2022.

[5] T. Carvalho, D. Duarte Novaes, and L. Gonçalves. Sliding Shilnikov connection in Filippov-type predator-prey model. *Nonlinear Dynamics*, 100:2973–2987, 2020.

[6] D. Chieregato Vicentin, P. F. Mancera, T. Carvalho, and L. Fernando Gonçalves. Mathematical model of an antiretroviral therapy to HIV via Filippov theory. *Applied Mathematics and Computation*, 387:125179, 2020.

[7] R. Cristiano, T. Carvalho, D. J. Tonon, and D. J. Pagano. Hopf and homoclinic bifurcations on the sliding vector field of switching systems in $\mathbb{R}^3$: A case study in power electronics. *Physica D: Nonlinear Phenomena*, 347:12–20, 2017.

[8] T. de Carvalho, R. Cristiano, L. F. Gonçalves, and D. J. Tonon. Global analysis of the dynamics of a mathematical model to intermittent HIV treatment. *Nonlinear Dynamics*, 101(1):719–739, 2020.

[9] F. Dumortier. Singularities of vector fields on the plane. *Journal of Differential Equations*, 23(1):53–106, 1977.

[10] F. Dumortier. *Singularities of Vector Fields*. Monografias de matemática. IMPA, 1978.

[11] F. Dumortier. *Techniques in the Theory of Local Bifurcations: Blow-Up, Normal Forms, Nilpotent Bifurcations, Singular Perturbations*, pages 19–73. Springer Netherlands, 1993.

[12] F. Dumortier and R. Roussarie. Canard cycles and center manifolds. *Memoirs of the American Mathematical Society*, 121:1–100, 1996.

[13] N. Fenichel. Geometric singular perturbation theory for ordinary differential equations. *Journal of Differential Equations*, 31(1):53–98, 1979.

[14] A. F. Filippov. *Differential Equations with Discontinuous Righthand Sides*, volume 18 of *Mathematics and its Applications*. Springer Netherlands, first edition, 1988.

[15] M. Guardia, T. M. Seara, and M. A. Teixeira. Generic bifurcations of low codimension of planar Filippov Systems. *Journal of Differential Equations*, 250(4):1967–2023, 2011.

[16] G. Hek. Geometric singular perturbation theory in biological practice. *Journal of Mathematical Biology*, 60:347–386, 2010.

[17] H. Jardón-Kojakhmetov and C. Kuehn. A survey on the blow-up method for fast-slow systems, 2021.

[18] C. K. R. T. Jones. *Geometric singular perturbation theory*, pages 44–118. Springer Berlin Heidelberg, 1995.

[19] D. Joyce. A generalization of manifold with corners. *Advances in Mathematics*, 299:760–862, 2016.

[20] V. Kozlova. Roughness of a discontinuous system. *Vestnik Moskovskogo Universiteta Seriya 1 Matematika Mekhanika*, (5):16–20, 1984.

[21] M. Krupa and P. Szmolyan. Extending geometric singular perturbation theory to nonhyperbolic points-fold and canard points in two dimensions. *SIAM J. Math. Anal*, 33(2):286–314, 2001.

[22] M. Krupa and P. Szmolyan. Extending slow manifolds near transcritical and pitchfork singularities. *Nonlinearity*, 14(6):1473–1491, 2001.

[23] C. Kuehn. *Multiple Time Scale Dynamics*. Springer International Publishing, 2015.

[24] C. Kuehn and P. Szmolyan. Multiscale geometry of the olsen model and non-classical relaxation oscillations. *Journal of Nonlinear Science*, 25(3):583–629, 2015.

[25] J. Llibre, P. R. Silva, and M. A. Teixeira. Sliding vector fields via slow fast systems. *Bulletin of Belgian Mathematical Society Simon Stevin*, 15(5):851–869, 2008.

[26] J. Llibre and C. Simó. Oscillatory solutions in the planar restricted three-body problem. *Mathematische Annalen*, 248(2):153–184, 1980.

[27] D. D. Novaes and G. Rondón. Smoothing of nonsmooth differential systems near regular-tangential singularities and boundary limit cycles. *Nonlinearity*, 34:4202–4263, 2021.

[28] D. Panazzolo and P. R. Silva. Regularization of discontinuous foliations: Blowing up and sliding conditions via fenichel theory. *Journal of Differential Equations*, 263(12):8362–8390, 2017.

[29] D. S. Rodrigues, P. F. A. Mancera, T. Carvalho, and L. F. Gonçalves. A mathematical model for chemoimmunotherapy of chronic lymphocytic leukemia. *Applied Mathematics and Computation*, 349:118–133, 2019.

[30] D. S. Rodrigues, P. F. A. Mancera, T. Carvalho, and L. F. Gonçalves. Sliding mode control in a mathematical model to chemoimmunotherapy: the occurrence of typical singularities. *Applied Mathematics and Computation*, 387:124782, 2020.

[31] J. Sotomayor and M. A. Teixeira. regularization of discontinuous vector fields. In *Equadiff 95 : International Conference on Differential Equations*. World Scientific, 1998.

[32] M. A. Teixeira and P. R. da Silva. Regularization and singular perturbation techniques for non-smooth systems. *Physica D: Nonlinear Phenomena*, 241(22):1948–1955, 2012.

[33] A. N. Tihonov. Systems of differential equations containing small parameters in the derivatives. *Mat. Sbornik N.S.*, 31/73:575–586, 1952.

[34] J. Valencia-Calvo, G. Olivar-Tost, J. D. Morcillo-Bastidas, C. J. Franco-Cardona, and I. Dyner. Non-smooth dynamics in energy market models: A complex approximation from system dynamics and dynamical systems approach. *IEEE Access*, 8:128877–128896, 2020.